Synthesis and Characterization of Nanostructured Semiconductor Materials by Self-assembling Methods

by

Hong Yang

A thesis
presented to the University of Waterloo
in fulfillment of the
thesis requirement for the degree of
Master of Applied Science
in
Chemical Engineering

Waterloo, Ontario, Canada, 2008

AUTHOR'S DECLARATION

I hereby declare that I am the sole author of this thesis. This is a true copy of the thesis, including any required final revisions, as accepted by my examiners.

I understand that my thesis may be made electronically available to the public.

Abstract

This thesis reported synthesis of TiO_2 nanostructures and Fe_2O_3 nanostructures and studied on self-assembling process. The morphologies, compositions, and physicochemical properties of the prepared samples were characterized by TEM, FESEM, XRD, FTIR, UV, and SQUID etc.

Nanoparticles of transition metal oxides own their special function to become an interesting hot research topic in the recent decades. In particular, superparamagnetic iron oxide nanoparticles can be used as drug delivery agent and new hard disc drive materials. They have wide application in environment industry as well. Titanium dioxide nanoparticles can be applied in photocatalysts, UV protectors and dye sensitive solar cell etc. Their wide industrial applications for advanced technology development motivate scientists to develop simple, economical and novel synthetic methods, and explore their applications, so that the commercialization of the production of the nanomaterials becomes feasible.

The objective of this project is to develop an effective, simple and economical technical route for synthesis of nanosized iron oxide and titanium oxide particles/rods/films. The approach and the progress are outlined as follows.

Based on extensive literature reading on the project related area, a novel self-assembling technical route for iron oxide nanostructure and architecture was proposed which has been confirmed to be effective. Detailed experimental investigation on the synthesis of nanoparticles/rods, and instrumental characterization of the particle size, structure, and crystallites, etc. via TEM, FESEM, XRD, FTIR, UV, SQUID are conducted. Uniform nanorods of hematite iron oxide and titanium oxide nanospheres, and anatase TiO_2 thin film with micropores have been successfully achieved. Some preliminary exploration for applications of the synthesized nanomaterials has also been carried out.

Firstly, a novel assembled scheme of iron oxide nanostructure and architecture by self-assembling process was investigated. The sol-gel technical route was employed to synthesize nearly uniform nanorods of hematite particles. Morphologies and physicochemical properties of iron oxide nanostructure were characterized by analytical instrument.

Secondly, titanium oxide nanospheres were synthesized via a hydrothermal process using titanium isopropoxide as the precursor. Titanium oxide nanospheres with inner nanospace and

highly organized crystallites in the shell structure and surface regions were synthesized. It demonstrated that the technical route developed in this work has a high versatility for structural engineering of various targeted morphological products.

Thirdly, a simple process of preparing anatase TiO_2 thin film with micropores was pursued. The synthesized nano thin film with micropores was used for the material of dye-sensitive solar cell; and effective electron transfer of titanium oxide electrode was confirmed by electrochemical voltammetry. Preparation of the titanium oxide electrode and its electrochemical analysis was studied. The application of the titanium oxide of microporous thin film material as a promoter for electrochemistry voltammetry measuring system was explored in this thesis.

In conclusion, the iron oxide nanorods with superparamagnetic property were successfully synthesized by a simple method with low cost materials. Titanium oxide hollow nanospheres were achieved by the assistance of copolymer template. Titanium oxide thin film with microporous structure with significantly high efficiency in electron transfer was realized. Further researches on the synthesis of hybrid iron oxide and titanium oxide nanoparticles, their crystal growth architecture and mechanism, as well as exploration of their applications are recommended.

Acknowledgements

I gratefully acknowledge the Natural Sciences and Engineering Research Council of Canada (NSERC) and Graduate Studies Office for the financial support.

I wish to express my deepest gratitude to my supervisor, Prof Qinmin Pan, for her painstaking modification of the publications and this thesis. Many thanks for her guidance and support.

Many thanks to our group members Dr J. Wu, D Fang, Truth Wei and L Zhang for their help in carrying out my research work in the Lab. Thanks to our group new members L. Yang, J. Xiao, Y. Liu and M. Liu, with them, life is enjoyable in Waterloo.

I am also acknowledging to all the staff in the General Office and Instrument Laboratories for their support in running some testing instrument.

Special thanks must go to my husband, my lovely sons and my parents for their kind understanding, encouragement, and support during my pursuit of MASC in Waterloo.

Table of Contents

Author's Declaration……ii
Abstract iii
Acknowledgements v
Table of Contents vi
List of Figures x
List of Tables xiii
Chapter 1 Introduction 1
1.1 Objectives 2
1.2 Outline 4
Chapter 2 Literature Reviews 5
2.1 Brief background 5
2.2 Self-assembly mechanism 5
2.3 Crystal structures and surface propeties 8
2.3.1 Nanostructures and surface properties of TiO_2 8
2.3.2 Nanostructures and properties of Fe_2O_3 10
2.3.2.1 Structure of α-Fe_2O_3 10
2.3.2.2 Magentic property of hematite nanoparticles 12
2.4 Synthesis methods for TiO_2 and Fe_2O_3 based nanostructures 14
2.4.1 Sol-gel method 14
2.4.2 Solvothermal method 15
2.4.3 Liquid phase deposition (LPD) method 17
2.4.4 Other sythetic methods 18
2.5 Application of TiO_2 and Fe_2O_3 nanomaterials 19
2.5.1 Application of TiO_2 nanocrystals 19
2.5.1.1 Photocatalytic properties 19
2.5.1.2 Cheaper and highly efficient solar cells 20
2.5.1.3 Multicolor photochromism 22
2.5.2 Application of Fe_2O_3 nanocrystals 22
2.5.2.1 Application in biotechnology 22
2.5.2.2 Catalystic reaction 23
2.5.2.3 Environment significance 24
2.5.2.4 Liquid pigments 24

2.6 Summary 25
Chapter 3 Research Approaches and Experimental Methods 26
3.1 Research approaches of anatase and hematite nanoparticles 26
3.1.1 Research approach of anatase nanoparticles 26
3.1.2 Research approach of hematite nanoparticles 27
3.2 Materials characterization analysis 28
3.2.1 Powder X-ray diffraction (XRD) 28
3.2.2 Transmission electron microscopy (TEM) 28
3.2.3 Scanning electron microscopy (FESEM/SEM) 29
3.2.4 Nanoparticle size analysis (NANOTRAC) 29
3.2.5 Fourier transform infrared spectroscopy (FTIR) 30
3.2.6 UV spectrophotometer 30
3.2.7 Magnetic property analysis (SQUID) 31
3.2.8 Surface area analysis (BET) 31
3.2.9 Electrochemical voltammetry 31
Chapter 4 Self-assembly of Iron Oxide Nanorods 33
4.1 Introduction 33
4.2 Experiment details 35
4.2.1 Materials for synthesis of iron oxide nanoparticles 35
4.2.2 Apparatus 35
4.2.3 Preparation of reagents 35
4.2.4 Synthesis of nanoparticles of iron oxide 36
4.2.5 Separation of the products 36
4.3 Characterization 37
4.4 Results and discussion 38
4.4.1 Crystal hematite nanostructures 38
4.4.2 Crystal nanorod growth and morphology 40
4.4.3 Nanoparticle size 49
4.4.4 Nanoparticles composition 51
4.4.5 Magnetic properties 52
4.4.6 UV-Vis diffuse reflectance spectroscopy 54
4.4.7 Surface area adsorption analysis 55
4.5 Summary 56

Chapter 5 One Step Synthesis of TiO_2 Hollow Nanospheres vis Coploymer Template 57
5.1 Introduction 57
5.2 Experiment details 59
5.2.1 Materials for synthesis of TiO_2 nanospheres 59
5.2.2 Reaction apparatus 59
5.2.3 Synthesis of TiO_2 nanospheres 59
5.2.4 Separation of the products 59
5.3 Characterization 60
5.4 Results and discussion 60
5.4.1 Surfactant assisted synthesis of TiO_2 nanoparticles 60
5.4.2 Crystal structure and size of TiO_2 nanospheres 61
5.4.3 Crystal morphology 63
5.4.4 Nanosphere composition 70
5.4.5 UV-visiable spectra 72
5.4.6 Physical phenomena 73
5.5 Summary 74
Chapter 6 Performance of High Porous TiO_2 Nanoparticles in Electron Transport 75
6.1 Introduction 75
6.2 Experimental section 76
6.2.1 Frabrication of TiO_2 nano thin film with pores structure 76
6.2.1.1 Synthesis of TiO_2 thin film 76
6.2.1.2 Separation of the products 77
6.2.2 Electrochemical impedance voltammetry 77
6.2.2.1 Measurement instrument and processing method 77
6.2.2.2 Titanium oxide electrode preparation 78
6.3 Results and discussion 78
6.3.1 The critical condition to make TiO_2 thin film 78
6.3.2 Crystal structure of the TiO_2 nanoparticles 78
6.3.3 Morphological of TiO_2 nanoparticles 80
6.3.4 Composition of thin film 85
6.3.5 UV-visiable spectra 86
6.3.6 Electrochemcial analysis for TiO_2 electrodes 87
6.4 Summary 90

Chapter 7 Conclusions and Recommendation 91
7.1 Conclusions 91
7.2 Recommendation for future work 92
7.2.1 Iron oxide series nanoparticles 92
7.2.1.1 Synthesis architected iron oxide nanoparticles 93
7.2.1.2 Synthesis iron oxide nanocatalyst 93
7.2.2 Titanium oxide series nanoparticles 93
Nomenclature 95
References 98
Appendix A 117

List of Figures

Figure 2.1: Self-assembly diagram via hydrogen bonds

Figure 2.2 : Rutile & anatase TiO_2 crystal unit cell

Figure 2.3: TiO_2 orthorhombic brookite unit cell

Figure 2.4: Structure scheme of regular hexagon

Figure 2.5: Nature hematite (kidney ore) mine picture

Figure 2.6: Simple illustration of a paramagnetic probe made up from miniature magnets

Figure 2.7A: Antiferromagnetic ordering

Figure 2.7B: Ferromagnetic ordering

Figure 3.1: Molecular formula of Tween 85

Figure 3.2: Hematite crystal 3D structure unit cell diagram

Figure 4.1: TEM images of Fe_2O_3 nanorods synthesized at 90ºC

Figure 4.2: Symmetric unit cell to one dimension nanorod of α-Fe_2O_3

Figure 4.3: XRD spectrum of hematite iron oxide nanorods

Figure 4.4: TEM image 1 of iron oxide nanoparticles

Figure 4.5: TEM image 2 of iron oxide nanoparticles

Figure 4.6: TEM image 3 of iron oxide nanorods

Figure 4.7: TEM image 4 of iron oxide nanorods

Figure 4.8: TEM image 5 of iron oxide nanorods

Figure 4.9: TEM image 6 of iron oxide nanorods

Figure 4.10: Diffraction result of iron oxide nanorods

Figure 4.11: HRTEM image 1 of iron oxide nanorods at 20 nm scale

Figure 4.12: HRTEM image 2 of iron oxide nanorods at 10 nm scale

Figure 4.13: SEM image 1 of iron oxide at 100 nm scale

Figure 4.14: SEM image 2 of iron oxide at 20 nm scale.

Figure 4.15: Nanotrac scheme of iron oxide nanodots at L11

Figure 4.16: Iron oxide particles size distribution of L3 solution

Figure 4.17: FTIR spectrum for iron oxide nanorods powder

Figure 4.18: EDX diagram of hematite iron oxide powder

Figure 4.19: SQUID (M-H) scheme of iron oxide nanoparticles

Figure 4.20: UV-Vis spectrum of iron oxide nanorods

Figure 5.1: Structure of Tween 85 unit cell

Figure 5.2: Anatase crystal 3D structure unit cell

Figure 5.3: XRD scheme of titanium oxide

Figure 5.4: Nanotrac scheme of TiO_2 nanospheres

Figure 5.5: TEM image 1 of TiO_2 nanospheres at 1μm scale

Figure 5.6: TEM image 2 of TiO_2 nanospheres

Figure 5.7: TEM image 3 of TiO_2 hollow nanospheres at 100 nm scale

Figure 5.8: HRTEM image 4 of TiO_2 hollow nanospheres 200 nm scale

Figure 5.9: HRTEM image 5 of TiO2 hollow nanospheres 100 nm scale

Figure 5.10: TEM image 6 of TiO_2 nanospheres at 200 nm scale

Figure 5.11: FESEM image 1 of TiO_2 nanospheres at 1μm scale

Figure 5.12: FESEM image 2 of TiO_2 nanospheres at EHT 15kv

Figure 5.13: FESEM image of titanium oxide nanospheres at EHT 5kv

Figure 5.14: EDX scheme of titanium oxide powder

Figure 5.15: FTIR spectrum of standard Tween 85

Figure 5.16: FTIR scheme of titanium oxide

Figure 5.17: UV-vis. Scheme of TiO_2/copolymer

Figure 6.1: XRD scheme of TiO_2/copolymer film

Figure 6.2: Nanoparticle size scheme of TiO_2 thin film

Figure 6.3: TEM image 1 of TiO_2 nano thin film at 6 hrs

Figure 6.4: TEM image 2 of TiO_2 nano thin film at 5 hrs

Figure 6.5: TEM image 3 of TiO_2 thin film at 4 hrs

Figure 6.6: TEM image 4 of TiO_2 nano thin film at 3 hrs

Figure 6.7: FESEM image of TiO_2 thin film

Figure 6.8: EDX scheme of TiO_2 thin film

Figure 6.9: FTIR scheme of TiO_2 thin film

Figure 6.10: UV-vis. Scheme of TiO_2 thin film

Figure 6.11: Potential vs. current of TiO_2 nanoparticles with/without pores

Figure 6.12: Potential vs. current of TiO_2 nanoparticle/standard glassy carbon

List of Tables

Table 2-1: Parameters of rutile, anatase and brookite TiO_2 crystallites

Table 2-2: Structural orientation of iron oxides

Table 4-1: EDX analysis of iron oxide nanoparticles

Table 4-2: Nanorods of iron oxide obtained by BET analysis

Table 5-1: Titanium Oxide morphologies observed at various reaction conditions (pH = 8-9)

Chapter 1
Introduction

In recent years, nanocrystalline materials have attracted great attention from chemists, physicists and material scientists due to their unique and special chemical, physical and mechanical properties. The most remarkable feature of nanoparticles in that they display distinct differences from their microcrystalline counterparts. For example, Reddy and his group (Reddy et al., 2001) have shown that nanoparticles of anatase TiO_2, synthesized by a precipitation technique, display direct bandgap semiconductor behavior, whereas microcrystalline TiO_2 is an indirect bandgap material.

Synthesis approach in this field has developed so rapidly that nano-crystalline materials with new functionalities show great promise for use in industry. For instance, semiconducting nanomaterials (Fe_2O_3, ZnO, Co_3O_4, CuO and TiO_2 etc) represent an interesting and important class of materials with potential applications in electronic, optoelectronic, electrochemical, electromechanical and other fields. (Murray et al., 2000)

Prospects on nanomaterials mainly depend on the success in fabrication processes. Various strategies have been employed to synthesize semiconducting nanomaterials such as vapor-phase evaporation and /or vapor-liquid-solid growth mechanism, and controllable solution growth at elevated temperatures. Among these, development of novel methods for mass production in low cost self-assembled nanostructures is a challenging topic. Accordingly, there has emerged a demand to study their synthesis-structure-property relationships in order to understand the fundamental concepts underlying the observed physical and mechanical properties (Morales et al., 1998; Gate et al., 2000).

Semiconductor metal oxide nanoparticles inclusive of iron oxide and titanium dioxide both have special functions to become an interesting hot research topic. In particular, superparamagnetic iron oxide nanoparticles can be used for drug delivery of biomedical, new hard disc drive materials, and environmental application etc. Titanium dioxide nanoparticles are used for photocatalysts, UV protectors and dry sensitive solar cells, etc.

The synthesis of uniform magnetic nanoparticles of iron oxide has been intensively pursued (Kong et al., 2004) because of their broad applications in magnetic storage media, ferrofluids, magnetic

resonance imaging (MRI), magnetically guided drug delivery and catalysts for the growth of carbon nanotubes. Many metallic magnetic ferrite nanocrystals have been synthesized (Park et al., 2000) via thermal decomposition of organometallic precursors or reduction of metal salts and ferrite nanoparticles have been synthesized using reverse micelles as nanoreactors (Guo et al., 2003). However a proper size selection process was usually required to obtain magnetic nanocrystals with a narrow particle size distribution. Recently, several groups (Sun et al., 2002) reported the direct synthesis of monodisperse ferrite nanocrystals via a thermal decomposition of metal-surfactant complexes followed by mild chemical oxidation without a size-selection process. Although several groups have reported the direct synthesis of uniform iron oxide nanoparticles, most of them selected to use relatively expensive organic-metallic materials as the starting materials. Development of a simple and low cost synthetic method for uniform iron oxide nanoparticles receives intensive attention.

TiO_2 nanoparticles are of particular interest as they have been widely used in various important areas, such as pigments, photocatalysts, catalyst supports, ceramics, energy storage, magnetic data storage, sensors, dye-sensitized solar cell and environment applications (Rao et al., 2002). TiO_2 nanoparticles have been fabricated by various methods including sol-gel, hydrothermal and coprecipitation methods (Zhong et al., 2000). Most methods mentioned above require multiple steps to obtain monodispersed particles. (Cheng et al., 1995) So far, three challenges still remain in preparing nanoparticles of titanium oxide for solar cell application: (i) to obtain a simple synthetic route so that it is easy to transfer to industrial production; (ii) to use low cost and nonhazardous raw materials to make nanomaterials (iii) to increase the quantum yields, which is defined as the number of reaction events occurring per proton absorbed. In face of those challenges, lately considerable attention has been focused on fabricating different TiO_2 nanostructures (nanospheres, nanowires, and nanoparticles, etc.) (Edisson et al., 2007) . As all synthetic procedures have their limitations, it is still difficult, however desired, to in produce nanocrystalline TiO2 particles by a simple route.

1.1 Objective

Magnetic iron oxide nanoparticles and titanium oxide nanoparticles have been extensively studied because of their various applications. However, there is still a shortage of simple and economical synthetic methods, particularly for a synthesis technology that can be transferred to industrial production. This objective of this thesis associated research is to develop a novel synthetic method and

to investigate architecture nanostructures of two series semiconductor metal oxides, iron oxide and titanium oxide.

This research includes two relelated sub-projects. The first one is to synthesize iron oxide nanorods and their characteristic analysis. Herein, a simple and low cost synthetic method for iron oxide nanorods and nanodots was pursued and considerable characterization was conducted. A simple and common raw inorganic material of diluted iron (III) chloride solution and diluted sodium hydroxide solution via sol-gel method with surfactant was used to synthesize nanorods and nanodots. Carbon nanotubes were applied as an additive for this synthesis under designed conditions. The uniform nanorods of iron oxide with 5 nm width and 30 nm-50 nm length were obtained and characterization analysis was pursued.

The second series of studies was to synthesize titanium oxide hollow nanospheres and titanium oxide microporous thin film via a novel synthetic route. Anhydrous titanium (IV) isopropoxide and anhydrous isopropanol reacted in a reactor for this synthesis. Surfactant of Tween 85 and 1-hexadecylamine were applied to fulfill titanium dioxide hollow nanospheres and titanium dioxide microporous thin film under different reaction time and reaction temperature. Electrochemical voltammetry with titanium oxide thin film electrode was investigated and characteristic analysis for TiO_2 nanospheres and TiO_2 thin films were carried out in this project. Hollow nanospheres of titanium oxide with diameters ranging from 100-200nm, and titanium dioxide microporous thin filmswith about 100nm in width and 200nm in length were achieved.

Work electrodes of titanium oxide thin films with/without pores were prepared and a linear sweep method was used for the potential testing. It demonstrated that the TiO_2 nano thin film with pores will affect the electron transfer in electrochemistry cells, and it enhances the efficiency of dye-sensitivity of solar cells with TiO_2 compared to TiO_2 particles without pores. Further research about dye-sensitive solar cell of TiO_2 electrode and electron transfer analysis is suggested.

1.2 Outline of the thesis

Chapter 1 is a simple introduction of the objective and achievement outlines of the content.

Chapter 2 is a detailed but critical literature review on some basic knowledge of nanomaterials, self-assembling processes, synthesis methods and crystallographic structure of TiO_2 and Fe_2O_3. The modern application of various TiO_2 and Fe_2O_3 nanostructures are introduced in this chapter. The detailed research progress in each field of Fe_2O_3 and TiO_2 nanostructures are reviewed in Chapter 4 -6 respectively.

Chapter 3 outlines the general experimental procedures and design for preparing TiO_2 based nanostructures with a self-assembling process. The research approaches of synthesis iron oxide nanorods and titanium oxide nanospheres are proposed and discussed in this chapter. The principles of the instrumental characterization methods by TEM, FESEM, XRD, BET, FTIR, and NACO are briefly discussed and the default experimental conditions are also indicated in this chapter.

In Chapter 4, the synthesis of hematite iron oxide nanostructure and morphology by self-assembling growth process are reported. Characterization analysis of the nanorods synthesized is also described in detail.

In Chapter 5, the synthesis of hollow anatase TiO_2 nanospheres and their intestines under hydrothermal conditions were investigated and reporte.

In Chapter 6, the synthesis of microporous TiO_2 thin film using a copolymer as the template via a hydrothermal route was studied and reported. Electrochemical voltammetry comparison analyses of TiO_2 thin films with pores and without pores were described.

In Chapter 7, brief conclusion of the thesis and recommendations for future research were provided.

Chapter 2
Literature Reviews

2.1 Brief background

Nanostructures have been defined as having at least one dimension less than 100 nm. They have received steadily growing interest because of their unusual properties and promising applications, which are superior to their bulk counterparts (Wang et al., 2003a; Xia et al., 2003a; Yin et al., 2001). The ability to fabricate such nanostructures is essential to modern science and technology. Despite recent advance in the preparation and characterization of various nanostructures, there are numerous challenges in this field, such as preparing uniform nanoparticles, design of simple synthetic route and reducing the cost of materials. It has been known that the physical and chemical properties of substances can be considerably changed when they are in nanoscopic scale (Patzke et al. 2002). Nanostructure semiconductor materials such as TiO_2 Fe_2O_3, CoO, Co_3O_4, ZnO, MoO_3, SnO_2, and CuO etc. have been extensively studied due to their unusual catalytic and photoelectronic properties. (Cozzoli et al., 2003; Alivisator, 1996a)

2.2 Self-assembly mechanism

Self-assembly (SA), in the classic sense, can be defined as the spontaneous and reversible organization of molecular units into ordered structures by non-covalent interactions. The first property of a self-assembled system that this definition suggests is the spontaneity of the self-assembly process. The interactions responsible for the formation of the self-assembled system act on a strictly local level, in other words, the nanostructure builds itself. At this point, one may argue that any chemical reaction driving atoms and molecules to assemble into larger structures, such as precipitation, could fall into the category of SA. However, there are at least three distinctive features that make SA a distinct concept.

First, the self-assembled structure must have a higher order than the isolated components, be a shape or a particular task that the self-assembled entity may perform. This is generally not true in chemical reactions, where an ordered state may proceed towards a disordered state depending on thermodynamic parameters.

The second important aspect of SA is the key role of weak interactions (e.g. Van der Waals, capillary, $\pi - \pi$, hydrogen bonds) with respect to more "traditional" covalent, ionic or metallic bonds. These weak interactions play an important role in material synthesis. It can be instructive to note how weak interactions hold a prominent place in materials, but especially in biological systems, although they are often considered marginally with respect to "strong" (i.e. covalent, etc.) interactions. For instance, they determine the physical properties of liquids, the solubility of solids, and the organization of molecules in biological membranes.

The third distinctive feature of SA is that the building blocks are not only atoms and molecules, but span a wide range of nano- and mesoscopic structures, with different chemical compositions, shapes and functionalities. These nanoscale building blocks can in turn be synthesized through conventional chemical routes or by other SA strategies (Korgel, 2004).

Important examples of SA in materials science include the formation of molecular crystals, colloids, lipid bilayers, phase-separated polymers, and self-assembled monolayers (Whitesides et al., 2002). The folding of polypeptide chains into proteins and the folding of nucleic acids into their functional forms are examples of self-assembled biological structures. Figure 2.1 exemplifies the SA building block by hydrogen bonding. (Beijer et al., 1998)

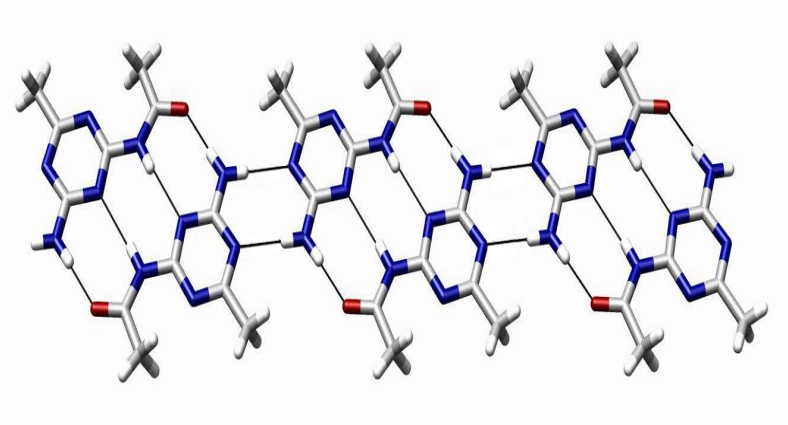

Figure 2.1: Self-assembly diagram of adenosine via hydrogen bonds (Beijer et al., 1998)

Another character that is common to nearly all self-assembled systems is their thermodynamic stability. In order for SA to take place without the intervention of external forces, the process must lead to a

lower Gibbs free energy, thus self-assembled structures are thermodynamically more stable than the single, unassembled components.

SA is a process which is easily influenced by external parameters: This can make synthesis more problematic due to the many free parameters that should be controllable; on the other hand, it has the exciting advantage that a large variety of shapes and functions on many length scales can be obtained (Lehn et al., 2002). By choosing precursors with suitable physicochemical properties, it is possible to exert a fine control on the formation processes in order to obtain complex architectures. Clearly, the most important tool when it comes to designing a synthesis strategy for a material, is the knowledge of the chemistry of the building units (Forster et al., 2002)

Most self-assembling mechanisms for inorganic nanostructures occur with the assistance of ligands (Polleux et al., 2004), surfactants (Larsen et al., 2003; Motte et al., 1996; Lisiechi et al., 2003; Messer et al., 2000; Li et al., 2005; Puntes et al., 2002), virus (Lee et al., 2003), fluidic channel structures (Huanget al., 2001), Langmuir-Blodgett technique (Yang , 2003; Whang et al., 2003), drying-mediated process (Zeng et al., 2002; Rabani et al., 2003), belong to the ”growth-then-assembly” process where the two discrete steps, growth and assembly, can be clearly divided. Recently, the shape effect in nanoparticle self-assembly was also investigated efficiently by Jana (Jana et al., 2004).

The “growth-cum-assembly” integrated process which is usually also called the self-organized growth process has also attracted great interest due to its simplicity and good results. External assistance such as magnetic field (Niu et al., 2004) and templates of microbial polysaccharides (Chan et al., 2004), self-assembled monolayer (Lee et al., 2002) and micro-patterned surfaces (Tian et al 2003a) have been explored to grow various crystals with in-situ self-assembling process(Imai et al., 2003; Tian et al., 2003b; Liu and Yu et al., 2004). Moreover, some bio-inspired approaches have also been used to fabricate micropatterned calcite single crystals with complex structure. (Aizenberg et al., 2003)

2.3 Crystal Structures and surface properties of TiO_2 & Fe_2O_3

2.3.1 Nanostructure and surface properties of TiO_2

As one of the most useful metal oxide, titanium dioxide has three major different crystal structures, rutile (tetragonal, D_{4h}^{14} space group: $P4_2/mnm$, $a=b=4.584$Å, $c=2.953$Å), anatine (tetragonal, D_{4h}^{19} –I spacegroup:$I4_1/amd$, $a=b=3.782$Å, $c=9.502$Å) and brookite (rhombohedra D_{2h}^{15} Space group: Pbca, *a*

= 5.436 Å , *b*=9.166Å, *c*=5.135Å) (Samsonov et al., 1982). Table 2.1 shows the parameters of brookite, anatase and rutile structure. In general, rutile and anatase is an important role in the application of TiO_2. The unit cells of rutile, anatase and brookite are illustrated in Figure 2.2 and Figure. 2.3. In both structures, each titanium ion is coordinated with six oxygen ions and each oxygen ion with three titanium ions. For anatase, the TiO_2 octahedra shares edges with four adjacent octahedral; while the corner-sharing octahedral forms (001) planes. (Diebold et al., 2003)

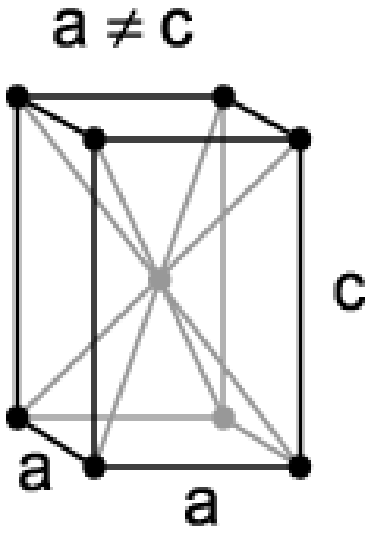

Figure 2.2: Rutile & anatase TiO_2 crystalline unit cell (Smyth et al., 1988)

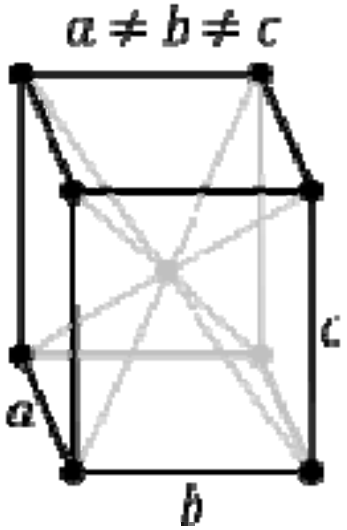

Figure 2.3: TiO_2 orthorhombic brookite unit cell (Smyth et al., 1988)

Table 2-1: Parameters of Rutile, Anatase and Brookite TiO_2 Crystals (Smyth, et al., 1998)

TiO_2 Crystal Type	Rutile	Anatase	Brookite
a(Å)	*4.5845*	*3.7842*	*9.184*
b (Å)			*5.447*
c(Å)	*2.9533*	*9.5146*	*5.145*
Crystal System	*tetragonal*	*tetragonal*	*orthorhombic*
Density g/cm^3	*4.27*	*3.895*	*4.123*
Mole Mass (g/mol)	*79.89*	*79.89*	*79.89*
Space Group	D_{4h}^{19}-$P4_2/mnm$	D_{4h}^{19}-$I4_1/amd$	D_{2h}^{15}-$Pbca$
Vol: a^{2}c and abc nm^3	*62.07*	*136.25*	*257.38*

Anatase is one of the most investigated polymorphs of TiO_2. The stability of the different low-index anatase surface has been predicted theoretically (Vittadini et al., 1998; Fahmia and Minot, 1994; Bullen et al, 2002). By using a periodic Hartree-Fock method, water adsorption on various crystallographic surfaces, (101) and (001), could be calculated. It is well known that the (101) face is the most thermodynamically stable surface for anatase TiO_2 nanocrystal (Lazzeri et al., 2001; Lazzeri et al., 2002). It might explain the fact that TiO_2 nanostructure in anatase phase is more stable than in rutile phase. Because anatase is a metastable phase, it transforms into rutile at relatively low temperature (Amores et al., 1995), and the transition temperature is dependent on impurities, crystal size, sample history etc.

Various TiO_2 nanostructures have been synthesized during the recent decade, including nanorods (Kim et al., 2003), nanofibers (Jung et al., 2002), nanotubes (Niederberge et al., 2002), nanowhiskers (Zhu and Ding, 1999), nanospheres (Iida et al., 1998), ordered holes (Yin et al., 2001) and other morphologies. Among which the contribution of Chemseddine et al. (1999) has given researchers in this field a deep impression because he very clearly indicated the TiO_2 nanocrystals exhibit different

sizes, shapes, and facets, depending on the pH value and the type of organic additives in the colloidal solutions. Typically, high pH value results in small cubic-like nanocrystals with {112} and {103} faces, while low pH value leads to truncated tetragonal nanocrystals with {101}, {001} and {010} faces. Excess dilution of the particle density appears to cause partial dissolution of the cubic-like TiO_2 nanocrystals to form spherical nanocrystals (Chemseddine et al., 1999).

Due to its wide applications, mesoporous TiO_2 has also attracted great interest and various porous nanostructures have been prepared successfully (Schűth et al., 2001, Yang et al., 1998; Moritz et al., 1997, Burnside et al., 1998).

2.3.2 Nanostructures and properties of Fe_2O_3

2.3.2.1 Structure of α-Fe_2O_3

Hematite (α-Fe_2O_3) is the mineral form of Iron (III) oxide (Fe_2O_3). Hematite crystallizes in the rhombohedral system and has hexagonal structure. Figure 2.4 shows the standard hexagon structure diagram of regular hexagon crystal and Figure 2.5 shows the natural hematite materials diagraph of kidney ore from Michigan. (Dang et al., 1998)

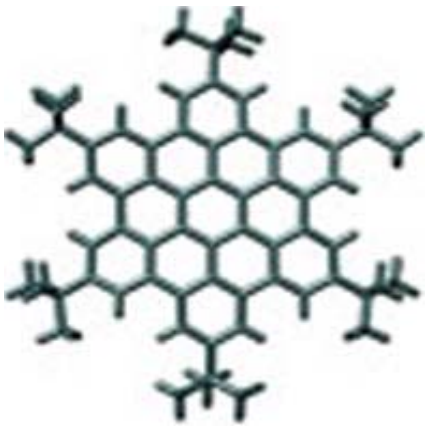

Figure 2.4: Structure scheme of regular hexagon (Dang et al., 1998)

Figure2.5: Nature hematite (kidney ore) mine picture (Dang et al., 1998)

The unit cell of hematite is hexagonal with a = 0.5034 nm and c = 1.375 nm (Bragg & Bragg, 1918). It consists of hexagonal close packing, where the sheets stack in ABAB [001]. Space group R3c arrays of oxygen ions stacks along the [001]. (Cornell, 2002) The arrangement of cations produces pairs of $Fe(O)_6$ octahedra, and each octahedron shares edges with three neighboring octahedras in the same plane and one face with an octahedron in an adjacent plane. Table 2-2 is the structural orientation of crystal plane and crystal direction of iron oxides.

Table 2-2: Structural orientation of iron oxides (Dang et al., 1998)

Crystal status	Crystal plane	Crystal direction
Goethite	(100)(004)(200)	[100]
Hematite	(001)(003)(110) (100)	[100]
Magnetite	(111)	[110]
Lepidocrocite	(100)	[110]
Maghemite	(001)	[110][111]

The crystal structure of hematite has a less directional effect on crystal habit than that of goethite. The principal habits of hematite are hexagonal plates and rhombohedra. Morphologies of synthetic hematite include plates and discs, rods, spindles, spheres, ellipsoids, double ellipsoids, rhombohedra, stars, cubes and peanuts.

2.3.2.2 Magnetic property of hematite nanoparticles

Hematite is an antiferromagnetic material below the Morin transition at 260K. It is also a weakly ferromagnetic with an extremely tiny moment (0.002mB) between the Morin transition (260K) and below its Néel temperature at 948K, where it is paramagnetic. Hematite particles when smaller than about 8 nm display superparamagnetic relaxation at room temperature. The magnetic behavior of hematite depends on its crystallinity particle size and the extent of cation substitution. (Cornell, 2002)

Figure 2.6 is a simplified illustration of a paramagnetic probe made up from miniature magnets. Figure 2.7A is a simplified illustration of antiferromagnetic ordering and Figure 2.7B is an illustration of ferromagnetic ordering.

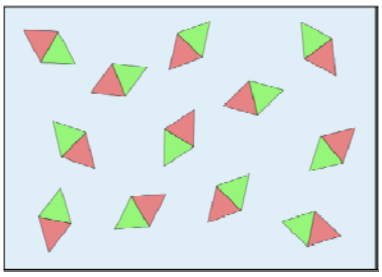

Figure 2.6: Simple illustration of a paramagnetic probe made from miniature magnets

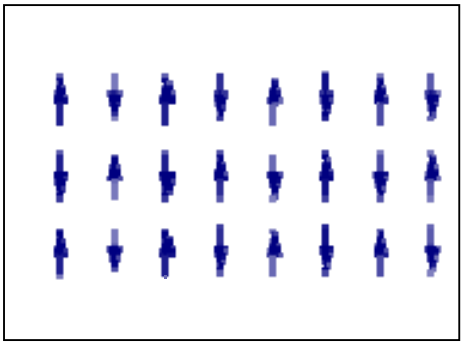

Figure 2.7A: Antiferromagnetic ordering

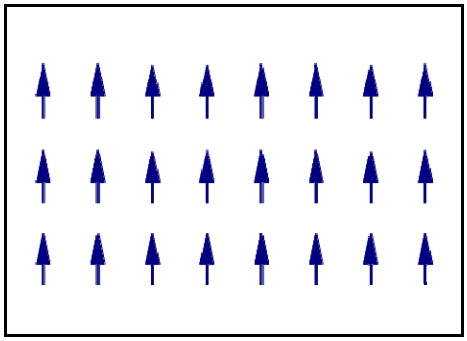

Figure 2.7B: Ferromagnetic ordering

The constituent atoms or molecules of paramagnetic materials have permanent magnetic moments dipoles, even in the absence of an external magnetic field. This generally occurs due to the presence of unpaired electrons in the atomic/molecular electron orbits. In pure paramagnetism, the dipoles do not interact with one another and are randomly oriented in the absence of an external field due to thermal agitation, resulting in a zero net magnetic moment as illustrated in Figure 2.6. When a magnetic field is applied, the dipoles will tend to align along with the applied field, resaulting in a net magnetic moment in the same direction as the applied field as shown in Figure 2.7B.

Superparamagnetism is such a phenomenon by which magnetic materials may exhibit a behavior similar to paramagnetism even at a temperature below the Curie or the Néel temperature. This phenomenon could occurr when the materials were composed of very small nanocrystallites (1-10 nm) and where the thermal energy was not sufficient to overcome the coupling forces between neighboring atoms (Cornell, 2002). However, the thermal energy was just sufficient to change the direction of magnetization of the entire nanocrystallite. Thus, the materials behaved in a manner similar to paramagnetism (Blake et al., 1966).

2.4 Synthetic methods for TiO_2 and Fe_2O_3 based nanostructures

2.4.1 Sol-Gel method

The sol-gel method is one of the common approaches to prepare well-dispersed nanoparticles and homogenous thin films by fabricating the structure of a primary precursor in which metal atoms distribute uniformly. The normal procedure of this method consists of mainly two steps, the hydrolysis

and polycondensation of a metal alkoxide. It ultimately yields a hydroxide or oxide of the metal under certain conditions. To obtain nanomaterials in sol-gel process, properly controlling experimental conditions such as pH, solution concentration, and temperature, etc. are especially important (Wang et al., 2003a). The resultant precipitate of metal oxide nanoparticles is subsequently washed and dried, which is then calcined at an elevated temperature to form crystalline metal oxide nanoparticles.

The hydrolysis of metal alkoxides involves nucelophilic reaction with water as follows:

$$M(OR)_y + xH_2O \longrightarrow M(OR)_{y-x}(OH)_x + x\ ROH$$

Condensation occurs when either hydrolyzed species react with each other and release water molecules, or hydrolyzed species react with unhydrolyzed species and release an alcohol molecule. The rates at which hydrolysis and condensation reactions take place are important parameters that affect the properties of the final product.

The technical route using sol-gel method to prepare metal oxide nanoparticles has been well developed in the recent twenty years, which has been used for synthesizing nanoparticles and alloy nanomaterials of metal oxides of Ti, Zn, Co, Al, and Fe, etc. The sol-gel method is also used for preparing magnetic nanoparticles, such as barium ferrite particles (Zhong et al., 1997), iron oxide/silica nanocomposite (Ohko et al., 2003), M-type barium hexaferrites (Dong et al., 2006), $CoFe_2O_4$-SiO_2 nanocomposites (Dasilva et al., 2006), Al-doped nickel ferrite nanocrystalline (Raghavender et al., 2007), and maghemite-silica nanocomposites consisting of 5 nm magnetic nanoparticles dispersed in silica xerogel (Sartoratto et al., 2007).

2.4.2 Solvothermal method

The solvothermal method (mainly hydrothermal) can be defined as a method of synthesis of single crystals which depends on the solubility of minerals in hot water under a high pressure. The crystal growth is performed in an apparatus consisting of a steel pressure vessel called autoclave, in which a nutrient is supplied along with water or solvent. A gradient of temperature is maintained at the opposite ends of the growth chamber so that the hotter end dissolves the nutrient and the cooler end causes seeds to take additional growth.

Possible advantages of the hydrothermal method over other types of crystal growth include the ability to create crystalline phases which are not stable at the melting point. Also, materials which have a high vapor pressure near their melting points can also be grown by the hydrothermal method. The method is also particularly suitable for the growth of large good-quality crystals while maintaining good control over their composition. Disadvantages of the method include the need of expensive autoclaves, good quality seeds of a fair size and the impossibility of observing the crystal as it grows (Laudise et al., 1987).

It has many advantages compared to other synthesis methods, for example it produces a highly homogenous crystalline product at a low reaction temperature. Its most important feature is that it favors a decrease in agglomeration between particles, narrow particle size distributions, phase homogeneity, and controlled particle morphology. It also facilitates to produce relatively uniform composition and pure product. The hydrothermal technique has been considered one of the best ways to prepare TiO_2 particles of desired size and shape with homogeneity in the composition and a high degree of crystalline (Byrappa and Yoshimura, 2001).

Qian et al. (1993) have reported the preparation of TiO_2 nanocrystals by hydrothermal H_2O_2 oxidation starting from metallic Ti. This can be done in two steps: i) oxidation of TiO_2 with an aqueous solution of H_2O_2 and ammonia to form a gel, and ii) hydrothermal treatment of the reactant system under various conditions. Chen et al. (1995) have also prepared TiO_2 nanocyrstals with different morphologies by oxidation hydrothermal combination method. The effects of carboxymethyl cellulose sodium (CMC), HNO_3, Al^{3+}, K^+, and other additives on the particle morphologies and crystalline structures were also discussed. The reaction time, temperature, solvent and minerals are also studied systematically.

Cheng et al. (1995) have studied the process to prepare uniform nanosize rutile and anatase particles under various hydrothermal conditions. The effects of temperature, acidity, minerals, and the concentration of the starting material on the formation, phase, morphology, and grain size of products were investigated and discussed based on the understand on coordination chemistry.

It is also possible to combine the hydrothermal process and sol-gel method (usually named sol-hydrothermal) to prepare TiO_2 nanocrystals, (Wang, et al, 1999; Wu et al., 2002; Sugimoto, et al., 2003) because the titanium alkoxides hydrolyze easily with water while the raw materials have been used in

the synthetic process. It is inevitablly to form the sol before the hydrothermal processing. With the chelating agent of triethanolamine (TEOA), ethylenediamine (EN), or trimethylenediamine (TMD), the uniform TiO_2 nanocrystals with different morphologies such as nanocubes, nanoellipsoidal, and nanorods have been prepared by Sugimoto et al. (2003).

Interestingly, Kim (2003) reported that narrowly dispersed nanorods and nanoparticles of TiO_2 could be prepared by a surfactant-aided synthetic method in toluene solution. With this novel method, the average size of the products is less than 6 nm. In organic media such as ethylene glycol (EG), uniform brookite-type TiO_2 has also been synthesized successfully by Kominami et al. (2000).

More importantly, under hydrothermal conditions, layered titanates such as Na_xH_{2-x} Ti_3O_7, $H_2Ti_3O_7$, $H_2Ti_4O_9.1.2H_2O$, and $H_2Ti_5O_{11}.3H_2O$ have been synthesized in protonic forms and their ion-exchange and intercalation properties have been studied extensively (Sun et al., 2003; Sasaki, et al., 1996; Sasaki et al., 1997; Sasaki et al., 1998). Through the swelling/exfoliation process, these layered titanates could produce single nanosheets and then reassemble into porous aggregates. On the other hand, single crystal nanotubes and nanowires of the layered titanates can be easily obtained.

In summary, solvothermal method is widely used to synthesize TiO_2 based nanostructured materials though the morphologies of the products are still limited to nanoparticles or nanorods with different aspect ratio. However, more elegant superstructures could be expected with this novel synthesis method. Recently, Guo et al. (2003) have fabricated mesoporous core-shell structured titania microspheres with 0.5μm diameter of well-defined hollow interiors which were directly prepared by a novel hydrothermal precipitation of $TiCl_4$ in the presence of urea and ammonium sulfate.

2.4.3 Liquid phase deposition (LPD) method

Liquid-phase deposition (LPD) is an aqueous technique for deposition of metal oxide films. LPD method is based on the processes of which at least two raw materials from at least two supply devices undergoing reaction of a saturation reaction system into a mixture trough. The processes involve stirring the mixture until saturation occurs and filtering out unnecessary solid-state particles. The next step is to provide saturated and filtered liquid into an over-saturated reaction trough of a steady flow over the saturation loop reaction system, then depositing a thin film onto the substrate when the saturated liquid becomes over-saturated.

The distinguishing characteristic of LPD is the use of a solution of titanium-fluoride complexes such as $(NH_4)_2TiF_6$ whose hydrolysis in water is modulated by adding boric acid (H_3BO_3) or aluminum metal. The fluoride ligand provides a slower and more controllable hydrolysis compared to the boric acid or aluminum functions as F- scavenger (Deki et al., 1996; Masude et al., 2002a; Wang et al., 1998; Masuda et al., 2002b). Using chemical equilibrium reactions between the titanium fluoro complex ion and titanium dioxide in the aqueous solution, titanium dioxide thin film could be deposited on the immersed substrates. This process is easy to apply to various kinds of substrates with large surface areas and/or complex morphologies without special equipment. However, other Ti sources such as TiF_4, $TiOSO_4$ and H_2TiO_3 have also been used in LPD process to fabricate rutile or anatase thin films (Imai et al., 2000; Imai et al., 1999; Imai et al., 2003; Shimizu et al., 1999; Yamabi and Imai, 2002a; Yamabi and Imai, 2002b).

2.4.4 Other synthetic methods

A micelle is an aggregate of surfactant molecules dispersed in a liquid colloid. A typical micelle in aqueous solution forms an aggregate with the hydrophilic head regions in contact with surrounding water, squestering the hydrophobic tail regions in the micelle centre. This type of micelle is known as a normal phase micelle (oil-in-water micelle). Inverse micelles have the hydrophilic headgroups at the micelle core and hydrophobic groups with the tails extending away from centre. These inverse micelles are approximately spherical in shape. Other phases, including shapes such as ellipsoids, cylinders, and bilayers are also possible. The shape and size of a micelle is a function of the molecular geometry of its surfactant molecules and solution conditions such as surfactant concentration, temperature, pH, and ionic strength.

At inverse micelle is a water-in-oil droplets stabilized by a surfactant, and the most often used surfactant is sodium 1,4-bis[2-ethylhexyl]sulfosuccinate. These droplets are displaced randomly and subjected to Brownian motion. They exchange their water content and re-form two distinct micelles and the size of the water-in-oil droplets increases linearly. It offers an excellent method for preparing nanoparticles with a very narrow size distribution and highly uniform morphology. For example, by coating a thin layer of gold, the nano-iron particles were protected from oxidation, the resulting nanoparticles were 7 nm in diameter coated with a 1 nm gold shell (Carpenter et al., 2001), further research was reported to prepare α-Fe_2O_3 nanoparticle with uniform size about 10nm by inverse micelle

method (Song et al., 2004). Kim et al. reported successful preparation of nanoionic surfactant coated nanoscale Fe_3O_4 particles with an average size of 2-6nm. (Kim et al., 2001)

Chemical vapor condensation (CVC) process was developed for preparing a variety of materials because a wide range of precursors for this method is commercially available. Choi et al. reported that magnetic nanoparticles of Fe were synthesized by CVC using iron carbonyl as the precursor under a flowing helium atmosphere. They realized the spherical nanoparticles with an average size of 5-13 nm distribution.Choi et al. (2001)

2.5 Applications of TiO_2 and Fe_2O_3 nanomaterials

2.5.1 Applications of TiO_2 nanocrystals

Titanium dioxide has wide applications in the fields of catalysis, solar cell gas sensors, white pigments and corrosion-protective coatings, etc. It also possibly finds applications as a gate insulator for a new generation of metal–oxide–semiconductor field-effect transistors (MOSFETS) and as a spacer material in magnetic spin-valve systems. It is also possibly useful being made into nanostructured foams for Li-based batteries and electrochromic devices. Nanocrystalline TiO_2 has become one of the mostly studied oxides. The technological potential of titania is expected to be remarkably extended if the particle morphology and surface property are completely controllable.

2.5.1.1 Photocatalytic properties

Degradation of volatile organic compounds (VOC) with photochemical processes has become a major area of investigation in environmental protection during the last decade (Legrini et al., 1993). The advanced oxidation process (AOP) is mainly related to heterogeneous photocatalysis using TiO_2. Starting with the photocatalytic splitting of water into hydrogen and oxygen in a photoelectrochemical cell (Fujishima and Honda, 1972), TiO_2, particularly in anatase form, has been very extensively employed in such photo degradations because of its high activity and chemical stability. The mechanism of the process is believed to involve absorption of a UV photon by TiO_2 to produce an electron (e-) – hole (h+) pair. The photogenereated electrons and holes migrate to the nanocrystal surface, where they act as redox sources and react with water to yield hydroxyl and superoxide radicals which oxidize the organic molecules (Linsebigler et al., 1995).

A large variety of organic compounds may be oxidized by TiO_2 photocatalysis in the presence of molecular oxygen. For instance, Kim and Anderson (Kim et al., 1994) used a porous TiO_2 thin-film electrode to degrade formic acid. Al-Ekabi and Serpone (Ai-ekabi et al., 1988) investigated the kinetic properties of heterogeneous photocatalysis degradation of chlorinated phenols in aqueous solutions over TiO_2 supported on a glass matrix. Photocatalytic oxidation has already been used to achieve elimination of odors and to study, in particular, the degradation of organic compounds such as ethanol, butanoic acid, toluene, methylmercaptan, triethylamine (Ai-ekabi et al., 1988). Blake and Griffin (Black et al., 1988) proposed the parallel formation of butane although this hypothesis was invalidated by the work of Pėral and Ollis (1992) who could not detect this compound. The mechanism for the oxidative degradation of 1-butanol (BU) by photocatalysis has not been established so far. Up to now, very few studies have been carried out on amines and none of them suggest a degradation mechanism (Benoit-Marquie, 2000). Generally, a photocatalytic reaction is governed by relative rates of various processes such as oxidation reactions by photogenerated holes at the TiO_2 surface, reducing reactions by photogenerated electrons at the TiO_2 surface, diffusion of the electrons and holes in the TiO_2 catalysts, and various electron-hole recombination processes at the surface or in the bulk of TiO_2 (Linsebigler et al., 1995).

2.5.1.2 Cheaper and highly efficiency solar cells

The large-scale use of photovoltaic devices for electricity generation is prohibitively expensive at present. Photovoltaic cell, created from low to medium-purity materials through low-cost processes, exhibits commercially realistic energy-converging efficiency (O'Regan and Grätzel, 1991; Grätzel 2001: Nazeeruddin et al., 1993). The devices, TiO_2 –based dye-sensitized solar cells (DSCs) or Grätzel cells are usually based on a 10μm-thick, optically transparent film of TiO_2 particles with a diameter of a range nanometers, coated with a monolayer of a charge-transfer dye to sensitize the film for light harvesting. Because of the high surface area of the semiconductor film and the ideal spectral characteristics of the dye, the device harvests a high proportion of the incident solar energy flux and shows exceptionally high efficiencies for the conversion of incident photons to electrical current. The large current densities and exceptional stability, as well as low costs, make practical application feasible. Dye-sensitized cells differ from the conventional semiconductor devices in such a way that they separate the function of light absorption from charge carrier transport. In the n-type materials, such as TiO_2, current is generated when a photon is absorbed by a dye molecule and gives rise to electron injection into the conduction bands of the semiconductor. Light harvesting or efficiency of the

devices is greatly determined by the surface area or roughness of the films and novel charge-transfer dye (O'Regan and Grätzel, 1991).

High-surface-area TiO_2 films are the base of solar cells because they offer highly efficient light harvesting while maintaining a pore size large enough to allow the redox electrolyte to diffuse easily (O'Regan and Gratzel, 1991). The intrinsic properties of thin-film nanocrystalline TiO_2 electrodes can be summarized as follows: (1) visible light transparency, (2) charge separation properties (3) electronic conductivity, (4) high surface affinity towards certain organic groups, and (5) large surface area. (Tachibana et al., 2002) The common "principle of efficiency" in these devices relies on fast electron transfer between the modified of the nanoparticles, and on the large surface area that amplifies optical and interfacial phenomena correspondingly (Campus et al., 1999). Recently, researchers found that the light-harvesting efficiency increases with the addition of relatively large particles to a transparent film, especially for near-infrared wavelengths (O'Regan et al., 1991). However, this lowers the light-harvesting efficiency over the whole visible wavelengths owing to enhanced light reflection at the conducting glass/ TiO_2 interface. Following a rigorous calculation using the results obtained from the light-harvesting efficiency and the short-circuit photocurrent measurements, it is demonstrated that the electron-transfer yield remarkably decrease with increasing optical thickness, that is, film light-scattering magnitude, by a maximum of about 60%. The origins of the change in the electron-transfer yield can be complex, involving multiple excitation or many electron-transfer processes. The analytical results obtained in this study suggest that an appropriate light-scattering magnitude in the TiO_2 film originating from particle size, their distribution, and the film thickness is a key parameter in controlling the electron-transfer yield as well as the light-harvesting efficiency and thus the short-circuit photocurrent (Tachibana et al., 2002).

Another key step for fabricating solar cells is sensitizing TiO_2 films with sensitizers such as cis-X_2 bis (2,2'-bipyridyl-4,4'-dicarboxylate) ruthenium (II) (where X=Cl-, Br-, I-, Cn- and SCN-) (Nazeeruddin et al., 1993), cis-(2,2'-bipyridyl-4-COOH, 4'-$COO^-)_2$ $(SCN)_2$ ruthenium (II) (Tachibana et al., 2002), etc. Recently, fluorescent quenching studies have been carried out to elucidate the processes of electron injection from the excited anhydro-1,1'-diethyl-3,3'-disulfobutyl-5,5'-dicyanimidazolo carbocyanine hydroxide (dye) into the conduction band of TiO_2 semiconductor colloid. The dye absorbed strongly on colloidal TiO_2 with an apparent association constant of $3478M^{-1}$, and its fluorescent emission was quenched by TiO_2 colloid with an efficiency of 92%. Fluorescent lifetime measurements gave the rate

constant for the electron injection process from the excited singlet state for the dye into the conduction band of the semiconductor as 4 x 10^9 S^{-1} (Chen et al., 1997)

2.5.1.3 Multicolor photochromism

Recently, multicolor photochromism of a TiO_2 film has been reported by Naoi et al. (2004) and Ohko et al. (2003). The TiO_2 film showing multicolor photochromism is loaded with Ag nanoparticles by photocatalytic reaction of Ag+ under UV light. More importantly, the Ag-TiO_2 films prepared by Naoi et al. are the first multicolor photochromic materials with apparently uniform structure. This kind of TiO_2 films has wide potential applications including a rewritable color copy paper, a multicolor smart glass, and a high-density multiwavelength optical memory. A color-changeable paint is an additional application, since the film is easy to prepare, low cost, and applicable to a large area. On the other hand, it is of great scientific interest that such simple materials exhibit the multicolor photochromism.

2.5.2 Application of Fe_2O_3 nanocrystals

For thousands of years, iron oxides have been used as coloring agents, as human progressed and technology developed the application of iron oxides as colorants were extended. Hematite can be used as pigment for paints and the construction industry, as catalysts for industrial syntheses, as materials for steel industrial, as magnetic materials for drug delivery research and it can also be used in the environmental area. Nanoparticles of iron oxide have higher rates of reactivity due to their high specific surface area and more reactive surface sites compared to bulk iron oxide materials, therefore, they can be used in: biotechnology research, for catalytic reaction, for environment application and high performance liquid pigment.

2.5.2.1 Application in biotechnology

Hematite nanoparticles seem to display different properties when composed of nano-ultrafine particles rather than larger particles in bio-pharmaceutics. Nanomaterials of hematite have an increased relative surface area compare with the same mass of materials in larger form; it increases materials chemical reactivity for chemical reaction in biotechnology (Georgakilas et al., 2005). Due to the fact that it is a semiconductor material, if a particle is in nano scale, quantum effects dominate the behavior of matter;

it will change its strength and electrical properties, even optical, magnetic properties at designated structure. The superparamagnetic properties of hematite nanoparticles have been of great interest for biomedical application in recent years such as therapeutic agents in cancer treatment e.g. hyperthermia, drug delivery (quantum dots), cell separation and protein immobilization. (Gupta et al., 2005) For example, reverse microemulsion techniques combined with templating strategies have led to the synthesis of homogeneous SiO_2 –coated Fe_2O_3 nanoparticles with controlled SiO_2 shell was reported by Yi et al. (2006). The magnetic nanotubes were assembled on sheep red blood cells in a phosphate buffer solution, forming magnetic cells, the blood cells attached with or without magnetic nanotubes can be selectively manipulated in a magnetic field (Gao et al., 2006). Hollow silica microspheres encapsulating ferromagnetic iron oxide nanoparticles were fabricated by a surfactant-aided aerosol process and subsequent treatment; it can serve as functional sites to graft biomolecules, such as protein and drugs on magnetic particles; it makes such silica coated nanoparticles a promising candidate for applications in bioseparations and targeted drug delivery under magnetic gradients.(Zheng et al., 2007)

2.5.2.2 Catalytic Reactions

The principal iron oxide nanoparticles used in catalysis of industrial reactions are magnetite and hematite. Both are semiconductors and can catalyze oxidation/reduction reactions. Owing to their amphoteric properties, they can also be used as acid/base catalysts.

The most intensively studied syntheses involving iron oxides as catalyst are the Haber process for the production of NH_3 from hydrogen and nitrogen and the Fischer-Tropsch synthesis of hydrocarbons (Campbell et al., 1970). Nanocrystals have a high ratio of surface area to volume; it can be used in coal liquidification (Huffman et al., 1993) and as an ultraviolet energy absorber. Ferrihydrite which is precipitated from aqueous Fe^{III} salt solutions has also been investigated for its suitability as a catalyst, and it has an average particle size of 3 nm and a surface area of around 200 m^2/g (Zhao et al.,1993). However, the nanosized catalyst powder quickly agglomerates, losing most of its active surface. In order to avoid this problem, crystallization inhibitors such as Si, Al (Zhao et al., 1994a) and Mo (Zhao et al., 1994b) and citric acid (Zhao et al., 1994d) can be added. Al_2O_3 as a structural promoter is distributed over the surface of the Fe nanoparticles can stabilize them against sintering and thus a reduction of the surface area during the operation of the catalyst can be minimized.(Kowsowski et al., 1993) K_2O acts as an electronic promoter and facilitates the chemisorptions of N_2 for NH_2 process (Topham, 1985).

2.5.2.3 Environmental Significance

Iron oxides have been recognized as being solid phase which has a significant effect on the behavior of a large range of environmentally relevant substances particularly heavy metals and other toxic elements and organic xenobiotics. Iron oxide can deactivate pollutants by surface absorption or by incorporation. These deactivation processes in the ecosystem are also used extensively in environmental technologies such as water purification and remediation of contaminated environment. For example, nanoscale iron oxide particles can be applied to reduce polyhalogenated methane and carbon tetrachloride (CT) with high efficiency (Li et al., 2006). McCormick et al. investigated carbon tetrachloride transformation on the surface of nanoscale biogenic magnetite particles. They indicated that within 120 h, over 93% of CT was reduced, with a significant fraction (-38%) reduced fully to carbon monoxide. Furthermore, an additional 9% of the CT was dechlorinated to CH_4 (McCormick et al., 2004). Another report indicated a similar result: at pH 7, about 20% of total CT was reduced to –C=O, and 40% to HCOO- (Elsner et al., 2004).Therefore, the large fraction of relatively benign products of carbon tetrachloride suggested that nanoscale iron oxide particle may have beneficial applications in the remediation of CT-contaminated groundwater or soil.

2.5.2.4 Liquid pigments

As pigments, iron oxides have a number of desirable attributes. They display a range of colors with pure hues and high tinting strength, and they are extremely stable, i.e. non-bleeding, non-fading and highly resistant to acids and alkalis, and can be exposed to outdoor conditions (Schnaitmann et al., 1998). Nanoscale iron oxide crystals are produced in a variety of shapes, such as spherical acicular, rhombohedra and cubic ones. By modifying the shapes and size of the particles, a variety of shades may be produced. Liquid pigments of nanoparticles are transparent, which has special characteristics such as being transparent reds and yellows. Transparent yellows consist of acicular nanocrystals of goethite; they can be transformed into the transparent reds of the same size and shape (50-100 nm) by calcinations at 400-500 °C. Blending of the reds and yellows gives a variety of transparent shades with different of refractive index and low binder. These liquid pigments with nanosized particles have more surface area and higher colorful optical effect compare with current commercial pigment; Nanosized liquid pigment can make a half tone tint which are widely used for valuemark documents for which microsized pigment cannot fulfill the special effect. It can provide a protection against detrimental

effects of exposure to sunlight or even fluorescent light. Owing to their high UV absorption, transparent iron oxides are also used to color plastic films and UV sensitive product (Cornell, 2002)

2.6 Summary

As a summary for this chapter, the progress in the nanotechnology associated with the iron oxides and titanium oxide were reviewed; the technique of self-assembling was described; crystal structure and surface properties of titanium oxide and iron oxide were described; The popular synthetic routes of nanoparticles such as sol-gel and hydrothermal were critically reviewd; The major applications of titanium dioxide and iron oxide nanocrystals were briefly highlighte. Both of them are fascinating materials for potential applications as semiconductors from an academic point of view. So much is known now about its structures, preparation, and properties; yet, so much is still to be learned. There are still many new synthetic approaches for example: physical synthesis, high temperature, new precursors, additives, surfactants and various growth media to surprise us with unexpected results. How to reduce the cost of raw materials to get the uniform particles is still interested to many researchers.

Chapter 3
Research Approaches and Experimental Methods

3.1 Research Approaches of Anatase and hematite nanoparticles

3.1.1 Research approach of Anatase TiO_2 nanoparticles

The principle of the chosen self-assembling reaction is based on the hydrolyzation of titanium isopropoxide to make TiO_2 and isopropanol; Hexadecylamine is used to maintain the pH of solution within 8-9 in order to speed up the hydrolyzation. The surfactant is polyoxyethylene sorbitan trioleate (Tween 85). It has a formula shown in Figure 3.1. (Acros Organics, 2006)

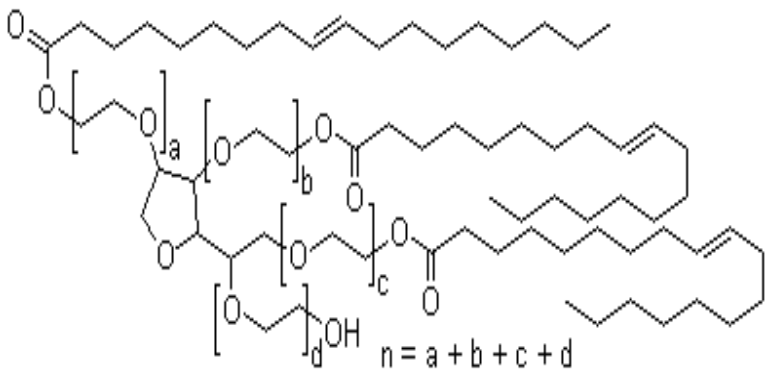

Figure 3.1: Molecular formula of Tween 85 (Acros Organics, 2006)

In this basic solution, anionic form of an alkylated oleic acid can be generated from Tween 85 while the Tween 85 serves as a micelle formation agent for controlling the size of nanocrystal titanium oxide. It was also discovered that the TiO_2 was formed from related layered hydroxide precursors, $[Ti_x^{IV} Ti_{I-x}^{V} (OH)_2 (A)_x nH_2O]$, where A was the anionic form of alkylated oleic acid. $Ti_x^{IV} Ti_{I-x}^{V} (OH)_2$ inside the micelle nanoreactors at 130 -140°C due to the surface capping formed on the TiO_2. (Yang et al., 2003)

3.1.2 Research approach of α-Fe_2O_3 nanocrystal

To achieve synthetic control, the nanostructures would be expected to show certain aesthetic expression apart from their basic functionality by controlling crystal growth directions, for instance, a resultant nanocrystalite may display crystal isotropy or anisotropy based on its underlying structural properties.

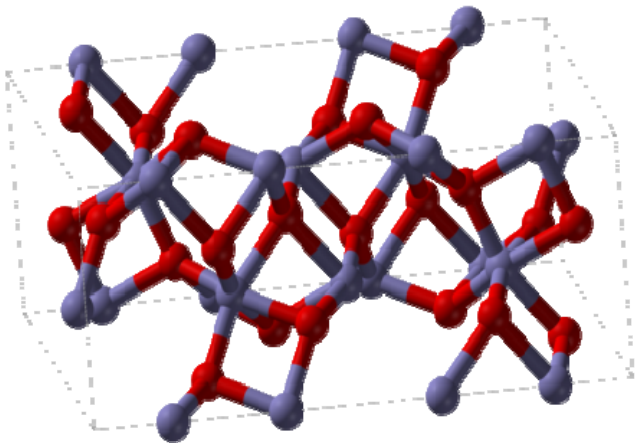

Figure 3.2: Hematite crystal 3D structure unit cell diagram (Cornell, 2002)

As shown in Figure 3.2, Fe_2O_3 nanoparticles are monodispersed with high crystalline, and the fast growing crystal ends are bounded with crystallographic facets (1011), (0111), (-1011), (-0111), (1101), (-1101) and (0001). (Zhao, et al., 2007) The array's habit of self-assembling depended on coupling forces in materials which was caused by the magnetic moments of neighboring atoms aligned. If the thermal energy of an individual atom is sufficient to overcome the coupling forces, the atomic moments would fluctuate in the one direction.

In our study, the raw materials, iron chloride and sodium hydroxide, a certain amount of the carbon nanotubes and excess surfactant of Tween 85 were added to make Fe_2O_3 nanorods. The sodium hydroxide concentration and the reaction temperature were important to make the Tween 85 micelles. A micelle looks like a "nanoreactor". Iron oxide molecules were connected in certain directions to form 2D nanorods within the "nanoreactor".The reaction time is also very important in controlling the particle size.

3.2 Materials characterization analysis

3.2.1 Powder X-ray diffraction (XRD)

The crystallographic information of all samples was investigated by powder X-ray diffraction (XRD, Brock D8 Advance, Cu, Kα radiation, λ =1.5406 Å, 40 kV, 40 mA). The samples were prepared in the form of fine homogeneous powder. A thin smooth layer of the samples mounted on a non-crystalline substrate such as fused silica was held in the path of X-rays. Calibration was carried out before each measurement. The diffracted X-rays correspond to all sets of planes in the crystal powder which could be orientated in every possible direction relative to the X-ray beam. The XRD patterns with diffraction intensity versus 2θ were recorded, usually from 10° to 80° at a scanning speed of 2° per min. The well–known Bragg's equation can be used to determine the interlayer space of the crystals $d= \lambda/ (2\sin \theta)$, where θ is the diffraction angle. The average crystallite sizes, D_{hkl}, can be calculated by the Debye-Scherrer formula with the full width at half maximum (FWHM) of the peaks $D_{hkl}=0.9 \lambda/ (\text{FWHM x} \cos \theta)$.

3.2.2 Transmission electron microscopy (TEM)

In TEM analysis, a highly focused and monoenergetic electron beam is used to bombard the sample specimen. The transmitted electrons form images on a fluorescent screen which provide morphological features and atomic arrangements of the samples. For high resolution transmission electron microscopy (HRTEM), interferences among beams scattered by the crystal in different directions form a "lattice image". Picometer-scale image provided by HRTEM is essential for nanomaterials science (Wang, et al., 2003b; Bulle-Lieuwma, et al., 1991; Wang, et al., 2000). During the specimen preparation, usually TiO_2 and Fe_2O_3 nanostructure materials were dispersed into deionized water or other solvent and a few drops of such solution mixture were spread on a cooper grid coated with carbon films for analysis in a Philips CM10 FEG electron microscope (80kV) , JEOL 3010 (300kV) and LEO 912AB (120kV) respectively.

3.2.3 Scanning electron microscopy (SEM)

Scanning electron microscopy (SEM) was also widely used in our work. As the electron beam hits each spot on the sample, secondary electrons are knocked loose from its surface. A detector counts these electrons and sends the signal to an amplifier. The final image is built up from the number of electrons emitted from each spot on the sample. In order to improve the conductivity of the samples, all our SEM samples were coated with a very thin layer of platinum by a sputter coater. Besides giving the images of the samples, SEM equipment can conduct Energy Dispersive X-Ray Spectroscopy (EDX) analysis which can also provide the information of the elemental composition of materials imaged by SEM. As the electron beam of the SEM is scanned across the sample surface, it generates X-ray fluorescence from the atoms in its path. The energy of each X-ray photon is the characteristic of the element which produced it. The EDX microanalysis system collects the X-rays, sorts and plots them by energy, and automatically identifies and labels the elements responsible for the peaks in this energy distribution. In order to produce clearer, less electro-statically distorted images, Field Emission Scanning Electron Microscopy (FESEM) was used in this work as well. For FESEM, a field-emission cathode in the electron gun of a scanning electron microscope provides narrower probing beams at low as well as high electron energy resulting in both improved spatial resolution and minimized sample charging and damage. FESEM and EDX of the samples were taken on a LEO 1530 Scanning electron microscopy operated at 5kV-15kV for this thesis.

3.2.4 Nanoparticle size analysis (NANOTRAC 150)

For this research work we used the Nanotrac 150 instrument to analyze nanoparticle size. The nanotrac 150 features an internal probe embedded in a stainless steel sample cuvette. The standard cuvette has a sample volume of 3 ml but is also available in a 0.2 ml version, and the measurement range is 0.8-6500 nanometer and the scan angle is 180°. The laser source is Laser Diode with 780 nm wavelength, 3 mW nominal, Class IIIB. The laser generator and detector were fixed in place and no alignments were required. The concentration limit range can be high up to 40% by solids in some cases and low down to 0.1 ppm for 200 nm polystyrene. Repeatability is 0.1% of 100nm polystyrene. The Microtrac FLEX operating software package is used for data analysis. (Microtrac Inc, 2007)

3.2.5 Fourier Transform Infrared spectroscopy (FTIR)

FTIR is a powerful tool for identifying types of chemical bonds in a molecule by producing an infrared absorption spectrum that is like a molecular "fingerprint". It can be applied to the analysis of solids, liquids and gases. The wavelength of light absorbed is a characteristic of the chemical bond as can be seen in the annotated spectrum which can be identified by comparison to a library of known compounds. FTIR can be used for some quantitative analyses. Solid samples for FTIR in our research were milled with potassium bromide (KBr) to form a very fine powder. This powder was then compressed into a thin pellet for analysis. In this thesis, all samples were recorded on Fourier transform infrared spectroscopy LEO 410 Bio-FT-IR instrument and handled at room temperature in air.

3.2.6 UV Spectrophotometer

UV/Vis spectrophotometer is ultraviolet-visible spectroscopy instrument. It is routinely used in the quantitative determination of solutions of transition metal ions and highly conjugated organic compounds. It measures the intensity of light passing through a sample (I), and compares it to the intensity of light before it passes through the sample (I_0). The ratio I/I_0 is called the transmittance, and is usually expressed as a percentage ($\%T$). The absorbance A, is based on the transmittance:

$$A = - \log (\%T)$$

The basic parts of a spectrophotometer are a light source where an incandescent bulb for visible wavelengths and a deuterium arc lamp in the ultraviolet. The spectrometer includes a holder for the sample, a monochromator to separate the different wavelengths of light and a detector. The detector is typically a photodiode used with monochromators, which filter the visible light so that only light of a single wavelength reaches the detector. In this thesis, a UV-visible Spectrophotometer Cary 300 instrument was used, and the scanning rate was 600 nm /min with a wavelength reange of 200 -900 nm. Spectra were acquired in transmission mode through the quartz tube at a 300kV accelerating voltage.

3.2.7 Magnetic property analysis (SQUID)

Superconducting Quantum Interference Device (SQUID) is very sensitive magnetometers. It is used to measure extremely small magnetic fields, based on superconducting loops containing Josephson

junctions. They have noise levels as low as 3 $fT \cdot Hz^{-1/2}$. Model 5000 DC SQUID controller made by Quantum Design was used for this research. SP5000 - High performance DC SQUID controller for up to eight channels, remote computer and GPIB port, simultaneous overall display of one to eight channels on the front panel LCD show that independent values for range, gain, bandwidth, status, and filter states and16-bit A/D converter is capable of multiplexing all eight channels of SQUID output. Magnetic hysteresis measurement at different temperature 300K was performed.

3.2.8 Surface area analysis (BET)

In this work, the Brunauer-Emmett-Teller (BET) method was used to measure the total surface area of the Fe_2O_3 based nanostructures and TiO_2-based nanostructures (Brunauer, et al., 1938; Brunauer, et al., 1940). The adsorption data were obtained from this testing. Full adsorption and desorption isotherm of nitrogen on our samples were determined at various pressures and the pore volume and pore-size distribution were calculated with the Barret-Joyner-Halenda (BJH) method (1951). In this thesis, the surface area was measured by Quantachrome NOVA-3000 and all smaples were degassed at 110°C for 3hrs by nitrogen at the atmosphere.

3.2.9 Electrochemical Voltammetry

The PGSTAT 30 is a high current potentiostate/galvanostat, with a compliance voltage of 30V and a bandwidth of over 1MHz. It is specially designed for electrochemical impedance spectroscopy. The maximum current is 2A; the current range can be extended to 20A. AutoLab PGSTAT30, the Potentiostat Galvanostat /voltammetric analysis instrument include Agilent 54624A Oscilloscope meter, a dummy cell and a differential electrometer amplifier from Eco chemie B.V. AutoLab PGSTAT 30 is used for analysis potential /current, for the performance of electron transfer, and for simulation of electrochemistry reaction etc. AutoLab and software provide a lot of methods and modulars, and include a staircase method, which is able to record these fast phenomena. In this method the analog current integrator is used. The integrator is reset at the beginning of each step. Subsequently, the integrated current or charge is sampled at the end of each step. In this thesis, PGSTA 30 instrument with linear sweep voltammetry was used for measuring electron transfer of titanium oxide working electrode.

Chapter 4
Self-assembly of iron oxide nanorods: experimental synthesis and instrumental characterization

4.1 Introduction

Iron oxide nanoparticles have been of great interest, not only because of their special fundamental properties, but also due to their multivalent oxidation states, abundant polymorphism and mutual polymorphous changes in crystal phase such as hematite (α-Fe_2O_3) and maghemite (γ-Fe_2O_3).

Hematite (α-Fe_2O_3), the thermodynamically stable crystallographic phase of iron oxide with a band gap of 2.2ev, is a very attractive material because of its wide applications in various fields, for instance, high density magnetic recording media, gas sensors, catalysts, pigment and clinical uses. Its nontoxicity, low cost, and relatively good stability are definitely very attractive features for these applications. (Willis et al., 2005; Li et al., 2007; Li and Zeng et al., 2005; Chang et al., 2005) There has been much interest in the development of novel synthetic methods to produce one-dimensional α-Fe_2O_3 nanostructures, such as vapor-solid growth techniques, (Yi et al., 2006; Fu et al., 2003; Chen et al., 2005) templated synthesis method, hydrothermal process and sol-gel process. (Wang et al., 2004; Mazeina et al., 2007) Among these processes, the sol-gel process can offer an advantage fabricating metal oxide nanoparticle with a wide range of compositions in improved homogeneity and high purity at relatively low temperature over the other fabrication techniques. (Sun et al., 2002)

In the recent few years, many studies on synthesis of iron oxide nanoparticles have focused on controlling the shape and size of nanoparticle via various synthesis methods. In particular, synthetic hematite iron oxide nanoparticles are expected to exhibit interesting magnetic properties because of shape anisotropy, for example, rodlike morphology hematite iron oxide exhibited variable magnetic properties at different temperatures. (Fu et al., 2002)

Some studies on synthesis of magnetic Fe_2O_3 nanoparticles have been reported in recent decade, and most of them focused on the synthesis of γ- Fe_2O_3, Fe_3O_4 nanoparticles and α- Fe_2O_3 nanospheres (Park et al., 2000; Gao et al., 2006; Tang, et al., 2006; Zhong et al., 2006). Only a few anisotropic magnetic nanorods have been investigated. Park et al. (2000) reported that they synthesized iron oxide nanospheres via thermal decomposition of organometallic precursor Fe $(CO)_5$ in the presence of

trioctylphosphine oxide (TOPO) surfactant at 340 °C under argon atmosphere and then the resulting solution was aged for 30 min at 320 °C. After the spherical nanoparticles of 2 nm were prepared, the produced nanospheres dissolved in 19 ml of pyridine containing 0.5g of didodecyldimethylammonium bromide for 12 h to make 2 nm (width) x 11 nm (length) nanorods. The magnetic properties of nanorods would be very interesting because they would demonstrate the effect of shape anisotropy (Park et al., 2000, Liu and Wang et al., 2004). Burleson et al. (2006) has addressed goethite growth by the phase transformation of six-line ferrihydrite nanoparticles to goethite nanoparticles followed by oriented aggregation to produce goethite nanorods. Data tracking goethite nanorods growth as a function of pH, temperature and time have been presented in his report. The final results showed that growth is faster at higher pH and higher temperature. Tang et al. (2006) synthesized α- FeOOH nanorods with diameters of 15-25nm and lengths up to 170-300nm in high yield via a facile and template-free hydrothermal method at low temperature. After calcining the as-synthesized α- FeOOH at 250°C for 2h, the α-Fe_2O_3 nanorods were obtained. It exhibited weakly ferromagnetic characteristics at low temperature and superparamagnetic property at room temperature. Zhong et al. (2006) developed a versatile method using alkylamines (octylamine and isobutylamine) as structure-directing agents for synthesis of various 1D transition metal oxides in aqueous solution. They prepared 1D pre-Fe_2O_3 powder by a hydrothermal processing, after calcinations at 300°C, the 1D pre- Fe_2O_3 was converted to single-crystalline α-Fe_2O_3 nanorods. If further reduction is applied, the nanorods can be converted to 1D Fe_3O_4. Two months ago, Zhong et al. (2007) just reported synthesis of porous α-Fe_2O_3 nanorods by a mild hydrothermal processing using tetraethylammonium hydroxide (TEAOH) as the structure director. The porous α-Fe_2O_3 nanorods have a pore size distribution in the range of 1-5nm, which is ideal to house very small gold particles. Final Au/ α-Fe_2O_3-nanorod catalyst exhibited higher catalytic activity than the normal Au/hematite catalyst for CO oxidation. However, so far there has not yet been a report on synthesizing uniform α-Fe_2O_3-nanorods using low cost materials via a sol-gel process with carbon nanotubes as the structure director.

In this chapter, a novel self-assembling method for synthesizing iron-oxide nanorods and nanodots has been investigated via the sol-gel technique with carbon nanotubes as the structure director and Tween 85 as the surfactant. Fe2O3 nanorods have been achieved using some low cost materials as the starting materials via an one-step process. The characteristic results showed that uniform nanorods were obtained. The mechanism of the self-assembling along a certain direction when carbon nanotubes were

used as the structure director in the growth of the hematite iron oxide nanorods from nanodots was discussed. Furthermore, some of future directions in nanomagnetism are also described.

4.2 Experiment Details

4.2.1 Materials

Tween 85 ($C_{100}H_{188}O_{28}$, polyoxyethylene (20) sorbitan trioleate; Polysorbate 85) and iron chloride (III), reagent grade 97% were purchased from Sigma-Aldrich (Oakville, Ontario, Canada). Sodium hydroxide (99%) powder was purchased from Fischer Chemical (Ottawa, Ontario, Canada). Multiwall carbon nanotubes-1030 (L-MWNT-1030, about 30nm width, long tube) powder was purchased from Shenzhen Nanotechnology Co. Ltd. (Shenzhen, Guangdong, China).

4.2.2 Apparatus:

A 250 ml three-neck-flask with a round bottom was used as the reactor, equipped with a condenser. An IEC CL 31 Multispeed centrifuge of Thermoelectron Corporation (Toronto, Ontario, Canada) was used for separating product of hematite iron oxide precipitation. A VWR Model 50HT Ultrasound Cleaner (Toronto, Ontario, Canada) was used for dissolution and precipitation operation during sample washing stage.

4.2.3 Preparation of reagents

10 g of sodium hydroxide was dissolved in deionized water to make 250 ml of 1 M sodium hydroxide solution, which was later diluted to 0.1 - 0.5 M, depending on the individual experimental requirements. 20.276g of $FeCl_3$ powder was dissolved in deionized water to prepare 250 ml of 0.5 M iron chloride solution, which was later diluted into 0.1-0.5 M, depending on individual experimental requirements. For each experiment, 30-50 ml of 0.1 - 0.5 M iron chloride solution, 12 ml of Tween 85, and 0-10 mg of carbon nanotubes (LMWNT-1030) were used.

4.2.4 Synthesis of nanoparticles of iron oxide

A sol-gel method was used to synthesize α-type iron oxide materials. The reaction time was controlled between 70 hrs -100 hrs and the reaction temperature was 90-100°C.The procedure for synthesizing paramagnetic iron oxide are as follows.

First, 10 mg of carbon nanotube powder was added into the 250ml of three-neck flask and then 30 ml of 0.5 M sodium hydroxide solution was added. Afterwards, the three-neck flask was placed in a silicon oil bath. When the temperature of the content in the flask reached 60 °C, 12 ml of Tween 85 was then added into the flask drop by drop with stirring of 500rpm for 15 min. Because the viscosity of the solution was high and the stirrer bar almost could not move when the temperature was below 60 °C, the operation temperature was set above 60 °C. After another 15 minutes of stirring, 30 ml of 0.5 M $FeCl_3$ solution was added into the flask drop by drop with continuous stirring at 60 °C. The viscosity of the solution decreased gradually as iron chloride solution was added, and the color changed from light yellow to deep yellow, and finally it became a turbid yellow solution; in the mean time, the system was heated for about 25 min so that the temperature of the system increased from 60°C to 100 °C. The stirring speed was maintained between 500 -600 rpm for the whole process. After the temperature of the solution reached 90°C-100°C, the reaction conditions were maintained for 70 - 100 hours. The heating was stopped but the stirring was still maintained at 500 rpm for another 12 hours to allow the temperature of the oil bath to cool down to the room temperature. For this series research, 30 individual experiments were conducted in the range of temperature and reaction time to find the suitable conditions to make hematite nanorods.

4.2.5 Separation of the products

250 ml of ethanol was used to wash the above synthesized products and a centrifuge operated at 6000 rpm was employed for 8-10 min to separate precipitation (yellowish black) from the solution. The resultant mixture had three layers. The top layer (denoted as L1) was an oily liquid with brown color, which was homogenous iron oxide with light oily liquid and Tween 85. The middle layer (denoted as L2) was a mixture of ethanol, water and Tween 85, and the bottom layer (denoted as L3) was a black precipitation, which was iron oxide nanoparticle sediment. These three layers were separated by centrifugation for further purification.

The sediment (L3) was washed at least 3 - 4 times using 99% ethanol and an ultrasound cleaner was applied for 15 min each time before it was put into the centrifuge so that the extra surfactant could be removed; the precipitate of iron oxide nanoparticles was then dried in a steam oven for at least 24 hours at 50 °C. Finally the sediment product was ground by a quartz grinder manually to powder for further characterization.

Using ethanol to dilute the L1 solution, a solution with a clear brown color was obtained. This so-called "Upsoln", a liquid mixture consisted of ethanol, iron oxide nanoparticles of about 1 nm, oily liquid and Tween 85, is very difficult to be further separated for characterization. To realize the separation, 20 ml of water was added into 50 ml of the "Upsoln" in a conical flask. The "Upsoln" then became a two-layer system, and the upper layer (denoted as L11) solution was about 4-5 ml with a deep yellow color, which was believed to be an iron oxide with oily liquid and the down layer (denoted as L12) was an emulsion of water and Tween 85 whose appearance was similar to yellowish milk. Most of iron oxide particles were capped by hydrophobic organic material and preferred to stay in the ethanol layer rather than water layer.

4.3 Characterization

Characterization of the synthesized iron oxide nanoparticles was conducted by a series of instrument to verify the nanorods. The crystal structure of hematite was analysed by XRD. The morphology of nanoparticles was investigated by HRTEM and TEM. The morphology on the surface of the nanoparticls was determined by FESEM. The chemical compositions of nanoparticles were analyzed by FTIR and EDX.

The nanoparticles size was measured by NanoTrac 150. The process of nanoparticles testing is as below. Using ethanol to wash products 2 times to get the brownish solutions L11 and L3, ultrasonic stirring solutions for 3 mins, then using dropper to collect 5 drops to 3 ml of ethanol solution for nanoparticle size testing. Characterization of the flurensence properties was carried on the UV-Visible Spectrophotometer Cary 300. Analysis of the magnetical properties was conducted by SQUID. Absorption properties were measured by BET.

4.4 Results and discussion

Iron oxide nanorods in our study were obtained. The results about the strucutures, morphology and the compositions of the nanoparticles were discussed in the section 4.4.1 through section 4.4.7.

4.4.1 Crystal hematite nanostructures

As shown in Figure 4.1, the Fe_2O_3 nanorods synthesized in our study are monodispersed and have high crystallinity with the diameter of 50 nm. In particular, the fast growing crystal ends were bounded with crystallographic facets (1011), (0111), (-1011), (-0111), (1101), (-1101) and (0001). (Zhao et al. 2007;

Cornell, 2002) It was found that individual one-dimensional Fe_2O_3 nanorods could also attach to one another to form a two dimensional array of nanorods, as shown in Figure 4.2 via their smoother prismatic side planes (10-10), (01-10), (-1010), (0-111), (1-100), and (-1100). Potentially the oriented attaching phenomenon observed here may offer new means for general freestanding single crystal sheets of inorganic materials.

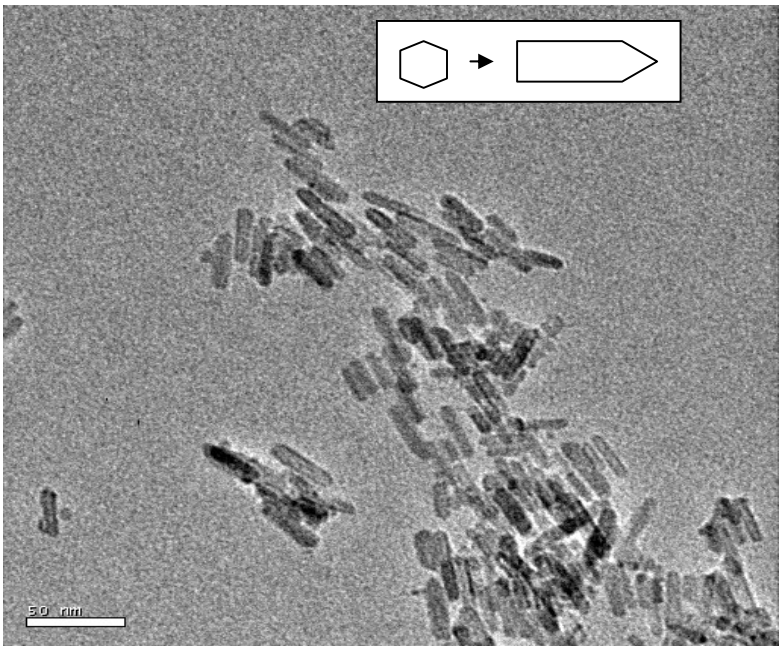

Figure 4.1: TEM images of Fe_2O_3 nanorods synthesized at 90ºC

25 ml of 0.5M FeCl3, 40 ml of 0.3M NaOH, 12 ml of Tween 85, 10 mg of carbon nanotube, reaction temperature : 90°C, reaction time: 72.5 hrs , scale shown on the image :50 nm.

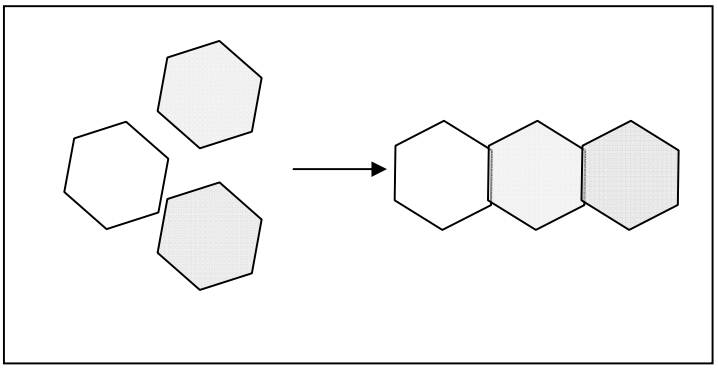

Figure 4.2: Symmetric unit cell to one dimension nanorod of α-Fe_2O_3

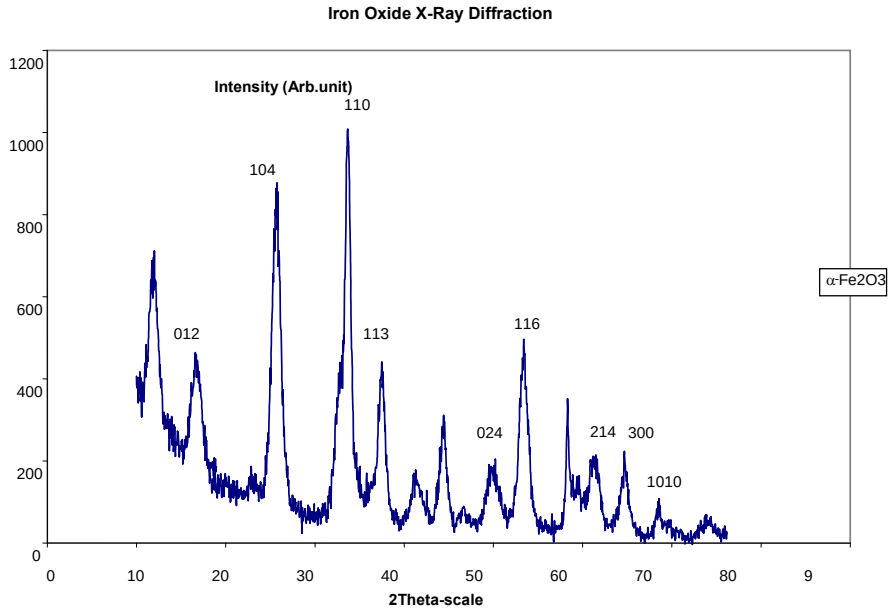

Figure 4.3: XRD spectrum of hematite iron oxide nanorods

XRD image of the powder of L3; reaction conditions: 5 ml of 0.5M $FeCl_3$, 40 ml of 0.3M NaOH, 12 ml of Tween 85 , reaction temperature :90º C, reaction time: 71.5 hrs.

The hematite nanocrystal structure verification was conducted by XRD. Figure 4.3 shows the XRD patterns of iron oxide nanorods from L3 layer. Obviously, this XRD pattern confirmed that the crystal structure of the product is the hematite α-Fe_2O_3 because the same pattern as the standard hematite XRD is obtained; especially the characteristic sharp peaks of hematite structure at 104, 110 and 116.

4.4.2 Crystal nanorods growth and morphology

The mechanism of the crystal growth and the morphology of the crystals depend on the solution conditions, particularly referring to the supersaturation on the crystal growing surface. Many functional inorganic materials are prepared according to their intrinsic structural anisotropies. The controlling of the structure, shape, and chirality of individual inorganic nanostructures is prevailingly achieved via organic capping assisted methods, which use various organic surfactants (Kwon et al., 2006), liquid

crystals, ligands, and chiral supramolecular assemblies (Choi et al., 2006) to guide the growth directions.

Reactions 1 and 2 below are the main chemical reactions involved in the formation of hematite:

$$FeCl_3 + 3NaOH = Fe(OH)_3 + 3Na^+ + 3Cl^+ \quad (1)$$

$$2Fe(OH)_3 = Fe_2O_3 + 3H_2O \quad (2)$$

The compounds of the Tween 85 belong to nonionic type surfactants and they are commonly used as an emulsifier to stabilize both water-in-oil and oil-in-water emulsion. The concentration of Tween-85 in our starting reaction mixture is much higher than its critical micelle concentration. During the synthesis, therefore, various types of micelles are expected to form. Our synthesized products indeed show that these micellar "nanoreactors" are working in controlling the particle size of Fe_2O_3. In all the cases, the resultant Fe_2O_3 nanorods were stably dispersed, and no precipitates were observed in the resultant emulsions, which can be ascribed to a tiered surfactant structure formed (i.e., a bilayer shell), where the hydrophilic headgroups of Tween-85 are pointing toward the aqueous phase.

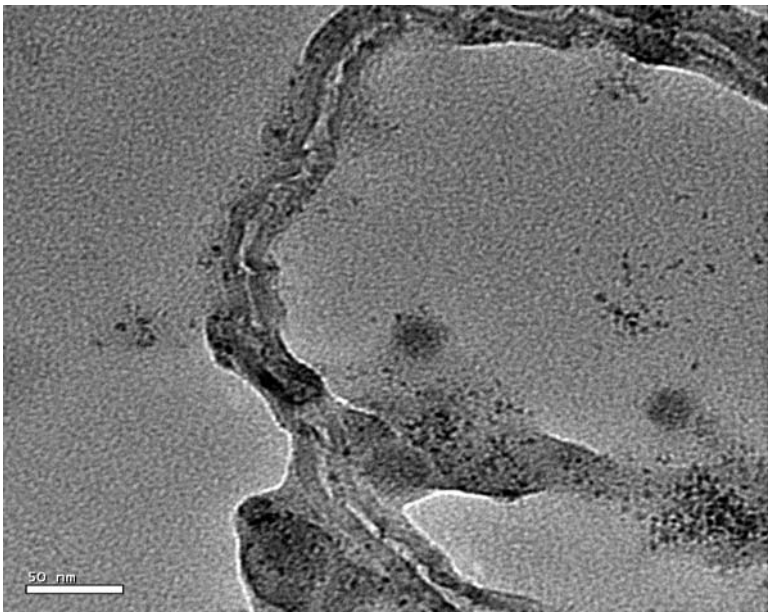

Figure 4.4: TEM image 1 of iron oxide nanoparticles

25 ml of 0.5M FeCl3, 40 ml of 0.3M NaOH, 12 ml of Tween 85, 10 mg of carbon nanotube, reactant solution temperature : 90°C ; reaction time: 20 hrs ; scale shown on the image : 50 nm. (Original sample without washing and directly diluted by ethanol, sample from mixture of L1, L2 and L3).

Figures 4.4 - 4.9 are the TEM imagesof the Fe_2O_3 generated when the reaction time was 20 hrs, 40 hrs, 50 hrs, 60 hrs , 71.5 hrs and 72.5 hrs respectively. In Figure 4.4 carbon nano tube can be observed clearly in the mixture and iron oxide nanodots were formed close to the carbon tubes. No nanorod of iron oxide was observed in this stage. From Figure 4.5 we can see small crystal nanodots arrayed to lines along the walls of carbon nanotubes which acted as a structure director.

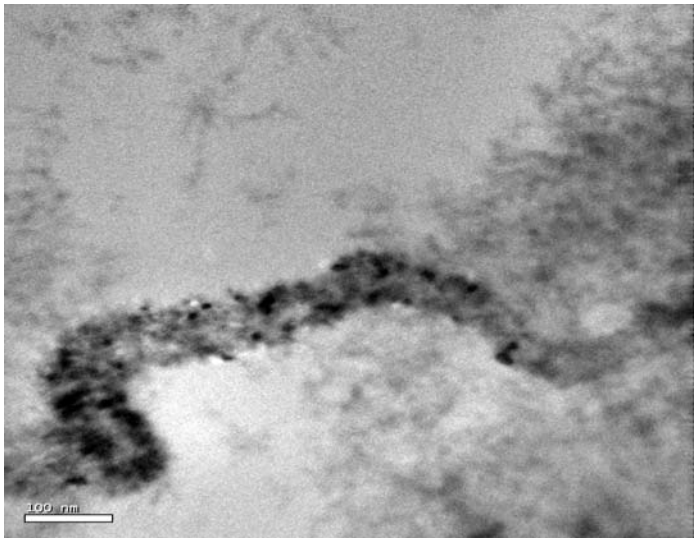

Figure 4.5: TEM image 2 of iron oxide nanoparticles

25 ml of 0.5M $FeCl_3$, 40 ml of 0.3M NaOH, 12 ml of Tween 85, 10 mg of carbon nanotube, reaction temperature: 90 °C; reaction time: 40 hrs; scale shown on the image :50 nm. (Original sample without washing and directly diluted by ethanol, sample from mixture of L1, L2 and L3)

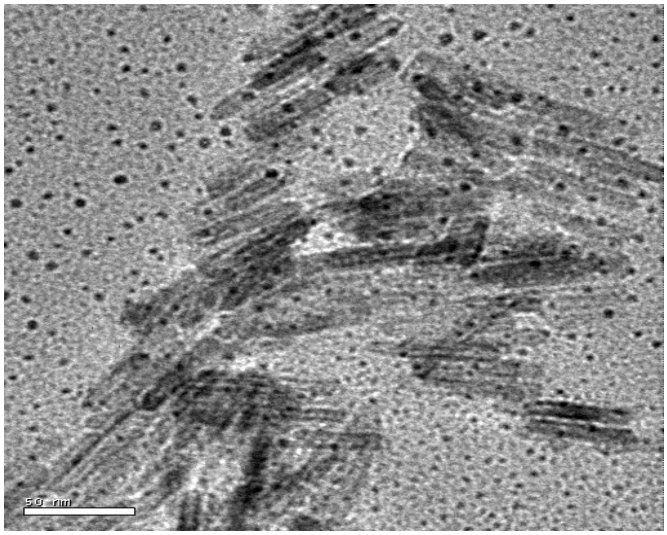

Figure 4.6: TEM image 3 of iron oxide nanodots and nanorods

25 ml of 0.5M $FeCl_3$, 40 ml of 0.3M NaOH, 12 ml of Tween 85, 10 mg of carbon nanotube, reaction temperature: 90 °C; reaction time: 50hrs; scale shown on the image: 50 nm. (Original sample without washing and directly diluted by ethanol, sample from mixture of L1, L2 and L3, scale bar in this Figure is 50nm)

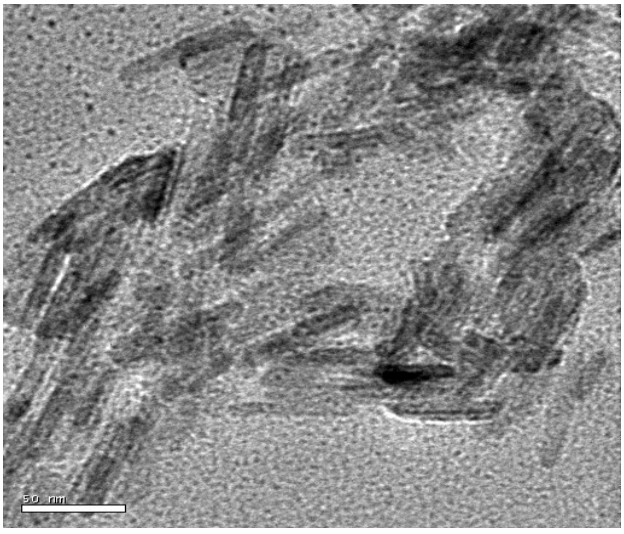

Figure 4.7: TEM image 4 of iron oxide nanorods

25 ml of 0.5 M $FeCl_3$, 40 ml of 0.3M NaOH, 12 ml of Tween 85, 10 mg of carbon nanotube, reaction temperature: 90°C; reaction time: 60hrs; scale shown on the image: 50 nm. (Original sample without washing and directly diluted by ethanol, sample from mixture of L1, L2 and L3)

The TEM image of Figure 4.5 showed that at 40 hrs, the extemal surface of the carbon tubes was attached with iron oxide dots; the channel of carbon tubes was filled by iron oxide particles although the long shape of carbon tube could still be observed. The carbon tubes changed into carbon dots. The iron oxide nano particles were generated after about 50 hours at 90 °C. Figure 4.6 shows that carbon nanotubes in the reaction system were broken, and then disappeared. A small amount of nanodots and some nanorods were formed. Carbon nanotubes in the initial stage could produce a traction force that induced the iron oxide molecules to be arranged in one sequence. After nanoparticles were formed, the carbon nanotubes would join the reaction as a reducer, and finally, the carbon nanotubes disappeared as shown in Figure 4.6 after 50hrs. In Figure 4.7 nanodots were observed less than that showed in Figure 4.6, and nanorods were formed more and more with the reaction time.

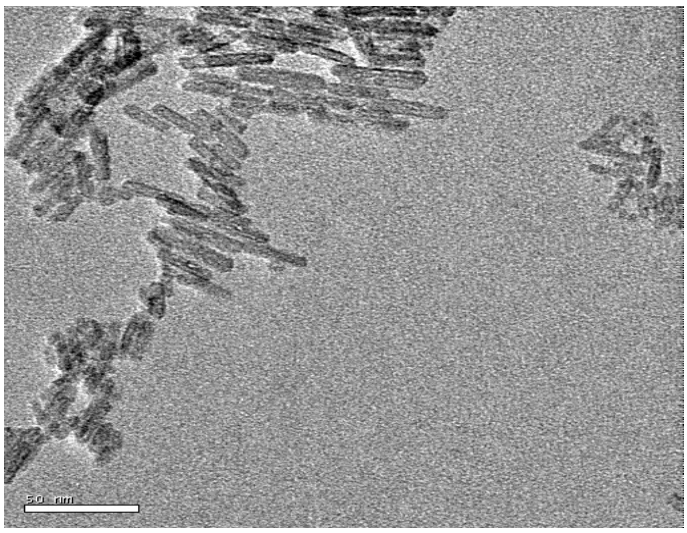

Figure 4.8: TEM image 5 of iron oxide nanorods

25 ml of 0.5M $FeCl_3$, 40 ml of 0.3M NaOH, 12 ml of Tween 85, 10 mg of carbon nanotube, reaction temperature: 90°C; reaction time: 71.5 hrs, shown on the image: 50 nm. (Original sample without washing and directly diluted by ethanol, sample from mixture of L1, L2 and L3)

Figure 4.8 showed the iron oxide nanorods self-assembled at 71.5 hrs. It can be observed that nanorods of iron oxide were successfully formed and carbon nanotubes disappeared completely.

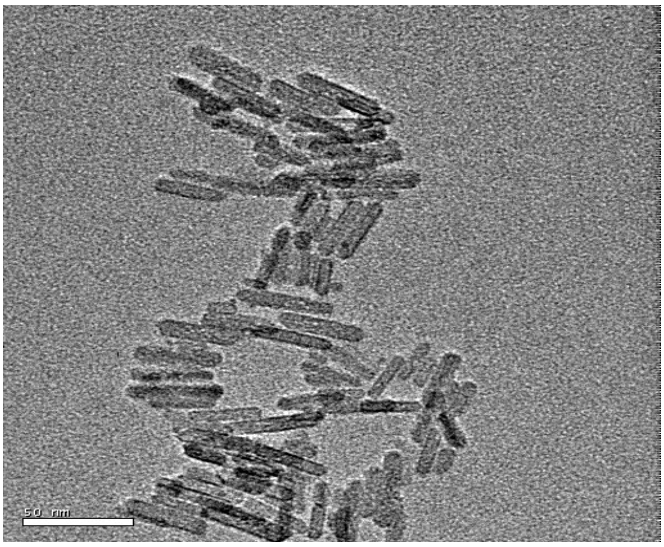

Figure 4.9: TEM image 6 of iron oxide nanorods at 72.5hrs

25ml of 0.5M $FeCl_3$, 40 ml of 0.3M NaOH, 12 ml of Tween 85, 10 mg of carbon nanotube, reaction temperature : 90 °C; reaction time: 72.5 hrs; L3 nanorods, shown on the image: 50 nm.

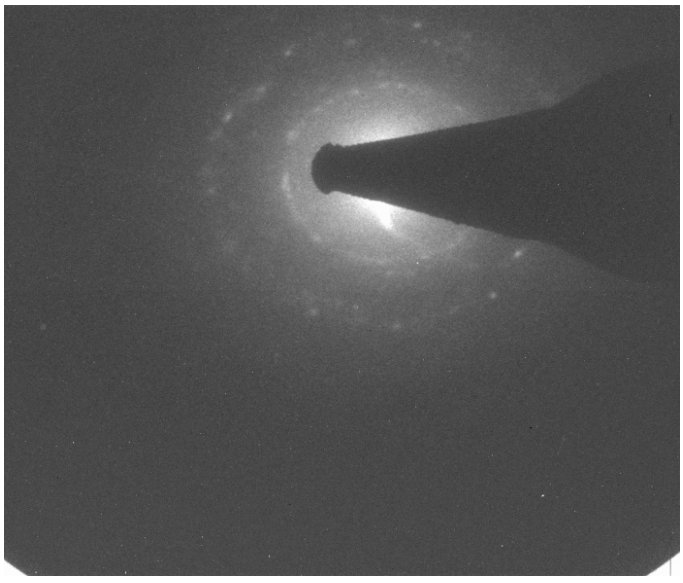

Figure 4.10: TEM Diffraction result of iron oxide nanorods of Figure 4.9

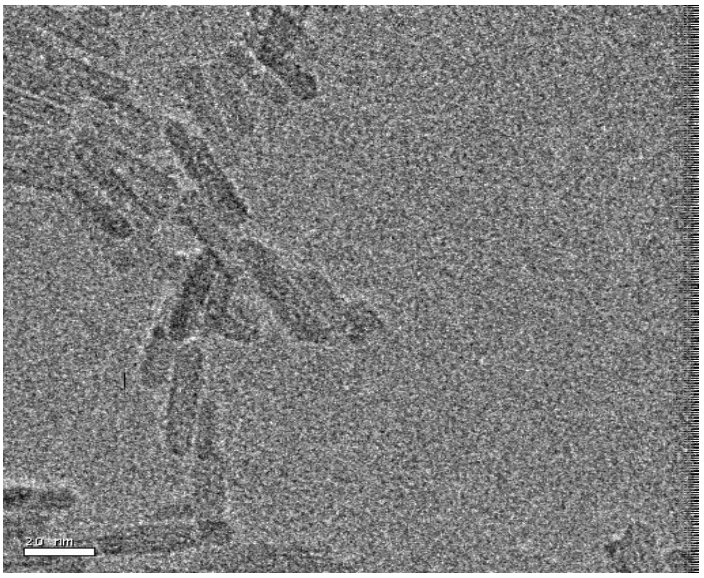

Figure 4.11: HRTEM image 1 of iron oxide nanorods at 72.5 hrs at 20 nm scale

25ml of 0.5M $FeCl_3$, 40 ml of 0.3M NaOH, 12 ml of Tween 85, 10 mg of carbon nanotube, reactiontemperature :90°C; reaction time: 72.5 hrs; shown on the image: 20 nm, sample is from L3.

TEM image shown in Figure 4.9 confirmed that the resultant iron oxide particles were nanorods and the size was 5 nm in width and 30-50 nm in length. From Figure 4.4 to Figure 4.9, the whole process of formation of iron oxide nanorods according to time variation has been observed.

Figure 4.10 showed the transmission electron diffraction (TED) image. It very clearly indicated that this particle was nanocrystaline as the diffraction crystalline rings were observed.

The nanorods were observed by HRTEM image (Figure 4.11) as well. It showed that the nanorods are uniform in size and in parallel arrangement within their groups.

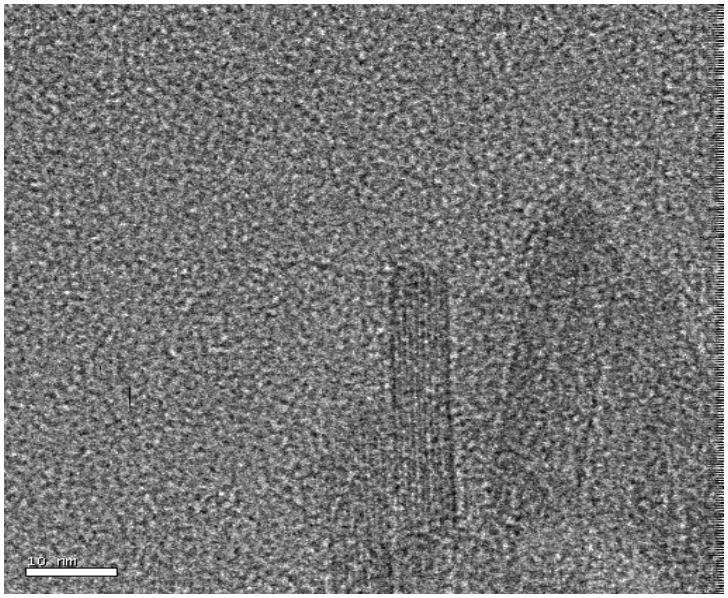

Figure 4.12: HRTEM image 2 of iron oxide nanorods at 72.5 hrs at 10 nm scale

25 ml of 0.5M $FeCl_3$, 40 ml of 0.3M NaOH, 12 ml of Tween 85, 10 mg of carbon nanotube, reaction temperature: 90°C; reaction time: 72.5 hrs, shown on the image: 10nm, sample from L3.

The HRTEM at 10 nm scale, Figure 4.12, showed that there were many pores in the nanorods. The nanorods consisted of self-assembled nanodots. These linear arrays will provide large surface area which is prefered when they are used as catalyst.

Field Emission Scanning Electron Microscopy (FESEM) is a high resolution imaging technique providing topographical and structural information in plan view or in cross-section. Figure 4.13 and Figure 4.14 showed the surface morphologies of iron oxide nanoparticles powders. Nanorods can be easily observed in the images. It means that the nanorod product still remained after the product was taken out from the solution.

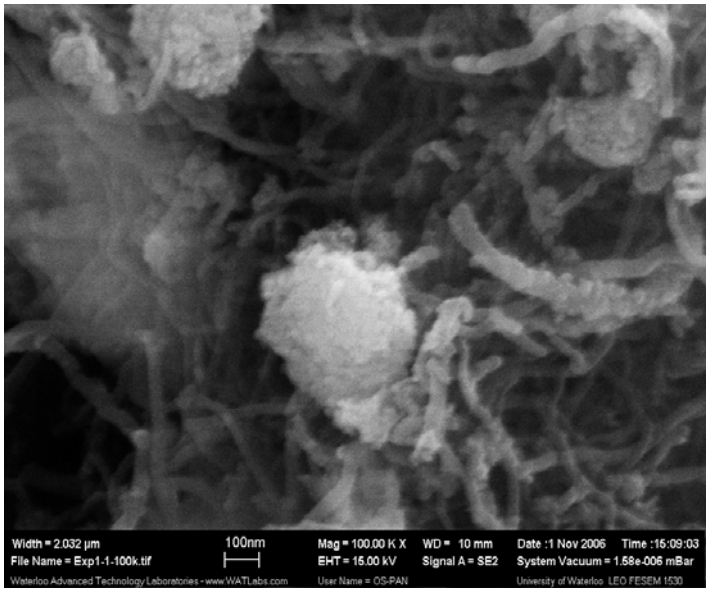

Figure 4.13: FESEM image 1 of iron oxide at 100nm scale

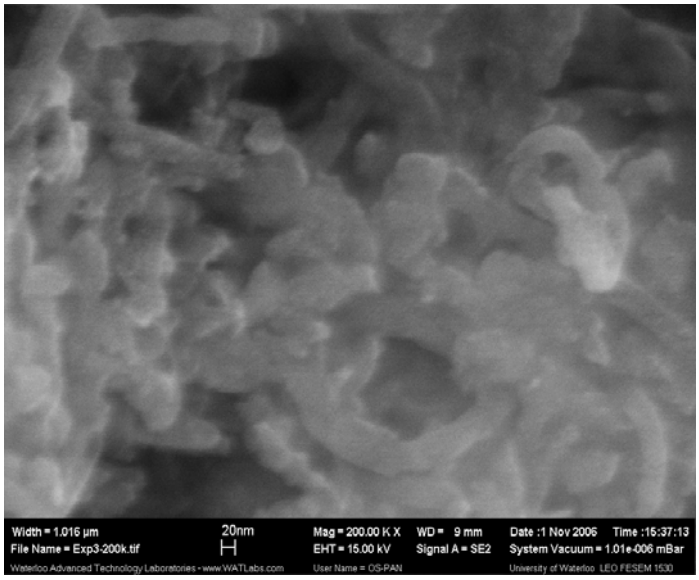

Figure 4.14: FESEM image 2 of iron oxide at 20nm scale.

Figure 4.13 and Figure 4.14: 25 ml of 0.5M $FeCl_3$, 40 ml of 0.3M NaOH, 12 ml of Tween 85, 10 mg of carbon nanotube, reaction temperature: 90°C; reaction time: 72.5 hrs; powder sample of iron oxide from L3; Scale image on Figure 4.13 and Figure 4.14 are 200 nm and 20 nm respectively.

4.4.3 Nanoparticle Size

Particle size distribution was measured for the L11 solution. The results shown in Figure 4.15 indicate that nanodots of iron oxide with a diameter of 1 nm were formed and the particle size distribution was very narrow.

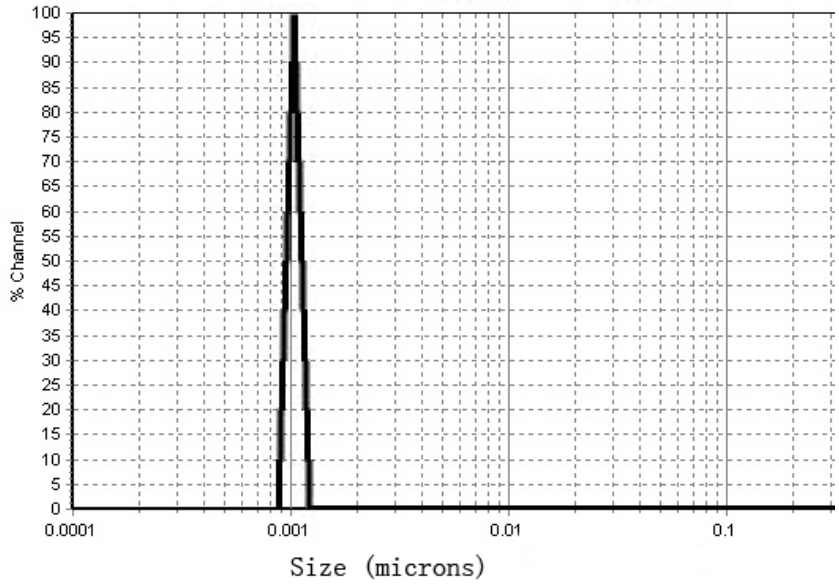

Figure 4.15: Iron oxide particles size distribution of L11 solution

30 ml of 0.5M $FeCl_3$, 30 ml of 0.5M NaOH, 12ml of Tween 85, 10 mg of carbon nanotube, reaction temperature: 100°C; reaction time: 72.5 hrs, Upper layer solution L11

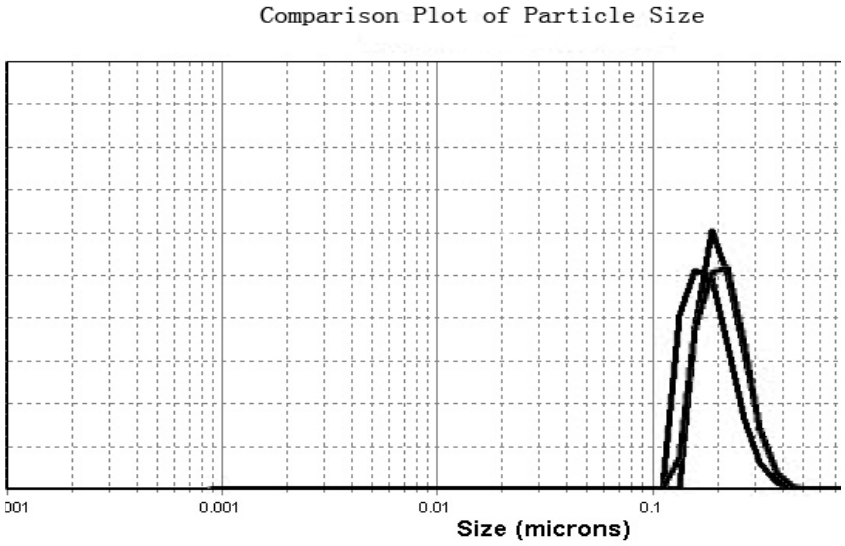

Figure 4.16: Iron oxide particles size distribution of L3 solution

30 ml of 0.5M $FeCl_3$, 30 ml of 0.5M NaOH, 12 ml of Tween 85, 10 mg of carbon nanotube, reaction temperature : 100°C, reaction time: 72.5 hrs, bottom particle, nanoparticles of L3.

Comparing Figures 4.15 and 4.16, the different results were obtained from the different layers of the same batch product. The result of nano-particle size analysis exhibited the existence of nanodots in the oily liquid of L11 layer, and their size is about 1 nm as shown in Figure 4.15; while the particle size in L3 is much large. The precipitate of L3 was washed and re-dispersed into ethanol solution before it can be done on particle size measurement.

4.4.4 Nanoparticle composition

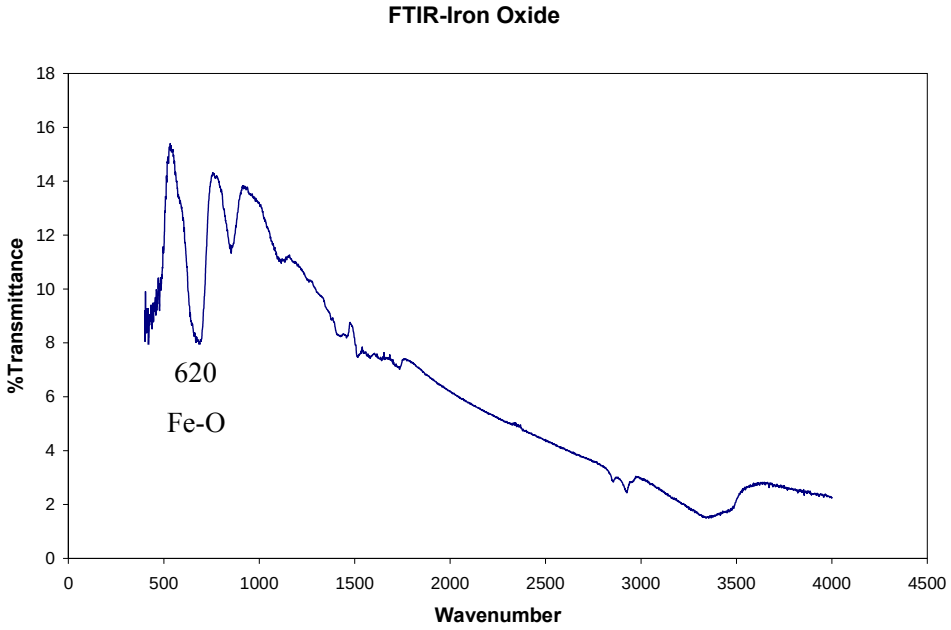

Figure 4.17: FTIR spectrum for iron oxide nanorod powder

25 ml of 0.5M $FeCl_3$, 40 ml of 0.3M NaOH, 12 ml of Tween 85, 10 mg of carbon nanotube, reaction temperature : 100°C; reaction time:72.5 hrs, powder sample of nanorods from L3.

The composition of the resultant iron oxide nanorod powder was analyzed by FTIR. The spectrum shown in Figure 4.17 clearly indicated the stretching vibration of Fe-O-Fe at 620 cm^{-1}.

Energy Dispersive X-Ray Spectroscopy (EDX) is used to qualitatively and quantitatively analyze the elements present in a selected area of the SEM image. Typical SEM applications include surface view and cross-sectional imaging for crystal surface structure analysis. EDX applications include specific elements analysis or compositional analysis. EDX result for our study was recorded and shown in Figure 4.18. Its component was tabulated in Table 4-1.

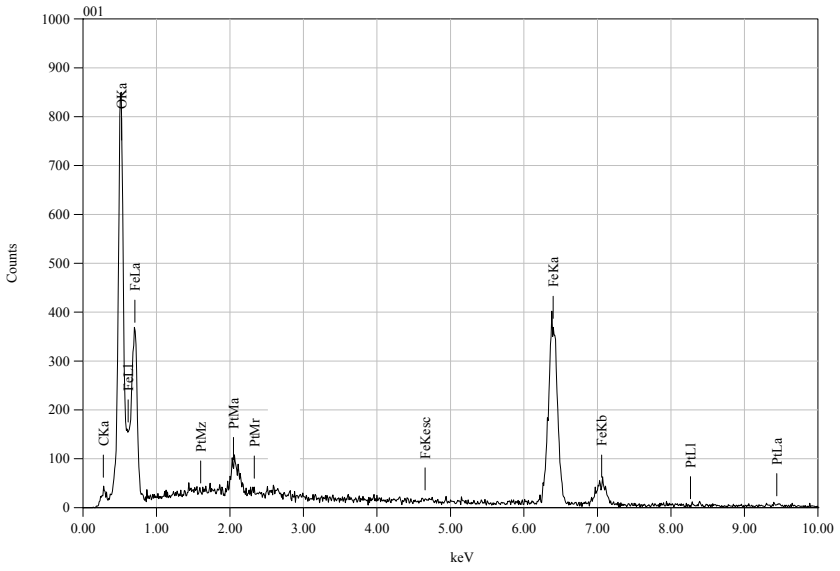

Figure 4.18: EDX diagram of hematite iron oxide powder

25 ml of 0.5M $FeCl_3$, 40 ml of 0.3M NaOH, 12 ml of Tween 85, 10 mg of carbon nanotube , reaction temperature: 90°C; reaction time: 72.5 hrs; powder sample of iron oxide nanorod from L3.

Table 4-1: The composition analysis of iron oxide nanorod by EDX report

Element	**Fe**	**O**	**C**	**Pt**	**Total**
Mass%	66.88	20.70	4.92	7.50	100%
Relative Atom Number	2	3	0	0	

EDX result corresponding to the materials on Figure 4.14 showed that the chemical component of the nanorods was iron oxide as the main composition is iron and oxygen. Contaminants of C, and Pt were introduced by platinum coating and double layer stick glue which have to be used during the sample preparation.

4.4.5 Magnetic properties

Bulk hematite, besides the Néel temperature (T_N= 948K), has a first-order magnetic transition at T_M=260K, which is called the Morin transition. Below T_M the crystal shows very weak ferromagnetic properties (Park et al, 2007; Georgakilas et al., 2005). Because of nanoscale confinement, nanomaterials can exhibit unusual magnetic behaviors that are quite different from those of conventional bulk materials. For example, α-Fe_2O_3 particles with diameter smaller than 20nm have shown a suppression of the Morin transition and stay in the weakly ferromagnetic state at least down to 5K. (Shull et al., 1951) Herein, we investigated the magnetic property of synthesized α-Fe_2O_3 nanorods by a superconducting quantum interference device (SQUID. The M-H curve (Figure 4.20) showed a very small hysteresis loop with coercive force of 187Oe and remnant magnetization of 0.0014 emu/g. This indicated paramagnetic property of the sample which is due to the small size of the nanorods and the nanodots. The nanoparticles change from multi domains to single domain when the size of the magnetic particles decreases. If the single-domain particles become small enough, the magnetic moment in the domain fluctuates in direction because of thermal agitation, which leads to paramagnetism.

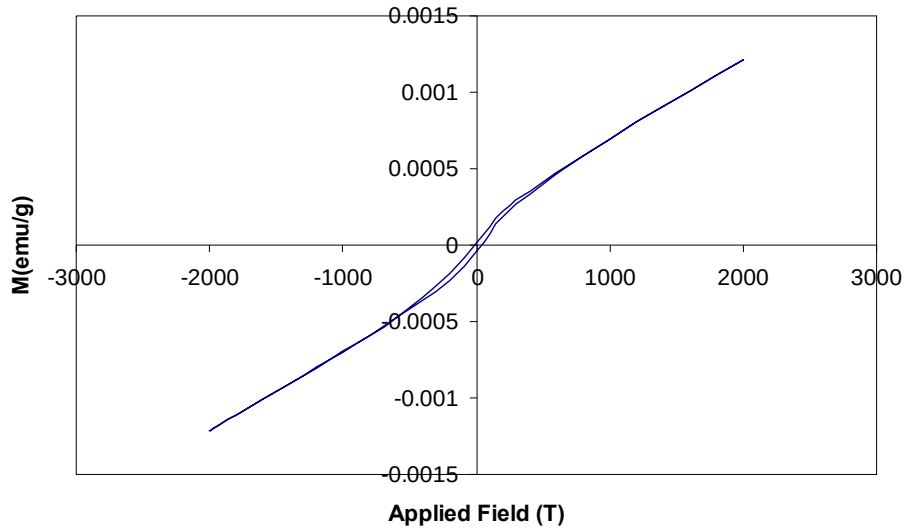

Figure 4.19: SQUID (M-H) scheme of iron oxide nanoparticles

25 ml of 0.5M $FeCl_3$, 40 ml of 0.3M NaOH, 12 ml of Tween 85, 10 mg of carbon nanotube, reaction temperature : 90°C, reaction time: 72.5 hrs, powder sample of iron oxide nanorod from L3.

4.4.6 UV-Vis diffuse reflectance spectroscopy

UV-visible spectra were also used for sample analysis. The results were illustrated in Figure 4.20.

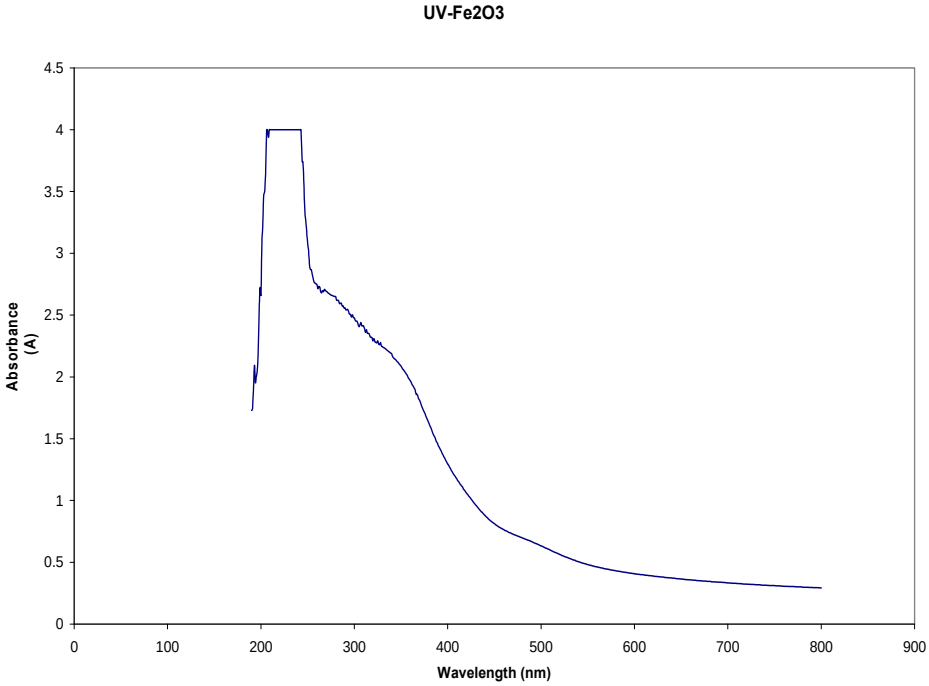

Figure 4.20: UV-Vis spectrum of iron oxide nanorods

25 ml of 0.5M $FeCl_3$, 40 ml of 0.3M NaOH, 24 ml of Tween 85, 10 mg of carbon nanotubes, reaction temperature : 90°C, reaction time: 72.5 hrs, sample from L3.

UV-Vis spectrum showed that the sample is α- Fe_2O_3 as the absorbent peak is at 280nm as shown in Figure 4.20. Generally, the UV absorption intensity of Fe_2O_3 nanocrystals was greater than that in the visible region, because the former one is allowed transition while the d-d transition was forbidde as in Figure 4.20. As well known, light scattering for visible light takes effect in the absorption spectra if the particle size becomes greater than 20 nm (Cheng et al., 2006). It means that the larger particles should show stronger reflectivity and the reflectivity of particles should shift to longer wavelength for larger particles (Cheng et al., 2006). In Figure 4.20, the absortance intensity was increased start from 600nm, but it was increased slowly during 500-600 nm; in the wavelength region 280-400 nm, the intensity increased fast; in the wavelength region 260-300 nm, the intensity increased sharply. This indicates that

the absorption intensity of the composite in the region 250-300 nm was much larger than that in the region 400-600 nm.

4.4.7 Surface area adsorption analysis (BET) .

Nanoparticles have a high specific surface area. The surface area of the iron oxide nanorods synthesized in the present work and analyzed by BET is compared with the surface area of activated carbon and the results are shown in Table 4-2.

Table 4-2: Nanorods of iron oxide BET analysis result

EXP Number	***Activated Carbon***	***Iron oxide (1)***	***Iron oxide (2)***	***Iron oxide (3)***
Degas Condition	300 °C, 1hr	80 °C, 12hr	110 °C, 3hr	110 °C, 2.5hr
BET Surface Area Sq.m/g	31.4279	95.6575	76.0389	60.9000
Langmuir Surface Area sq. m/g	49.4203	159.0984	127.7353	101.8017

BET testing results show that iron oxide nanoparticles have 2-3 times surface area higher than the activated carbon. This could mean that the iron oxide nanoparticles will be good for nanocatalyst materials because high surface area can increase the efficiency of catalytic reactions.

4.5 Summary

Uniform α-Fe_2O_3 nanorods with 5-10 nm in width and 30-50 nm in length were successfully prepared by a one-step sol-gel method with low cost raw materials, iron chloride, sodium hydroxide and Tween 85. The new synthetic method has of a potential commercial value due to the characteristics of the simplicity in the process and the low cost in the starting materials. The crystal nanostructure and

morphology were characterized by XRD, TEM, and SEM. The SQUID study confirmed that the nanorods have a paramagnetic character. The particles size of nanodots and nanorods was analyzed by a NanoTAC 150. The composition of iron oxide nanorods was confirmed by FTIR and EDX. The BET analysis showed the nanoparticles have 2 - 3 times surface area higher than the normal activated carbon.

Chapter 5
One step synthesis of TiO_2 hollow nanospheres via copolymer template

5.1 Introduction

Unique properties of titanium dioxide have received extensive attention in diverse areas such as catalysis, sensing, electronics, optics and separation science. In recent years, the large-scale commercialization of self-cleaning glazing products which include titania nanocrystals has received increasing attention due to their extreme physical properties. Potential applications include self-cleaning surfaces for use in architecture, construction, optical equipment and antimicrobial coating (Wei, et al, 2006; Kim et al., 2002; Salafsky et al., 2001).

A number of publications aimed at studying synthesis of titanium dioxide nanospheres by several different methods. For example, Colvin and co-workers reported the first solution-based nonhydrolytic synthesis of transition metal oxide nanocrystals. Those researchers exploited "nonhydrolytic sol-gel" chemistry that had been developed previously for the manufacture of bulk titanium (Trentler et al., 1999). Tang's group have reported a new synthesis of TiO_2 nanospheres that is based on the gentle oxidation of a very reactive organometallic complex of reduced titanium.(Tang et al., 2005) Philip Evans et al. had studied nanocrystals grown using titanium isopropoxide (TTIP) and demonstrated the differences in the resulting nanoparticles arising from a structure-directing role played by the precursors. A nitrogen carrier gas over the temperature range 450-650°C via chemical vapor deposit (CVD) at atmospheric pressure to growth of TiO_2 on stainless steel was reported by them.(Philip et al., 2006)

Macro-mesoporous structures of organic-inorganic hybrid of TiO_2 nanospheres have received a lot of attention in recent years because they offer multiple benefits arising form each pore size regime. For instance, dual templating techniques using surfactants and latex spheres can produce TiO_2 powder with bimodal pore size distributions (Coakley et al., 2005; Holland et al., 1998). Collins et al. had demonstrated that macro-mesoporous structures can be prepared in the presence of a single surfactant and even under a template free condition. (Collins et al., 2004) Konishi et al. reported the fabrication of TiO_2 monoliths with multiscale porous structure from titanium "alkoxy-derived" sol-gel system under

template free conditions. (Konishi et al., 2006) Weng and Wei have reported an approach of synthesizing nanoparticles with modified surfactants. They reported on dispersing surfactant-modified TiO_2 nanoparticles into either block of a PS-b-PMMA diblock copolymer with an ordered lamellar phase. TiO_2 was first synthesized in tetrahydrofuran (THF) instead of in a water or alcool pase. Cetyl trimethylamimonium chloride (TMAC) amphiphilics or 3-(methacryloyloxypropyl)-trimethoxy silane (TMS) surfactant was used to modify the TiO_2 nanoparticles. (Weng et al., 2003)

There are many reports on synthesis of TiO_2 nanocrystals via single surfactant with template free or "nonhydrolytic sol-gel" method which belong to the "growth-then-assembly" process, where the two discrete steps, growth and assembly, can be clearly divided. To meet the future challenges imposed by rapid development of nanoscience and nanotechnology, it would also be desirable to develop "growth-cum-assembly" processes, in which the growth and assembly take place at the same time, preferably under "one-pot" or continuous synthetic conditions. (Yang and Zeng, 2003; Seo et al., 2001) However, without the substrate prefabrication, arrays of nanostructured materials with distinct geometrical arrangement, structural repetition (superlattices), "one-pot" industrial reaction control and structural repetition have not been achieved directly on simple pristine TiO_2 nanospheres so far.

Our new approach, in which a novel type of TiO_2 nanoparticle consisting of crystalline nanospheres with hollow polymer rings are synthesized. The micro-mesoporous titania nanospheres with hydrophobic character and excellent UV absorption ability are achieved via one step self-assembling method, by hydrothermal processing. The significance is that the method developed in this work is very simple and can be easily developed into an industrial process of producing TiO_2 nanoparticles encapsulated by hollow spheres of the polymer, which implies that this has a great potentiality to be used widely in industrial applications, such as sunscreen coating materials and cosmetic materials.

5.2 Experimental Details

5.2.1 Materials

The polyoxyethylene sorbitan trioleate (Tween 85), titanium (IV) isopropoxide (99.999%) and hexadecylamine (99.5%) were purchased from Sigma-Aldrich (Oakvile, Canada). Isopropanol (99.9%), HPLC grade and Ethanol (99.5%) were purchased from Merck (Quebec, Canada).

5.2.2 Reaction apparatus

The reactor used for the reaction operations was a Parr reactor of 200ml (PARR 4843 Controller system of Parr instrument Inc.).

5.2.3 Synthesis of TiO_2 nanospheres

Mixing 40 -70 ml of isopropanol and 3 - 6 ml of Tween 85 into a glass container with stirring for 3 min at room temperature untill the solution became a clear with slight yellow color. 0.5 -1 g of hexadecylamine (white powder) was added into the solution with continuing stirring for about 20 min so that the powder hexadecylamine was dissolved in the solution. 1 ml of titanium isopropoxide solution was fetched and quickly injected into the glass container by using a pipette. The glass container was put into an autoclave equipped with atemperature sensor. The autoclave was sealed tightly. The temperature was set to 110 -150 °C at atmospheric pressure and the reaction time was set up at the range of 3 – 11 hrs. We have conducted 30 experiments in the range of temperature and reaction time in order to find the suitable condition to obtain the nanospheres.

5.2.4 Separation of products

After the reaction, the reactor was cooled down by setting control temperature to 25 °C. After 2-3 hrs, the reactor was opened a white precipitate and yellow solution were observed in the glass container. Ethanol was used to wash the white precipitate; then a centrifuge at 6800 rpm was applied for 10 min to separate the white precipitation. Before starting centrifugation, the products were put in an ultrasonic cleaner for 5 minutes. The above washing operation was repeated for at least 3 times. The obtained white precipitate was put into a steam oven, which was set at 40 °C to dry, for about 10-12 hrs. Finally, the product was grinded into a white powder.

5.3 Characterization

The crystal structure was verified by XRD diffraction, and the crystal morphology was observed by TEM. The nanoparticles size was acquired on NanoTrac 150. The surface structure was measured by FESEM; the composition of materials was analyzed by FTIR and EDX. UV visible spectra were acquired on UV-visible Spectrophotometer Cary 300 instrument, for which the scanning rate was 600nm/min and the wavelength range was 200-900nm through the quartz tube at a 300 kV accelerating

voltage. The surface area was measured by BET (Quantachrome NOVA-3000) and all samples were degassed at 110°C for 3 hrs by nitrogen at atmospheric pressure.

5.4 Results and discussion

5.4.1 Surfactant-Assisted Synthesis of TiO_2 Nanoparticles

The principle of the synthesis is based on hydrolysis of titanium isopropoxide.

$$Ti\{OCH(CH_3)_2\}_4 \rightarrow TiO_2 + 2(CH_3)_2CHOH + 2CH_3CHCH_2$$

Polyoxyethylene sorbitan trioleate (Tween 85) was employed as surfactant to template the formation of nanoparticles. The structural image of Tween 85 is shown in Figure 5.1. One important structural feature of Tween 85 is its dissociable ester segment (dashed line). By controlling reaction conditions (e.g., pH), in principle, ester hydrolysis may further occur, giving a newsurfactant product (i.e., alkylated oleic acid, whose anionic form is indicated as "A" in Figure 5.1). Hence, without preintroduction of complex surfactants, tiered surfactant combinations can be selfgenerated from a single-source surfactant Tween-85 during the synthesis of nanoparticles. (Xu, et al., 2004) In order to speed up the hydrolysis, hexadecylamine was used to maintain the pH of the solution at 8.

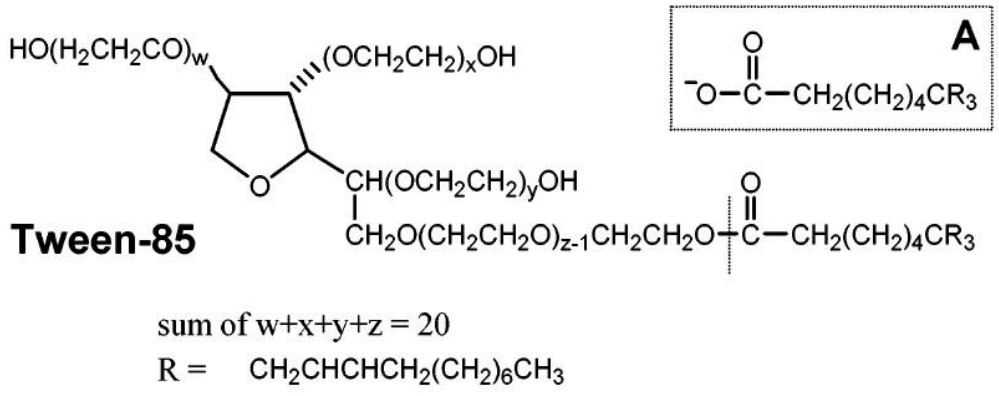

Figure 5.1: Structure of Tween 85

5.4.2 Crystal structure and size of TiO_2 hollow nanospheres

The crystal structure of anatase titanium dioxide is tetragonal, D_{4h}^{19}-$I4_1/amd$, a=b=3.782Å, c=9.502 Å, a: c=1:2.54. Each titanium ion is coordinated by six oxygens, and each oxygen ion is linked by three titaniums to form an octahedral TiO_6 crystal unit as shown in Figure 5.2.

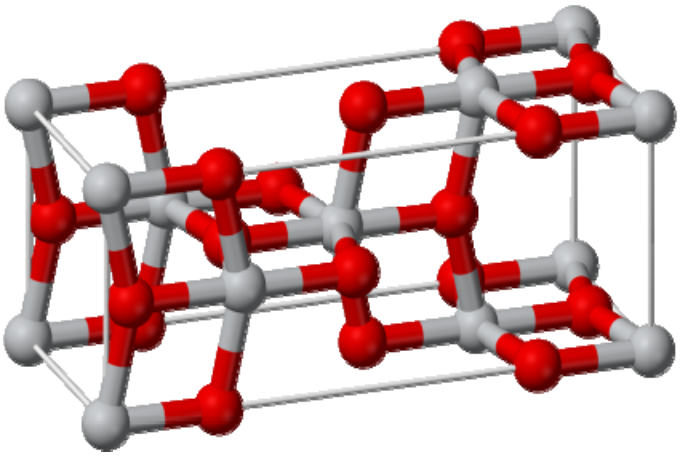

Figure 5.2 **:** Anatase crystal 3D structure unit cell (Smyth et al., 1988)

Crystals are typically acute dipyramidal [101], often highly modified; obtuse pyramidal or tabular on [001]; less commonly prismatic on [001], with [110], [010].

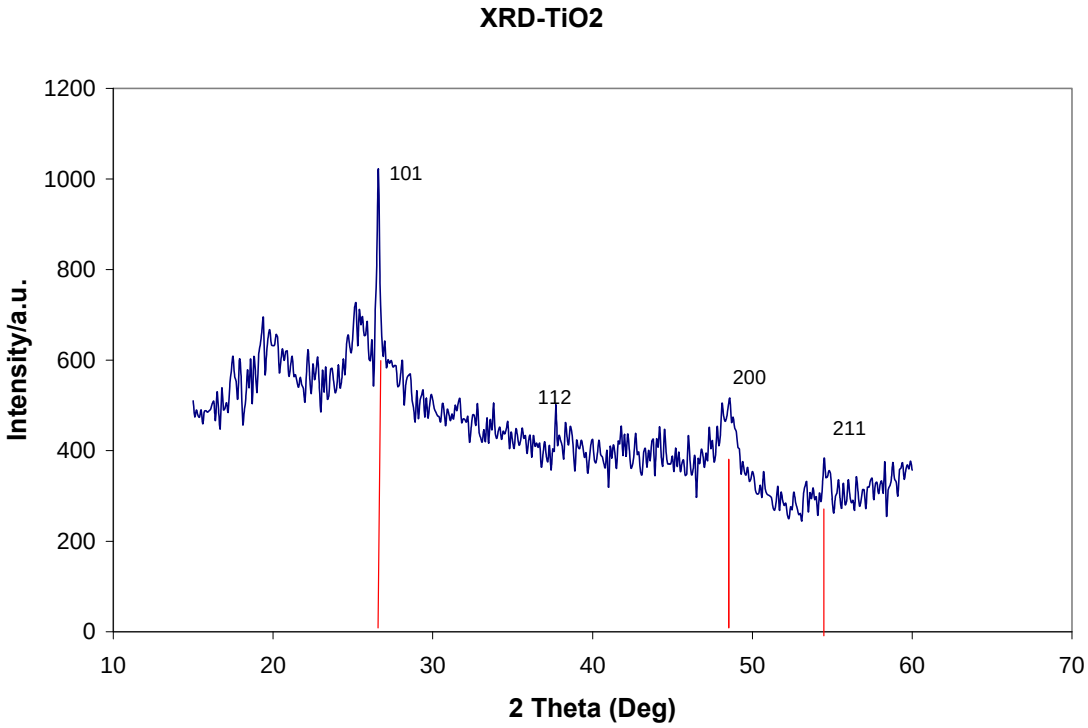

Figure 5.3: XRD scheme of Titanium oxide

40 ml of isopropanol, 3 ml of Tween 85, 1ml of titanium (IV) isopropoxide, 1g of 1-hexadecylamine, reaction temperature: 140°C, reaction time :6 hrs.

Displayed in Figure5.3 is the XRD spectrum of synthesized titanium oxide nanoparticles. The characteristic peaks of anatase titanium oxide crystallites at [101], [200] and [211] are obviously observed with the strongest peak at [101].

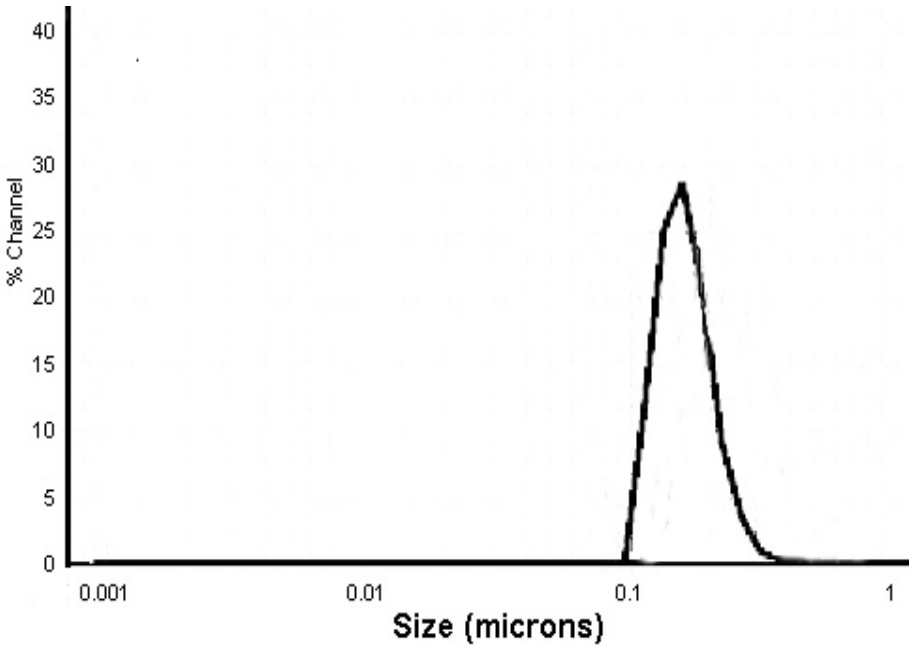

Figure 5.4: Nanotrac scheme of TiO_2 nanospheres

50 ml of isopropanol, 6 ml of Tween 85, 1ml of titanium (IV) isopropoxide, 1g of 1-hexadecylamine, reaction temperature: 130°C, reaction time : 6 hrs.

The particle size was measured by sampling 0.01mg of TiO_2 white powder which was redissolved in ethanol with ultrasonic agitation. The result shows that the TiO_2 nanospheres particle size is about 100 nm- 500 nm, the size of most particles is located in the range of 200 -300 nm. This result will be further verified below by TEM images.

5.4.3 Crystal morphology

Transmission electron microscope analysis is one of the best analysis methods to show the crystal morphology by direct and simple images. 0.01 mg of titanium oxide was dispersed by 10 ml of ethanol for the TEM analysis.

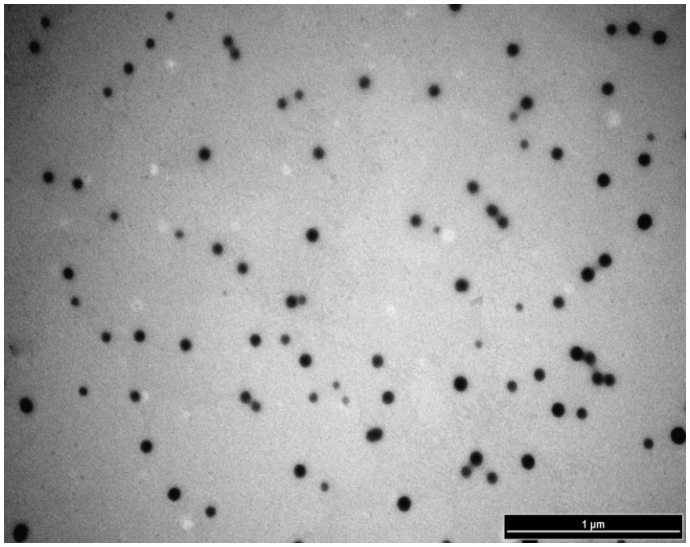

Figure 5.5: TEM image 1 of TiO_2 nanospheres at 1µm scale.

40 ml of isopropanol, 3ml of Tween 85, 1ml of titanium (IV) isopropoxide, 1g of 1-Hexadecylamine, reaction temperature:140 °C, reaction time: 6 hrs, scale shown on the image : 1µm.

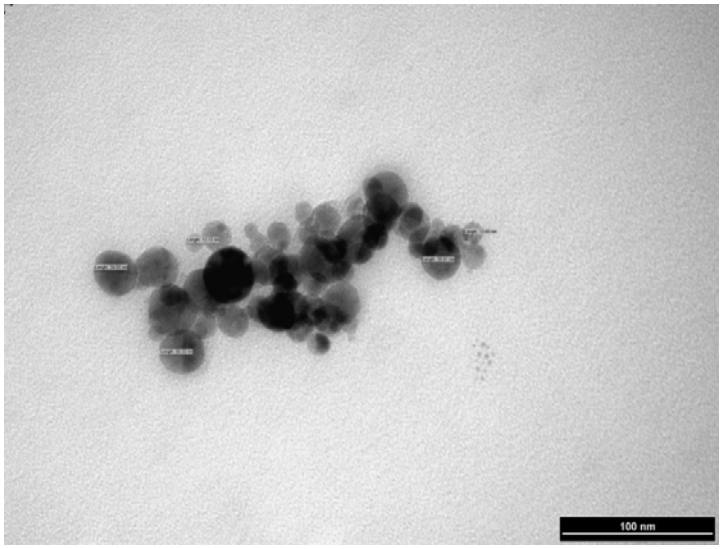

Figure 5.6: TEM image 2 of TiO_2 nanospheres

40 ml of isopropanol, 3ml of Tween 85, 1ml of titanium (IV) isopropoxide, 1g of 1-hexadecylamine, reaction temperature: 140 °C, reaction time : 6 hrs, scale shown on the image : 100 nm.

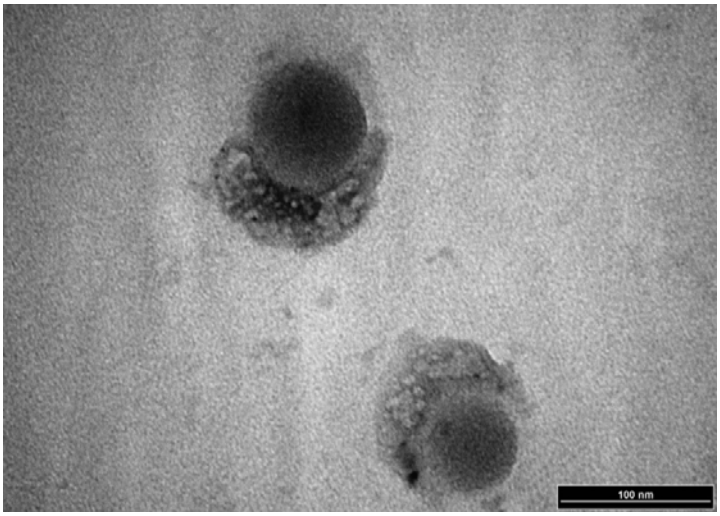

Figure 5.7: TEM image 3 of TiO_2 nanospheres 100 nm scales

40 ml of isopropanol, 3 ml of Tween 85, 1ml of titanium (IV) isopropoxide 99.999% solution, 1g of 1-hexadecylamine, reaction temperature:140 °C, reaction time : 6 hrs, scale shown on the image :100 nm.

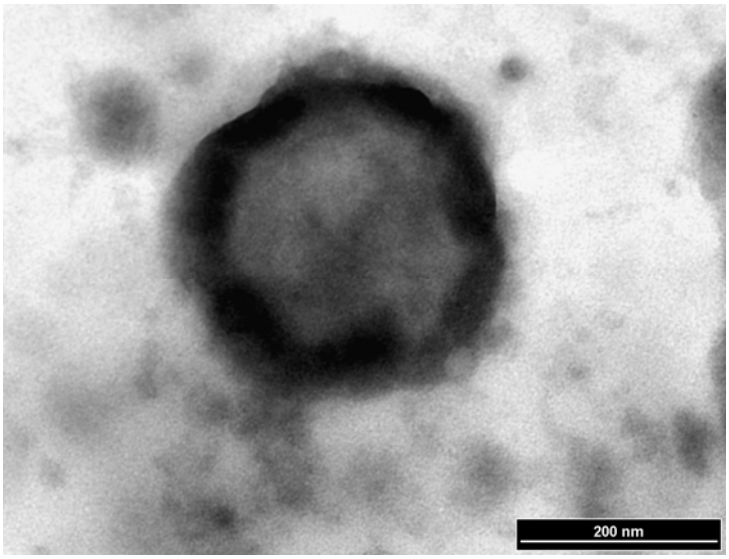

Figure 5.8: TEM image 4 of TiO_2 hollow nanospheres at 200 nm scale

40 ml of isopropanol, 3 ml of Tween 85, 1ml of titanium (IV) isopropoxide 99.999% solution, 1g of 1-hexadecylamine, reaction temperature: 135 °C; reaction time: 5 hrs, scale shown on the image : 200 nm.

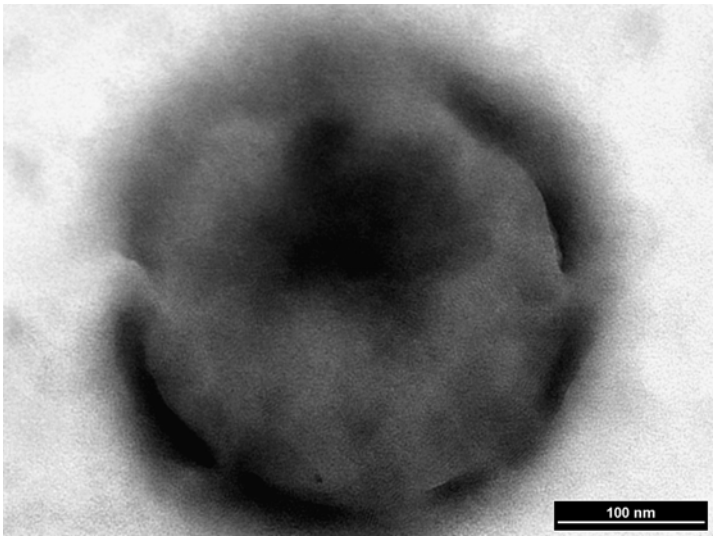

Figure 5.9: HRTEM image 5 of TiO_2 hollow nanospheres at 100 nm scale

40 ml of isopropanol, 3 ml of Tween 85, 1ml of titanium (IV) isopropoxide 99.999% solution, 1g of 1-hexadecylamine, reaction temperature:135 °C, reaction time: 5 hrs, scale shown on the image:100 nm.

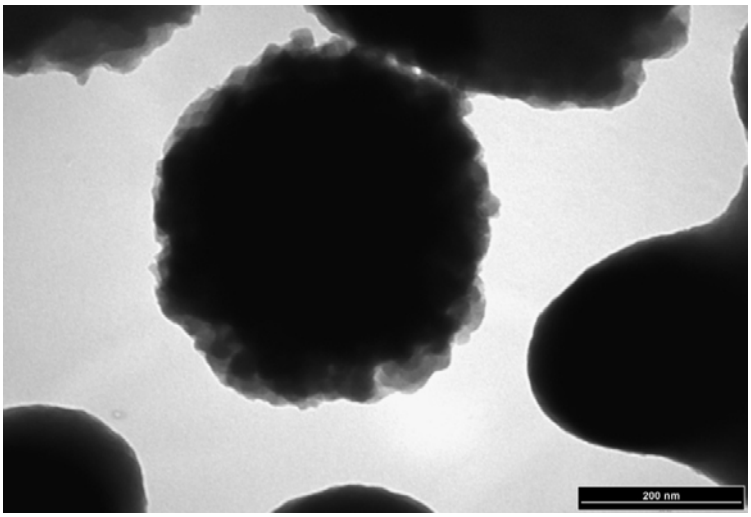

Figure 5.10: TEM image 6 of TiO_2 hollow nanospheres at 200 nm scale

40 ml of isopropanol, 3 ml of Tween 85, 1ml of titanium (IV) isopropoxide 99.999% solution, 1g of 1-hexadecylamine, reaction temperature:150 °C; reaction time:6 hrs, scale shown on the image: 200 nm.

We obtained titanium oxide nanospheres and shown in Figure 5.5 is the overall distribution image. The size of nanospheres is about 10-30 nm in diameter as shown in Figure 5.6. Some nanospheres were capped by porous copolymer ring as shown in Figure 5.7.

The hollow nanospheres were obtained as shown in Figures 5.8 - 5.9 when reaction temperature was 135°C. The diameter of the hollow spheres was about 200 nm in both figures. There were some titanium oxide particles in the center of spheres, and the transparent parts of spheres were recognized as hollow parts.

The reaction temperature and reaction time affect the particles size. Figure 5.10 indicated that when the temperature was 150°C, the size of the nanospheres increased to 300-350 nm.

Observations of the morphorlogies of the nanosized TiO_2 synthesized at diffent reaction temperature and time were made and the morphorlogies are listed in Table 5-1, in which other conditions such as material formula, pH etc.were kept unchanged.

Table 5-1: Titanium oxide morphologies observed at various reaction conditions (pH = 8-9)

Reaction Temp (°C)	**130**	**135**	**140**	**150**
Reaction time (4hrs)	Amorphous	Amorphous	Amorphous	Nanoparticles
Reaction time (5hrs)	Amorphous	Nanosphere	Nanosphere	Nanoparticles
Reaction time (6hrs)	Amorphous	Nanospheres	Nanospheres	Microspheres
Reaction time (7hrs)	Amorphous	Microspheres	Microspheres	Microspheres

It was noted that if the reaction temperature is lower than 135°C, it was difficult to make nanocrystal, and the titanium oxide powder was almost amorphous. At 135°C- 140°C, if reaction time was less than 4 hrs, most of the particles still had not been changed to crystal status. When the reaction time was about 5- 6 hrs, the nanospheres of titanium oxide were formed. However, at a longer reaction time (more than 6 hrs) the nanosphere became large or even became a microsphere. Controlling reaction time and reaction temperature is very important to obtain spherical nanoparticles. The optimal reaction temperature and reaction time are of 135-150°C and 4-6 hrs respectively.

The conditions to obtain hollow nanosphere titanium oxide are very interesting. We tried a lot of experiments and found that the favorite condition is at temperature of about 135°C and reaction time of about 6 hrs.

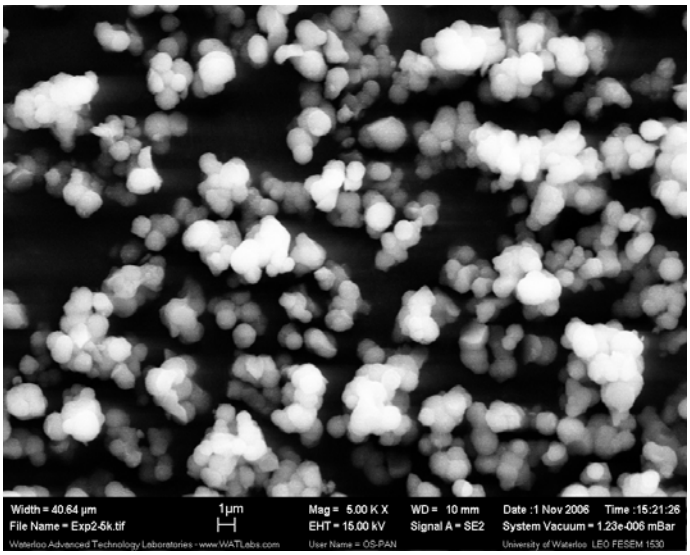

Figure 5.11: FESEM image 1 of TiO_2 nanospheres at 1µm scale

40 ml of isopropanol, 3 ml of Tween 85, 1 ml of titanium (IV) isopropoxide 99.999% solution, 1g of 1-hexadecylamine, reaction temperature:140°C, reaction time: 6 hrs, scale shown on the image :1µm; EHT:15kV.

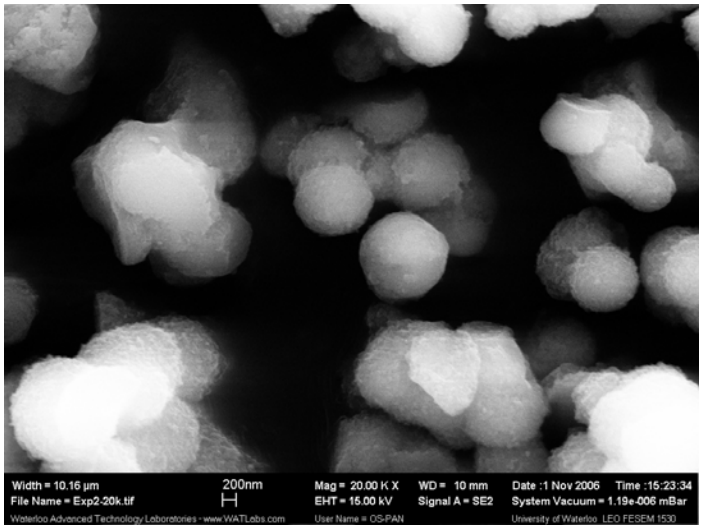

Figure 5.12: FESEM image 2 of TiO_2 nanospheres at 15kV EHT

40 ml of isopropanol, 3 ml of Tween 85, 1 ml of titanium (IV) isopropoxide 99.999% solution, 1g of 1-hexadecylamine, reaction temperature:140°C, reaction time : 6 hrs, scale shown on the image :200nm; EHT:15kV.

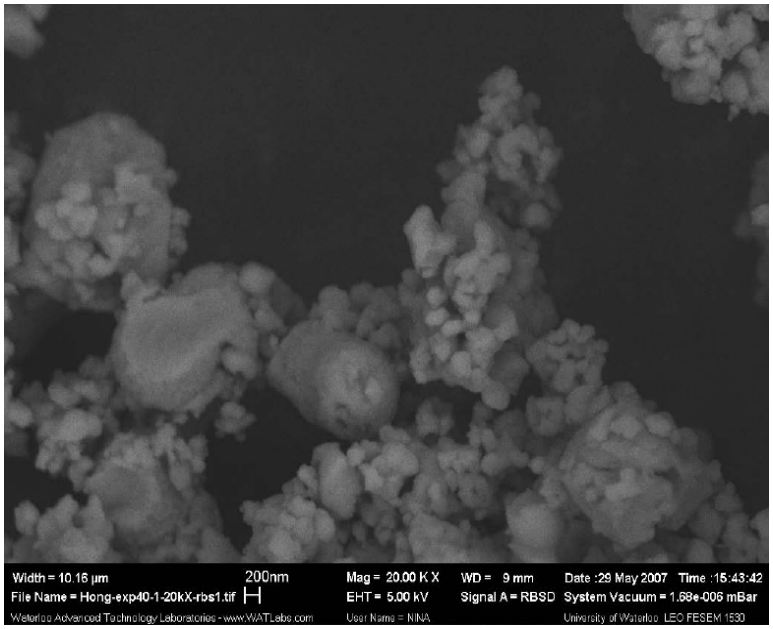

Figure 5.13: FESEM image 3 of titanium oxide nanoshperes at 5kV EHT

Figure 5.13: 40 ml of isopropanol, 3 ml of Tween 85, 1 ml of titanium (IV) isopropoxide 99.999% solution, 1g of 1- hexadecylamine, reaction temperature:135 °C, reaction time:5 hrs, scale shown on the image :200nm ; EHT:5kV.

FESEM images of Figures 5.11 to 5.13 showed that the nanospheres of TiO_2 were capped by copolymer to form hollow spheres. The size of the polymer nanospheres, as shown in Figure 5.11, is about 100 – 300 nm. It is similar to the results as shown in Figure 5.9 by the TEM technique.

5.4.4 Nanosphere compositions

Powder FESEM patterns, shown in Figure 5.14, indicates that our synthesized nanosphere is pure TiO_2.

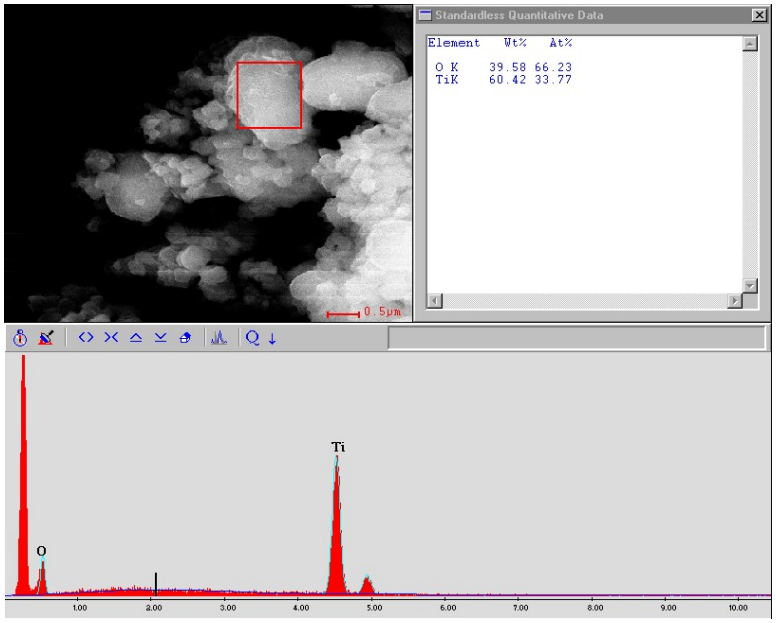

Figure 5.14: EDX scheme of titanium oxide powder

40 ml of isopropanol, 3 ml of Tween 85, 1 ml of titanium (IV) isopropoxide 99.999% solution, 1g of 1- hexadecylamine, reaction temperature: 135°C, reaction time:5 hrs, scale shown on the image: 0.5µm; EHT:15kV.

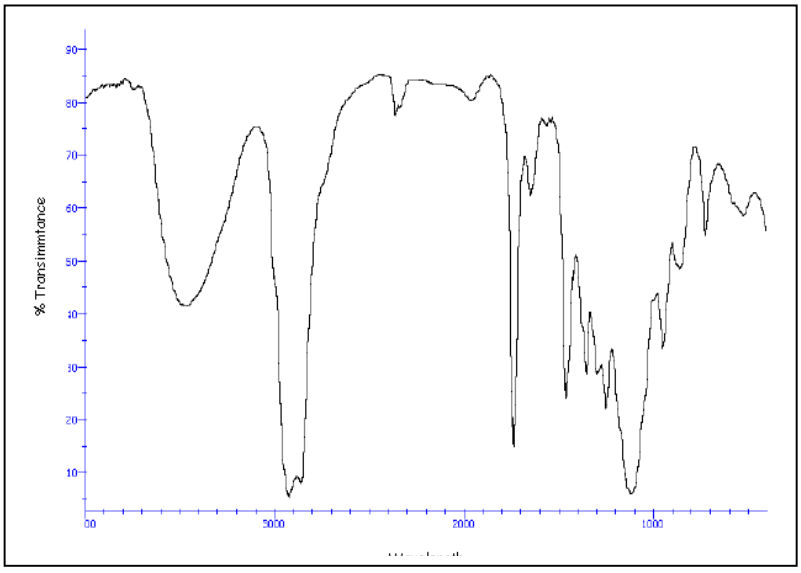

Figure 5.15: FTIR spectrum of Tween 85

Figure 5.15 is the FTIR spectrum of standard Tween 85 (Acros Organics, 2006). The characteristic peaks are 2927 and 2850.

FTIR spectrum in Figure 5.16 shows that Tween-85 remains largely intact in the bulk mixture, as all its fingerprint absorptions can be clearly observed in the spectrum. For instance, the broad bands at 3435-3452 cm^{-1} and the peaks at 1639-1644 cm^{-1} attribute to the O-H stretching and bending modes of Tween-85, respectively. The peaks at 2927 and 2850 cm^{-1} are due to asymmetric and symmetric C-H stretches of the hydrophobic chains. The sharp and symmetric peaks at 1736 - 1737 cm^{-1} are attributed to stretching mode of the ester carbonyl in the molecule. The broad peaks at 1103- 1111cm^{-1} can be assigned to C-O-C stretching mode. The IR spectrum of the capped nanocrystals is dominated by the antisymmetric and symmetric stretching vibrations of carboxylate anions by two characteristic bands centered at 1527 and 1467cm^{-1} respectively. Finally, the characteristic peak for TiO_2 phase is indicated by a vibration band of Ti-O-Ti groups at 900-400 cm^{-1}.

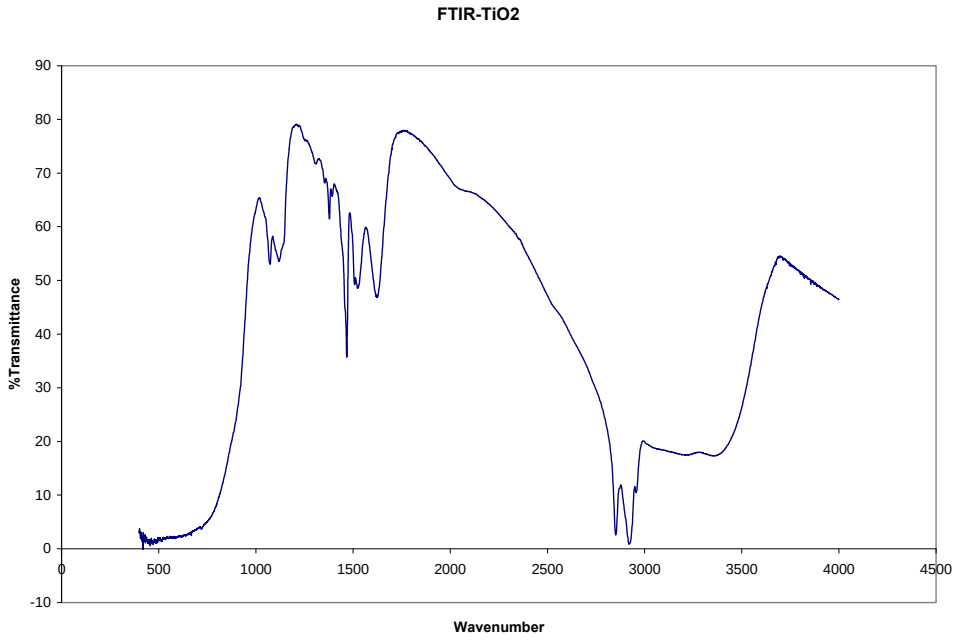

Figure 5.16: FTIR scheme of titanium oxide

50 ml of isopropanol, 6 ml of Tween 85, 1 ml of titanium (IV) isopropoxide 99.999% solution, 1g of 1-hexadecylamine, reaction temperature:130°C, reaction time: 6 hrs.

5.4.5 UV-vis Spectra

Figure 5.17 shows diffuse reflectance UV –Visible spectrum of TiO_2-polymer sample. An absorption band is centered at 230 nm which is attributed to the charge –transfer transition associated with isolated Ti^{4+} framework sites in tetrahedral coordination. The other peak around 320 – 350 nm indicates the presence of polytitanium $(Ti\text{-}O\text{-}Ti)_n$ clusters (Serpone et al., 1995; Mohamed et al., 2006). The small peak at 365 nm indicates that it is a typical anatase TiO_2 crystal. The intensity of this peak increases with Ti loading and the concentration. Figure 5.17 showed UVA and UVB absorption peak while UVB absorption range runs from the range of 280-320 nm, UVA range runs during 320 – 400 nm. For this sample the peak of UVB absorption is more intense than that of UVA adsorption.

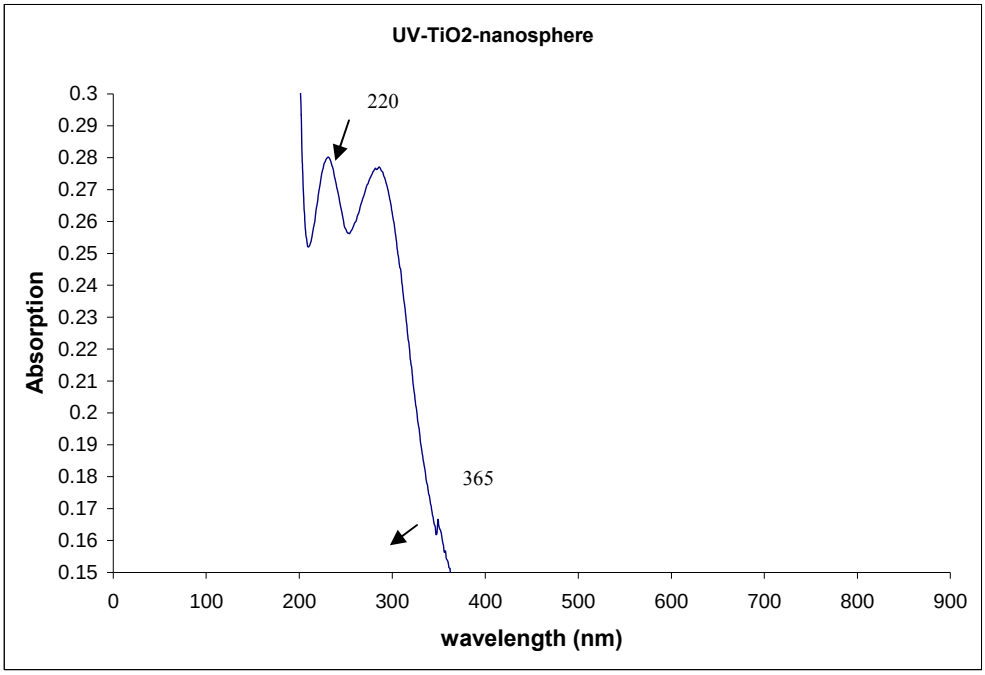

Figure 5.17: UV-vis. Spectrum of TiO_2/copolymer in ethanol

40 ml of isopropanol, 3ml of Tween 85, 1ml of titanium (IV) isopropoxide 99.999% solution, 1g of 1-hexadecylamine, reaction temperature: 135°C, reaction time:5 hrs.

5.4.6 Physical phenomena

The apparent density of the modified TiO_2 is less than the density of deionized water. This was found by adding 0.1 mg titanium oxide into 3 ml deionized water in a bottle. After stirring for 2 minutes and then leaving at room temperature and atmospheric pressure for 10 - 30 days, it was found that the sample of titanium oxide still floated on the water, and no precipitation was observed. It implied that the titanium oxide synthesized was completely hydrophobic. This hydrophobic property of titanium oxide can be applied to make anti-fogging coating varnish and auto-cleaning glass, especially for optical sunscreen glass that has a large potential market around the world.

5.5 Summary

The synthesis of TiO_2 microporous/ mesoporous materials by one step reaction via self-assembling mechanism was reported in this chapter. The effect of temperature on the systhsis was studied for making self-assembling nanocrystallites. The results confirmed that the method described by using cheap raw materials to make titanium dioxide nanocrystallites particles was achieved. Characteristic analyzes were conducted by TEM, XRD, FESEM, and FTIR. The synthesized hydrophobic titanium oxide nanoparticles may be potential of use in anti-fogging coating materials.

Chapter 6
Performance of Highly Porous TiO_2 Nanoparticles in Electron Transport

6.1 Introduction

Titanium dioxide thin films are chemically stable, possess a high refractive index, which is 2.55 for anatase thin film (Ottermann et al., 1996), and have excellent transmittance in the visible and near- IR spectral regions (Hagfeltd et al., 2000). This has therefore led to extensive applications of titanium oxide in antireflective coating, photo induced water splitting, organic compound degradation, dye-sensitized solar cell and self-cleaning properties (Philip et al., 2006; Tian et al., 2003c).

In particular, dye-sensitized nanocrystalline TiO_2 solar cell is a promising class of molecular photovoltaics because of their potential low cost and relatively high power conversion efficiency. The dye sensitization is initiated by the excitation of a sensitizer adsorbed onto a surface of a semiconductor electrode followed by electron injection into a conduction band of the electrode. Specifically, in 1991 Grätzel and others developed solar cells based on the sensitization of highly porous TiO_2 by ruthenium dyes with the highest power conversion efficiency which maks practical applications feasible (Hou et al., 2005; Grätzel et al., 2001; Kavan et al., 2001; Piotrowiak et al., 2003; Beltran et al., 2006). Pioneered by Stucky et al (Gerfin et al., 1997), some synthetic routes using block copolymers-base surfactants were proposed to prepare mesoporous TiO_2 layers. Yang reported syntheses of organized TiO_2 that were based on solvolysis of $TiCl_4$ in ethanol containing amphiphilic triblock copolymer of ethylene oxide and propylene oxide as the structure directing agent. They synthesized mesoporous TiO_2 in the form of powders or xerogels (Yang et al., 1999). Later, Domaradzki (Domaradzki et al., 2001) obtained thin films on glass or silicon by dip or spin coating. This simple technique involves a complex mechanism, called evaporation-induced self-assembly. Marketa Zukalova and his group have achieved high efficiency on electron transportation from the organized mesoporous TiO_2 film (Marketa et al., 2005). They made pluronic templated mesoporous TiO_2 film via layer-by-layer deposition and characterized this mesoporous TiO_2 film by a novel methodology based on the absorption of n-pentane. Motonari (2004) and his group presented the preparation of a TiO_2 network structure of single-crystal-like nanowires by an “oriented attachment” mechanism. They concluded that high efficiency dye-sensitized solar cells with a titania thin film electrode composed of a network structure of single-

crystal-like TiO_2 nanowires (Adachi et al., 2004). Recently, Zhu et al (2006) reported the influence of surface area on charge transportation and recombination in dye-sensitized TiO_2 solar cells. The nanotube arrays were prepared from electrochemically anodized Ti foils, and were characterized by scanning and transmission of electron microscopies. They reported that the oriented TiO_2 nanotube arrays could enhance charge-collection efficiency and light scattering. Although much work has been done on dry-sensitized solar cells, some of the work has been done about the effect of electrode porosity on electronic transportation. But the systematic comparison of the electron properties of various TiO_2 electrodes by Potentiostat Galvanostat instrument and the usage of low cost and simple synthesis method to fabricate the oriented TiO_2 thin film have not been carried out.

In this chapter, the synthesis of TiO_2/copolymer (Tween 85) thin film by a hydrothermal processing and self-assembling mechanism is investigated. Detailed information on the preparative method, crystallographic and surface structure is described. Comparison of electronic transfer properties of the TiO_2 nanoparticles and oriented TiO_2 thin film with micropores is studied. We find that the difference of surface structure affects the performance of potentiostat Galvanostat on dummy cells that consist of electrodes made from these nanocrystal materials. Better performance can be achieved using oriented thin film.

6.2 Experimental section

6.2.1 Fabrication of TiO_2 thin film

6.2.1.1 Synthesis of TiO_2 thin film

After 40-50 ml of IPA and 3-4 ml of Tween 85 in a glass container were mixed with stirring for 3 min at room temperature, the solution turned out clear and light yellow. 0.8-1.2 g of hexadecylamine white powder was added into the solution, and the mixture was stirred for 20 minutes more so that the powder dissolved into the solution. A pipette was used to fetch 1 ml of titanium isopropoxide, followed by transferring it quickly into the above prepared solution in order to avoid oxidation in air. The glass container was put into the stainless steel reactor. After closing the reactor and connecting it with control system, the temperature was set to 135°C-150°C and reaction time of 3-5 hrs. For this research, 20 experiments within the temperature and reaction time range were conducted in order to find a suitable condition to make the porous thin film.

6.2.1.2 Separation of products

After the reaction period, the temperature of control system was reset at 25°C. After the reactor was cooled to 25°C, it was opened and white precipitate and yellow solution was obtained.

The white precipitate was washed using anhydrous ethanol, and the wet precipitate was separated from ethanol using a centrifuge at 6500 rpm for 8 minutes. Before starting centrifugation, the products were put in ultrasonic cleaner to be agitated for 5 minutes. After repeating the washing process at least 3 times, a white precipitate was obtained. After putting in a vacuum oven at 30°C to dry for about 24 hrs, the sample was grinded in a mortar, and the white powder product was obtained.

6.2.2 Electrochemical impedance voltammetry

6.2.2.1. Measurement method and instrument

AutoLab PGSTAT30, the Potentiostat Galvanostat /voltammetric analysis instrument inclusive of Agilent 54624A Oscilloscope meter, a dummy cell and a differential electrometer amplifier from Eco Chemie B.V. was used for analyzing potential /current scan of solar cells. The software of general purpose electrochemical system (GPES) with cyclic and linear sweep voltammetry (stair case) electrochemical technique for solid electrodes was applied for this experiment. The Autolab dummy cell box was connected to the cell cable via the plug connector. There were three connectors on the front panel of PGSTA T30, and the cell cables were connected to the working electrode, reference electrode and counter electrode. For this experiment, the counter electrode was the platinum electrode supplied by Eco Chemie B.V, the working electrode was a TiO_2 electrode, and the reference electrode was a Ag/AgCl electrode. For all experiments, the parameters were set up in a way that the potential was 10 V in the beginning and -2V at the end, the step potential was 0.00244v/m, the scanning rate was 0.05 V/s, and the interval time was 50 sec. The linear sweep method can define start- and end- potential, whereas for 2 vertex potentials, the potential increasing was applied as steps at the end of each interval time. After this time for each step expired, the potential was increased with the step potential. The current was measured at the end of the each time interval. An option was available to change the sampling time interval by adjusting the α value. The background was also changed accordingly. In the experiments, the current was sampled at the end of each interval time: $\alpha = 1$. Usually, the staircase mode (Eco Chemie B V, 2001) is advantageous since it diminishes the current in the same manner as pulse voltammetry.

6.2.2.2 TiO_2 electrode preparation

A TiO_2 electrode was prepared by coating TiO_2 thin film on a small round shape copper master plate. The surface of the copper plate was polished using sand paper, and this plate was dipped into TiO_2/ethanol concentrated solution with ultrasonic agitation for 5 minutes. This polish step was repeated 4 times. The attached TiO_2 copper plate was sintered at 300° C in an oven for 30 min, then it was dipped into TiO_2/ethanol concentrated solution again for 10 hrs, and finally dried at room temperature. If the plate is not 100% coated by TiO_2, the preparation experiment needs to be conducted again. Only a completed coated plate could be used for working electrode. This process was repeated to prepare two kinds of electrodes using TiO_2 thin film and TiO_2 particles. The prepared electrodes were installed into silicon tip holder as a TiO_2 working electrode for the electrochemistry voltammetry measuring.

6.3 Results and discussion

6.3.1 The critical condition to make TiO_2 thin film

We used the same raw materials as those of Chapter 5 to prepare nano thin film composed of nanoparticles, but the critical condition such as chemical formula, reaction temperature and time had to be changed. The pH value was controlled to 9 by adding 10% more n-hexadecylamine, and the reaction temperature was 150°C. After 3 hrs of the reaction time TiO_2 nanoparticle thin film was obtained.

6.3.2 Crystal Structure of the TiO_2 nanoparticles in the thin film

The crystal structure of the TiO_2 in the thin film was verified by Powder X-ray diffraction.

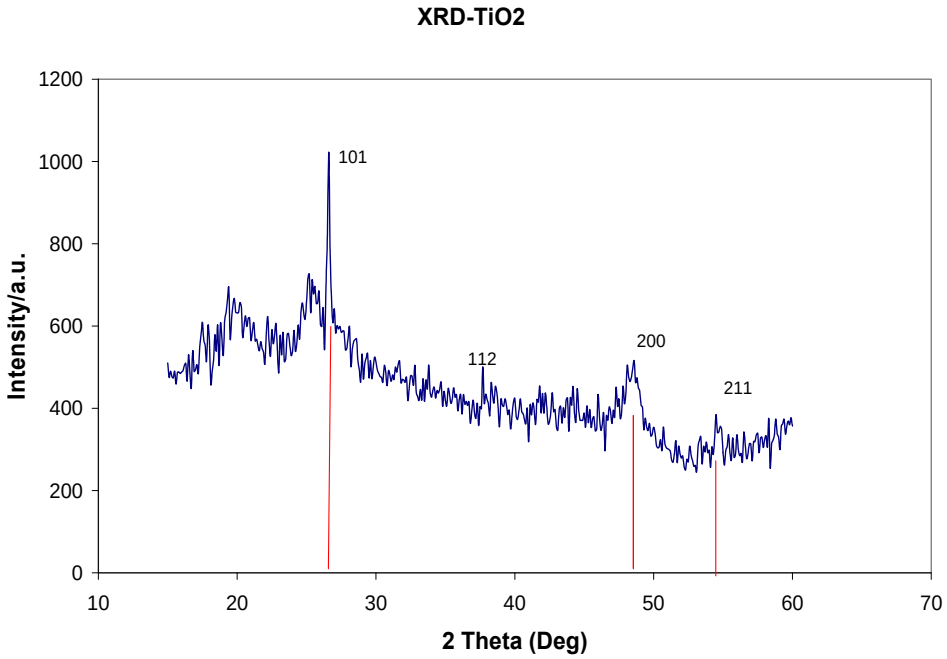

Figure 6.1: XRD scheme of TiO_2/copolymer film

40 ml of isopropanol, 3ml of Tween 85, 1 ml of titanium (IV) isopropoxide 99.999% solution, 1.1g of 1-hexadecylamine, reaction temperature:150 °C, reaction time: 4hrs.

Wide-angle X-ray diffraction was used to determine the crystal phase structure of the synthesized titania based materials. Results shown in Figure 6.1 indicated that the peak positions and diffraction intensities matched with the database spectra [101] of anatase titanium oxide crystal very well.

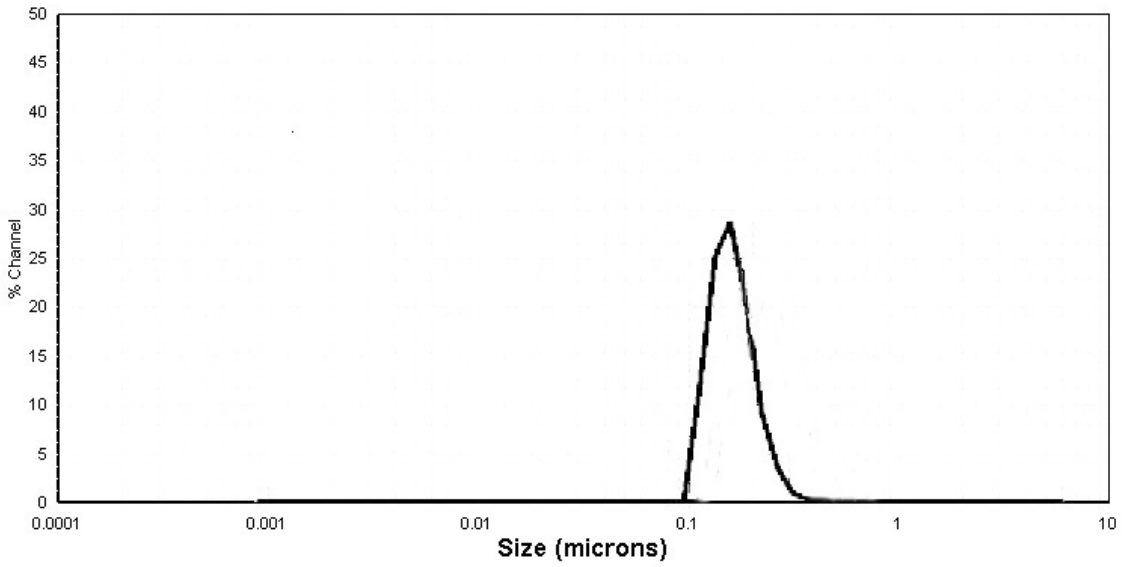

Figure 6.2: Nanoparticle size scheme of TiO_2 thin film

40 ml of isopropanol, 3 ml of Tween 85, 1ml of titanium (IV) isopropoxide 99.999% solution, 1.1g of 1-hxadecylamine, reaction temperature :150 °C, reaction time: 4 hrs.

The particle size was measured and the result is shown in Figure 6.2. The size of titanium oxide thin film is about 200 nm. The result will be verified by transmission electron microscope image.

6.3.3 Morphology of TiO_2 thin film

Titanium dioxide thin film was observed via TEM images. 0.01 mg of wet white precipitate titanium oxide was dissolved in 3 ml of anhydrous ethanol to make a sample solution for TEM testing.

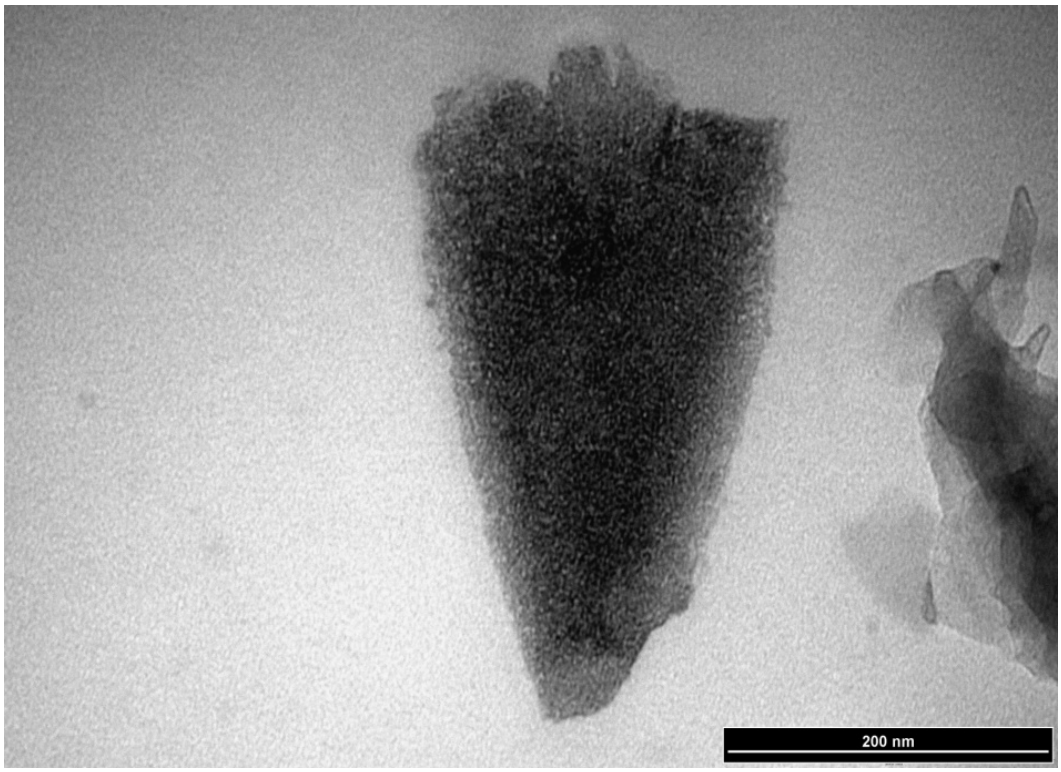

Figure 6.3: TEM image1 of TiO_2 nanoparticles at 6 hrs.

40 ml of isopropanol, 3 ml of Tween 85, 1ml of titanium (IV) isopropoxide 99.999% solution, 1.1g of 1-hexadecylamine, reaction temperature: 150 °C, reaction time: 6 hrs, scale shown on the image : 200nm.

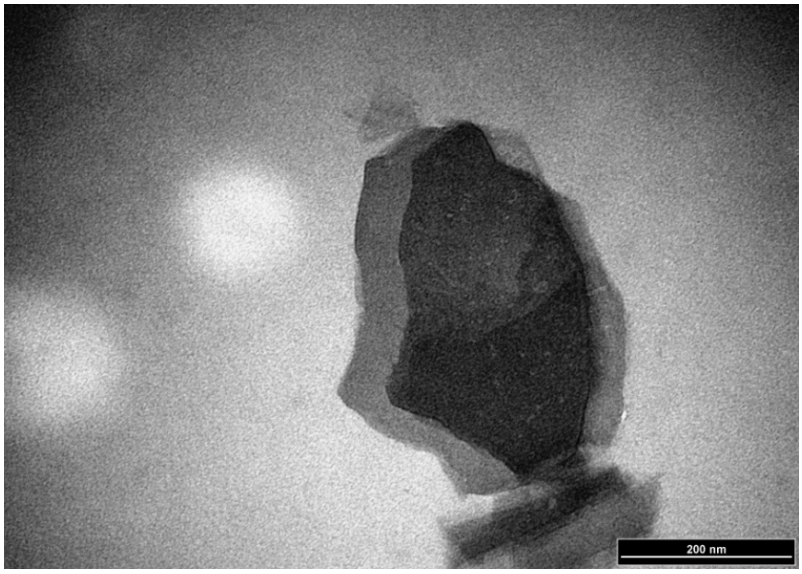

Figure 6.4: TEM image 2 of TiO_2 nano thin film at 5 hrs.

40 ml of isopropanol, 3 ml of Tween 85, 1 ml of titanium (IV) isopropoxide 99.999% solution, 1.1g of 1-hexadecylamine, reaction temperature : 150 °C, reaction time:5 hrs, scale shown on the image : 200nm.

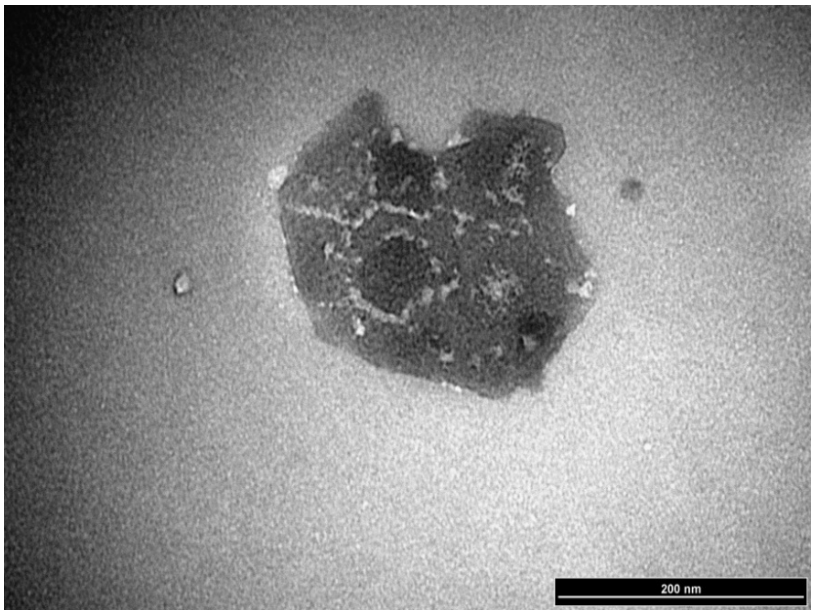

Figure 6.5: TEM image 3 of TiO_2 thin film at 4 hrs.

40ml of isopropanol, 4 ml of Tween 85, 1 ml of titanium (IV) isopropoxide 99.999% solution, 1.1g of 1-hexadecylamine, reaction temperature : 150 °C, reaction time:4 hrs, scale shown on the image : 200nm.

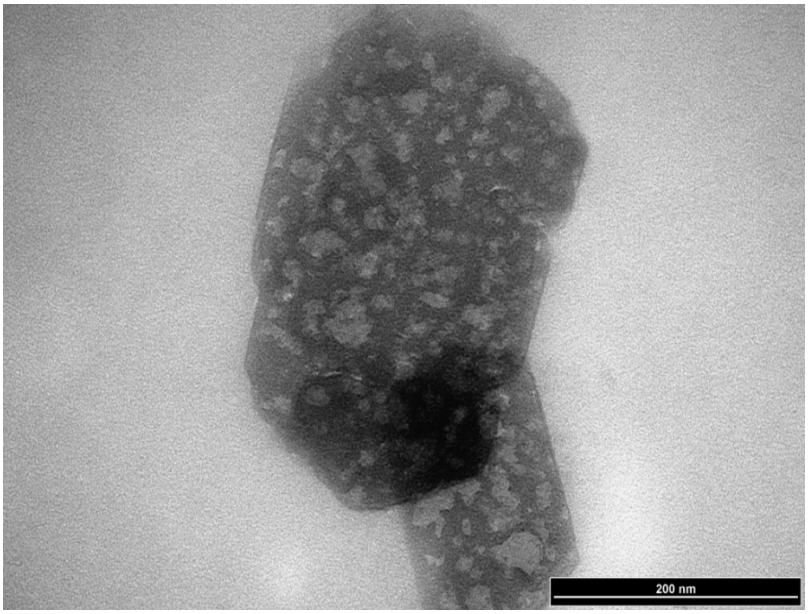

Figure 6.6: TEM image 4 of TiO_2 nano thin film at 3 hrs.

40 ml of isopropanol, 3 ml of Tween 85, 1 ml of titanium (IV) isopropoxide 99.999% solution, 1.1g of 1-hxadecylamine, reaction temperature: 150 °C, reaction time: 3 hrs, scale shown on the image : 200 nm.

Figure 6.3 shows the triangle titanium dioxide thin film sheet with few pores, the triangle sheet size was about 300nm in length and 200 nm in top width. Figure 6.4 shows that the sheets of titanium dioxide/copolymer were overlaid. Titanium dioxide nanoparticles formed thin film at the same temperature as Figure 6.3 except that the reaction time was changed to 5 hrs. The thin film sheet is very thin and it is easy to find two overlaid thin films in Figure 6.4. Some signs of porosity can be observed in the sheet. The sheet size is about 100-200 nm in width and 300 – 400 nm in length. In figures 6.5-6.6, thin films of titanium dioxide with a lot of micropores were observed. The pore sizes were 10-30 nm in average. The reaction time was about 4 hr and 3 hrs respectively. The formation of microporous micelles and the pore size depended on reaction time. It is noted that at long reaction time, the nanoparticles of TiO_2 tend to aggregation and less pores in the thin film was observed. Crystal nanoparticles of TiO_2 initially formed about 1nm nanodots. They gathered as striated dots array, and then formed solid sheet. Titanium oxide film was the electronic acceptor and absorption takes place in solar cell materials. Therefore, high porous film will improve the effectiveness of electron transfer.

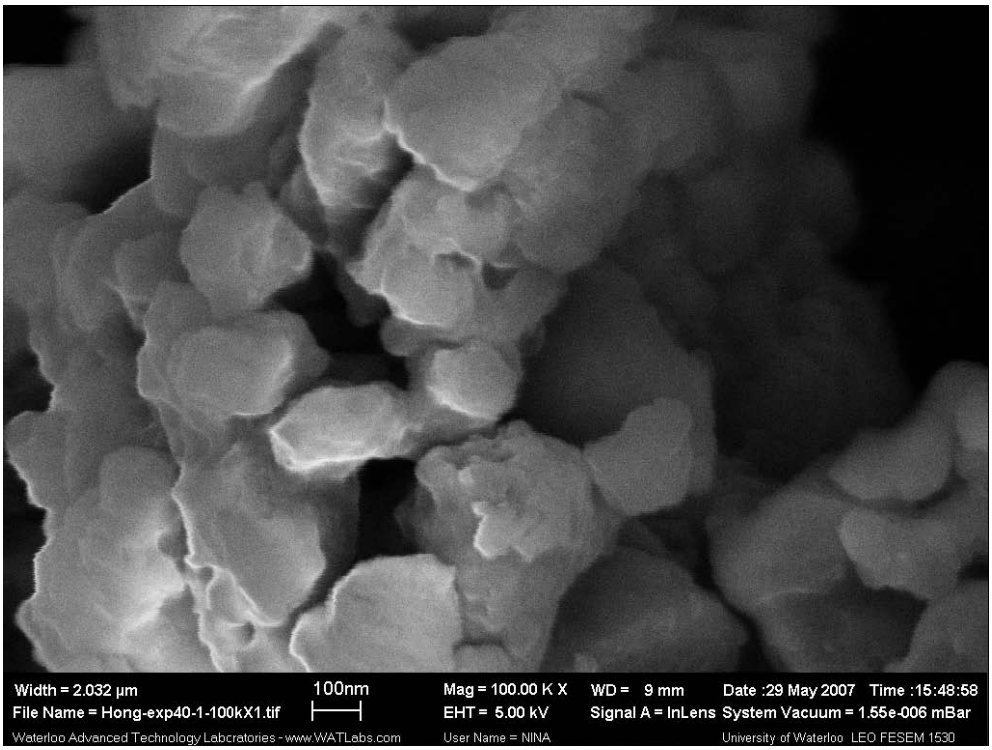

Figure 6.7: FESEM image of TiO_2 thin film at 100 nm scale

40 ml of isopropanol, 3 ml of Tween 85, 1 ml of titanium (IV) isopropoxide 99.999% solution, 1.1g of 1-hexadecylamine, reaction temperature:150 °C, reaction time :4 hrs, scale shown on the image: 100 nm, EHT = 5kV

The thin film structure is supported by FESEM analysis as well. The FESEM image of the TiO_2 powder shown in Figure 6.7 presents that the powder has a thin sheet like shape although the sheet size and shape are not even. The nanosheets in dry sample are overlaid each other into multiple layers.

6.3.4 Composition of the Thin Film

EDX analysis shown in Figure 6.9 indicates that the sample had a purity of 100% TiO_2 crystal nanospheres.

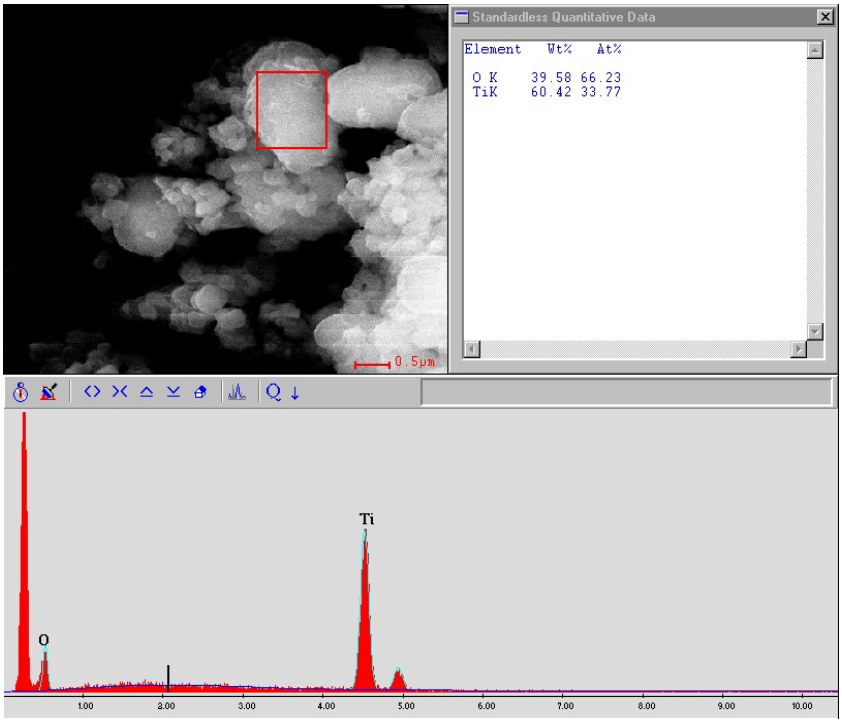

Figure 6.8: EDX scheme of TiO_2 thin film

40 ml of isopropanol, 3 ml of Tween 85, 1 ml of titanium (IV) isopropoxide 99.999% solution, 1.1g of 1-hexadecylamine, reaction temperature:150 °C, reaction time : 4 hrs. EHV =15kV

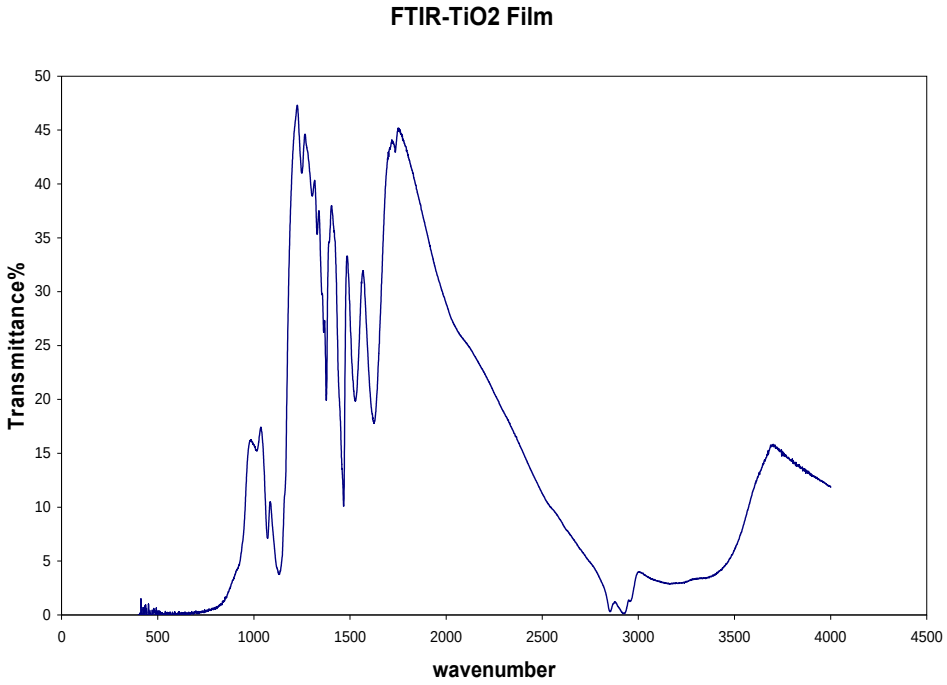

Figure 6.9: FTIR scheme of TiO_2 thin film

40 ml of isopropanol, 3 ml of Tween 85, 1 ml of titanium (IV) isopropoxide 99.999% solution, 1.1g of 1-hexadecylamine, reaction temperature : 150 °C, reaction time:4 hrs.

FTIR spectrum is shown in Figure 6.9. Same as in chapter 5, Tween 85 was confirmed to exist in the bulk solid sample as all its fingerprint absorptions can be clearly observed in the spectrum. The characteristic peak for TiO_2 phase was indicated by a vibration band of Ti-O-Ti groups at 900-400 cm^{-1}.

6.3.5 UV-visiable Spectra

To prepare samples for UV-vis. analysis, 0.001 mg of wet sample of TiO_2 was added into 3 ml of anhydrate ethanol, and then the mixture was mixed by Ultrasonic cleaner for 2 min stirring for UV-vis. analysis.

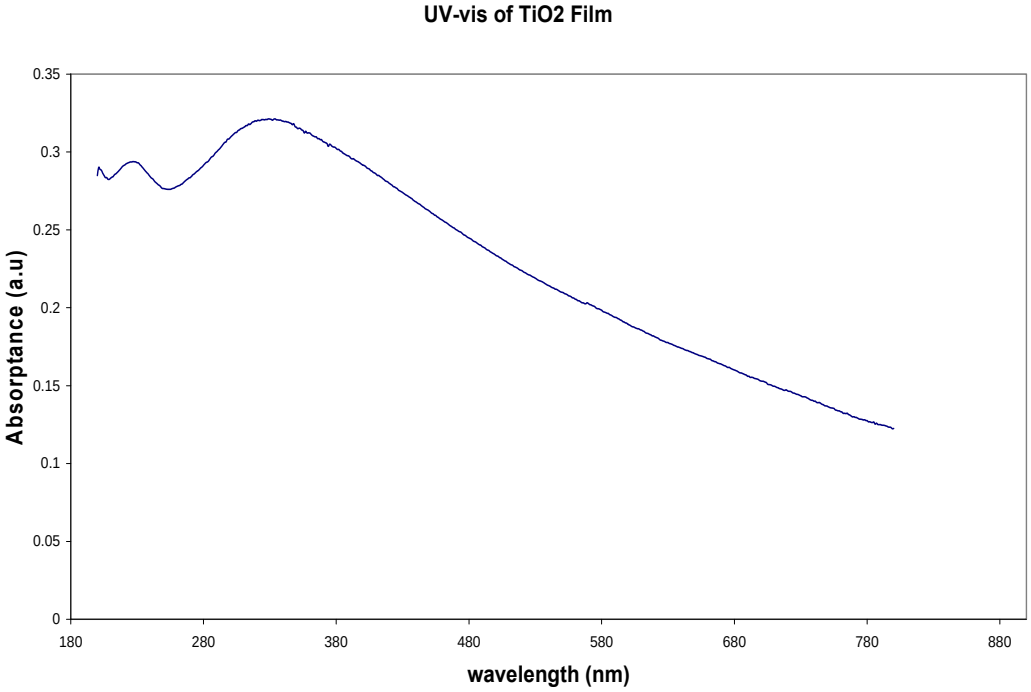

Figure 6.10: UV-vis. scheme of TiO_2 thin film

40 ml of isopropanol, 3 ml of Tween 85, 1ml of titanium (IV) isopropoxide 99.999% solution, 1.1g of 1-hexadecylamine, reaction temperature: 150 ° C, reaction time : 4 hrs.

Figure 6.10 shows the UV-vis. absorption spectrum of TiO_2 microporous nanoparticles, in which two bands are observed at 350 nm and 265 nm respectively. The spectrum has been normalized at sort band of the absorbance edge at about 380 nm in wave length for TiO_2 film and excitation peak at 350-360 nm.

6.3.6 Electrochemical Potentiosant Voltammetry analysis

To approach whether the synthesized TiO_2 nanomaterials are suitable for dye-sensitive solar cell materials, or for TiO_2 working electrodes, experiments of electrochemical potentiosant voltammetry are conducted. A typical plot of the potential (E/V) vs. the current (i/A) for TiO_2 film working electrode and TiO_2 nanoparticles working electrode, under Galvanostate Potentiosant Electrochemical System program is demonstrated in Figure 6.11.

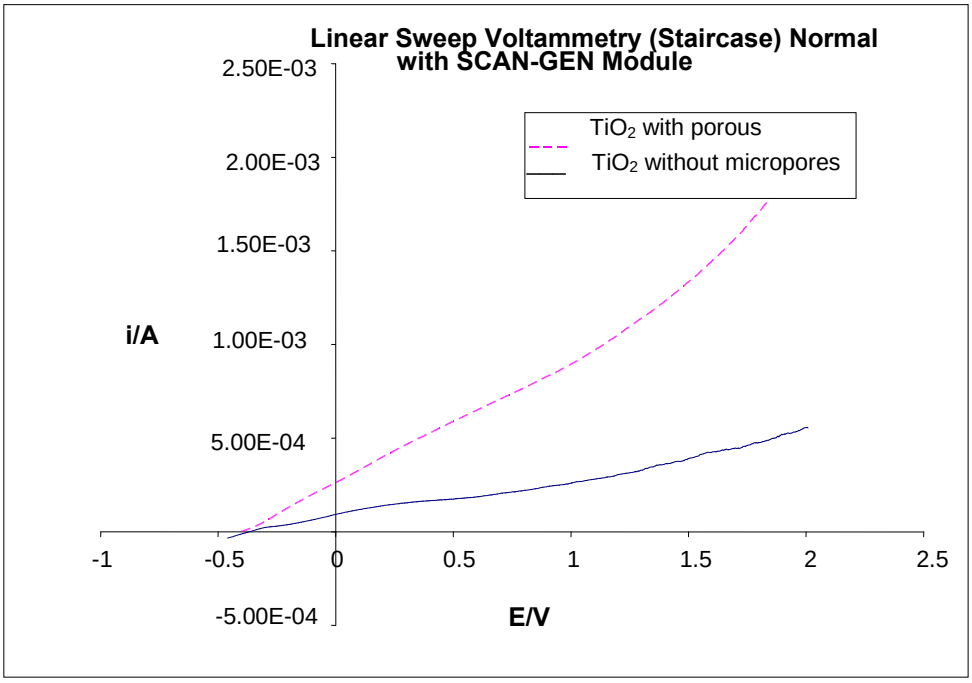

Figure 6.11: Potential vs. current of TiO_2 nanoparticle with/without micropores

Compare scheme of potential vs. current of TiO_2 nano thin film with micropores which was made from 40ml of isopropanol, 4 ml of Tween 85, 1 ml of titanium (IV) isopropoxide 99.999% solution, 1.1g of 1-hexadecylamine at reaction temperature: 150 °C, reaction time: 3 hrs (sample is the same as Figure 6.6), and TiO_2 nanoparticles without porosity which was made by the same formula of TiO_2 nano thin film but reaction time is changed to 6 hrs (sample is the same as Figure 6.3). The dashed line is the potential resultant from the TiO_2 thin film with micropores; while the solid line represents the result of the TiO_2 nanoparticles without micropores. Diluted (0.01M) hydrochloride solution was used for electrolyte solution.

In Figure 6.11, the solid line and dashed red line show the response of the potential to the electric current with TiO_2 electrodes. It measured the variation of the current with potential vs. current curves. Some quantitative analyses (Lagemaat et al., 2000; Mahori et al., 2006) indicated that the electron transfer yield in nanocrystalline TiO_2 solar cell dependents on the electron diffusion coefficient (D). The diffusion coefficient was affected by particle size and density. It was proposed $D \propto n^{-\alpha}$ (Legematt et al., 2000; Mahori et al., 2006; Hou et al., 2005), where α is a parameter of time interval

from 0 to 1, D is electron diffusion coefficient, n is particle density. If the particle density decreases, the electron diffusion coefficient will increase and the electron transportation speed will be enhanced.

Comparing with the dashed line, the current on the electrode make from by the TiO_2 nanoparticles without micropores, the solid line has a smaller increment with the same increase in potential. The microporous structure inTiO_2 nanoparticles apparently help enhance the electron transportation, which is desired for application of TiO_2 materials in making dye-sensitive solar cells.

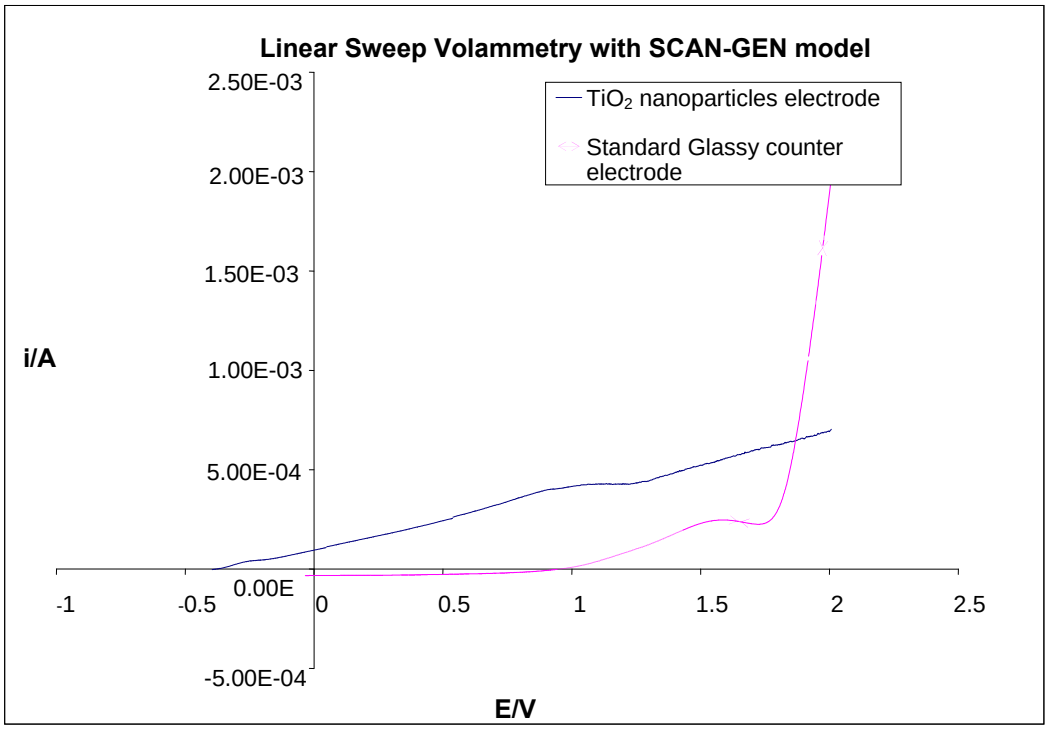

Figure 6.12: Comparison plot of TiO_2 nanoparticle electrode (without pores, sample is same as Figure 6.3) with standard glassy carbon electrode (provide by origin supplier, eco chemie B V)

A comparison measurement was conducted between standard glassy carbon electrode (provided by supplier, Eco Chemie B V) and TiO_2 electrode which is made of the materials without pores synthesized in this work. The other conditions remain the same as when platinum counter electrode was used, Ag/AgCl was used as reference electrode and 0.01M HCl was used as electrolyte. The results are

shown in Figure 6.12. The linear sweep voltammetry model on dummy cell was used for these experiments.

The conductivity of glassy carbon was shown by dashed line and the curve is obviously abruptly up at 1.75v where the TiO_2 curve changes it original manner. This is because the conductivity of glassy carbon is higher than TiO_2 nanoparticle.

Electrochemical voltammetrical analysis for TiO_2working electrode at dummy cell: To achieve high quantum yields in an electron transfer process when the electron is in its excited state, the electrolyte needs to be in ideally intimate contact with the surface of semiconductor. The porous TiO_2 layer in the TiO_2 electrode must exhibit efficient connectivity between nanocrystals to ensure the electron transfer to the collector electrode. Extremely high surface area is required to increase the electron-hole pair density generated at the hybrid interface, and large open pores can promote hole-transporting electron.

We verified the microporous nanoparticles of TiO_2 will increase electron transfer by electrochemical voltammetry measurement.

6.4 Summary

Synthesis of titanium oxide/copolymer films with and without micropores was studied in this chapter. These titania microporous thin films have been characterized through the use of complementary techniques such as XRD, UV-vis., TEM, FESEM, Nanoparticle size analyzer, FTIR, and EDX. Their electrochemical potentiosant voltammetry were analyzed by Current-Voltage testing. Our results indicated that these highly crystallized microporous TiO_2 thin films, compared to the nanoparticle TiO_2 without pores, can enhance the electron transport in electrochemistry voltammtery testing. Due to its favorite electron transportation property, the microporous TiO_2 film is potentially an attractive material for the solid-state dye-sensitized solar cells.

Chapter 7
Conclusions and Recommendations

7.1 Conclusions

Syntheses of the nanostructured Fe_2O_3 and TiO_2 by wet chemistry methods and a self-organized growth mechanism have been studied in this research and reported in this thesis. Organic titanium (TTIP) was used as the precursor for the synthesis of TiO_2 nanomaterials, and $FeCl_3$ was used as the precursor for the synthesis of hematite nanoparticles. Some new discoveries and significant achievements have been made, which are outlined as follows.

1. Uniform hematite nanorods with superparamagentic properties achieved

The controllable of nucleation mechanism in the growth of hematite Fe_2O_3 under a narrow temperature range from 90 to 110 °C has been examined (Chapter 4). Simple starting materials were used. Carbon nanotubes functioned as an inducer which helped with controlling the transformation from Fe_2O_3 nanodots to Fe_2O_3 nanorods. It is revealed that Fe_2O_3 first formed in 1 nm nanodots which were dispersed into the inside and outside of carbon tubes during the initial heterogeneous nucleation. Then the elongated nuclei grew into the rod shape morphology owing to a significant increase in homogeneous nucleation rate. Both temperature and reaction time affect the crystal morphologies and the self-assembling behaviors. The 0.3M concentration and the surfactant percentage also affect the nucleation growth, such that high temperature and high concentration will speed up the nucleation growth to get large crystal morphologies. In particular, using cheap raw materials to make uniform (5 nm in width and 30 nm -50 nm in length) rod shape with super paramagnetic hematite nanomaterial was achieved in this thesis. The nanorods exhibit weakly ferromagnetic and superparamagnetic behavior at room temperature for the powder of Fe_2O_3 nanorods bottom layer (L3). Such synthesized Fe_2O_3 nanorods could potentially find applications in hard disc drives and drug delivery methods of biomedical systems.

2. Anatase TiO_2 hollow nanospheres achieved

Simple "one pot" approach to prepare hollow anatase TiO_2 nanospheres under hydrothermal (or solvothermal as well) conditions was studied (Chapter 5). TTIP was hydrolysized at a temperature range over 130 °C to form small TiO_2 dots, which later moved into a round hollow ring template of oligomers. Internal nanopores and highly organized crystallites in the shell structure and surface regions can be created with a wide range of controlling parameters. The formation of hollow structures in TiO_2 nanospheres could be attributed to the existence of the oligomers. Eventually, a novel method of simple and one step to synthesize TiO_2 hollow nanospheres (100 nm diameter) was reported.

3. TiO_2 microporous thin film achieved

A novel one step self-assembling of titanium oxide/copolymer monolayers nano thin film with micropores has been achieved (Chapter 6). Simple synthesis materials were used to make anatase TiO_2 thin film with micropores (thin film sheet is about 100 - 200 nm width and 200-300 nm length). Two types of TiO_2 electrodes were prepared using TiO_2 thin film with and without nanopores, respectively. The performance of TiO_2 electrodes made by porous TiO_2 thin film on electron transport was examined by electrochemical potential/voltammetry analysis technique. Better performance using anatase TiO_2 microporous thin film has been observed.

Through the thesis, it could be noted that the basic analytical techniques, such as XRD, TEM, HETEM, SEM, FESEM, NanoTRAC, SQUID, FTIR, EDX, BET and electrochemistry voltammeter, etc. are essential and important in the characterization and determination of materials structures and properties.

7.2 Recommendations for future research

7.2.1 Iron oxide nanomaterials

Iron oxide has broad applications which have attracted significant attention of many scientists. Based on our research progress made in this work, the future research is recommended as follows.

7.2.1.1 Synthesis of architected iron oxide nanoparticles

1. Further study on synthesis of iron oxide nanoparticles that are flower shaped and cubic shaped is recommended. Their special characteristics with regards to magnetic properties are to be investigated. Development of new experimental methods / techniques by which only cheap materials are required needs to be investigated so that the economical commercialization could be feasible.

2. Synthesis of core-shell structured iron oxide based nanosized polymer materials is suggested which will have wide application in biomedical and cosmetic areas.

7.2.1.2 Synthesis of iron oxide nanocatalyst

Synthesis of efficient nanocatalysts is a very interesting research topic, and development of novel synthetic routes, advanced characteristic analysis techniques and applications of nanocatalysts calls for more investigation and studies.

1. Investigation on the synthesis of the hybrid metal oxide is desired such like iron oxide and cobalt oxide. The new high efficient catalyst can be used as Fischer-Tropsch catalyst for the petroleum industry.

2. Iron oxide is a photo-catalyst within the visible light wave range. Iron oxide photocatalysts can be used for decomposition of contaminants in the environment; it also can be used for a photocatalyst for many reaction/separation processes in the chemical industry. However, there is insufficient research in this area; therefore, the research on synthesis of iron oxide based photocatalysts and their applications are desired.

3. Further investigation on crystallization of the top layer of nanodots (L11 in chapter 4) via different conditions, such as supercritical fluid condition under recommended.

7.2.2 Titanium oxide based nanoparticles

TiO_2 has unique physicochemical properties, and thus it has a wide range of applications. Based on our research, future work is suggested in these following areas.

1. Further synthesis of TiO_2 nanoparticles with different shapes that possess super photo-catalytic activities for efficient self-cleaning and high UV adsorption ability by wet-chemistry and crystallization is suggested.

2. Synthesis of TiO_2 nanocomposites with copolymers that possess super hydrophilicity for anti-fogging application is recommended. The improved performance of coating with these properties would be very useful for developing new-generation of optical lenses and general glass coating.

3. More electrochemical experiments on TiO_2work electrode aspects need to be carried out based on our current results of TiO_2 microporous thin film in Chapter 6 for electron transfer. Usage of TiO_2 in the dye-sensitive solar cell is a very interesting research topic.

4. TiO_2 is an excellent promoter for a lot of metal catalysts such as iron, cobalt and nickel, etc. Hybrid semiconductor metal oxides are expected to be more efficient catalysts for applications in chemical and biomedical areas. Therefore, synthesis of highly efficient hybrids is another interesting topic for future research.

5. Based on the results of Chapter 5 further studies are desired on the synthesis of hollow nanospheres of TiO_2 aiming at applications for data storage and gas storage.

Nomenclature

α	parameter of time interval
σ_s	saturation magnetization (m^2 kg^{-1} /K)
AC	adventitious carbon
AFM	atomic force microscope
AOP	advanced oxidation process
APCVD	atmospheric pressure chemical vapor deposition
B_{hf}	magnetic hyperfine field (tesla, wb/m^2)
BE	binding energy (eV)
BEs	binding energies (eV)
BET	Brunauer-Emmett-teller method
BJH	Barret-Joyner-Halenda method
BU	1-butanol
CMC	carboxymethyl cellulose sodium
CTAC	cetyltrimethylammonium chloride
CVD	chemical vapor deposition
d	distance between two planes
d_{hkl}	distance between reflection planes (hkl)
Dp	average crystallite size (nm)
DSCs	dye-sensitized solar cells

ED	electron diffraction
EDX	energy dispersive X-ray
EG	ethylene glycol
ESSD	electrostatic sol-spray deposition
FESEM	field emission scanning electron microscopy
FWHM	full width at half maximum
FTIR	fourier transform infrared spectroscopy
HRTEM	high resolution transmission electron microscope
K_{eff}	anisotropy constant (J m^{-3})
LPD	liquid phase deposition
MBE	molecular beam epitaxy
MOCVD	metal-organic chemical vapor deposition
λ	wavelength of X-ray diffraction measurements (nm)
λ_e	wavelength of electron beam (nm)
θ	diffraction angle in the X-ray diffraction measurements (°)
OTE	optical transparent electrode
RMS	root mean square
ROS	reactive oxygen species
SA	Self-assembly
SAED	selected area electron diffraction

SAMs	self-assembling monolayers
SANS	small-angle neutron scattering
SAXS	small-angle X-ray scattering
SPC	superparamagnetic Clustering
SQUID	superconducting quantum interference devices
T	temperature (°C)
T_c,	Curie temperature
T_M	Morin temperature,
TEM	transmission electron microscope
TEOA	triethanolamine
TGA	thermogravimetry analysis
THF	tetrahydrofuran
TMD	trimethylenediamine
TTIP	titanium (IV) isopropoxide 99.999% solution
UV	ultraviolet
VOC	volatile organic compound
XRD	X-ray diffraction

References

Acros, Organis, Inc. : MSDS Catatlog number: P096050, 2006

Adachi, M., Yusuke M. , Jun T., Jiu J., Sakamoto, M., Wang F., Highly Efficient Dye-Sensitized Solar Cells with a TitaniaThin-Film Electrode Composed of a Network Structure of Single-Crystal-like TiO_2 Nanowires Made by the "Oriented Attachment" Mechanism, *J. Am. Chem. Soc*. 126, pp14943-14949, 2004.

Aizenberg, J., Muller, D. A., Grazul, J. L., Hammann, D. R., Direct Fabrication of Large Micropatterned Single Crystals, *Science,* 299, pp1205-1208, 2003.

Al-ekabi, H., Serpone, N., Kinetic-Studies in Heterogenious Photocatalysis 1. Photocatalytic Degradation of Chlorinated phenols in Aerated Aquious-Solutions over TiO_2 Supported on a Glass Matrix, *J. Phys. Chem.*, 92, pp5726-5731, 1988.

Alivisatos, A. P., Semiconductor Clusters, Nanocrystals, and Quantum Dots, *Science,* 271, pp933-937, 1996a.

Amores, J.M.G., Escribano, V.S., Busac. A., Anatase Grystal-growth and Phase-Transformation to Rutile in High-Area TiO_2, MoO_3-TiO_2 and Other TiO_2-Supported Oxided Catalytic-systems, *J. Mater. Chem.,* 5, pp1245-1249, 1995.

Barrett, E. P., Joyner L. G., Halenda P. C., The Determination of Pore Volume and Area Distributions in Porous Substance I. Computations from Nitrogen Isotherm, *J. Am. Chem. Soc.,* 73, pp 373-380, 1951.

Beijer, F. H., Kooijman H, Spek, A. L. Sijbesma, R. P. and Meijer, E. W., Self-Complementarity Achieved through Quadruple Hydrogen Bonding, *Angewa. Intern, Editi,* 37, pp75-78, 1998

Beltran, E. L., Philippe Prene, Boscher C., Belleville P., Buvat P., Lambert S., Guillet, F., Bossiere, C., Grosso, D., Sanchez, C., Nanostructured Hybrid Solar Cells Based on Self-Assembled Mesoporous Titania Thin Films, *Chem Mater.* 18, pp 6152-6156, 2006.

Benoit-Marquie, F., Wilkenhonera, U. , Simonb, V., Braunc, A. M., Oliverosc, E., Maurettea, M. T., VOC Photodegradation at the Gas-Solid Interface of a TiO_2 Photocatalyst: Part 1: 1-Butanol and 1-Butylamine, *J. Photochem. Photobiol. A: Chem.*, 132, pp 225-232, 2000.

Black, N.R., Griffin, G. L., Selectivity Control during the Photoassisted Oxidation of 1-Butanol on Titanium Dioxide, *J. Phys. Chem.,* 92, pp 5697-5701, 1988.

Blake R L , Hessevick R E , Zoltai T , Finger L W , Refinement of the hematite structure, *American Mineralogist* , 51, pp 123-129, 1966

Bragg, W.H., Bragg. W. L.<< X-rays and Crystal structure>>, *G. Bell and Sons, London*, 3rd ed., pp 50-80, 1918.

Brunauer, S., Emmett, P. H. and Teller, E., Adsorption of Gases in Multimolecular Layers, *J. Am. Chem. Soc.*, 60, pp 309-319, 1938.

Brunauer, S., Deming, L. S., Deming, W. S., and Teller, E., A Theory of the Van der walls Adsorption of Gases, *J. Am. Chem. Soc.*, 62, pp 1723-1732, 1940.

Bullen, H.A.,Garrett, S. J., TiO_2 Nanoparticles Arrays Prepared Using a Nanosphere Lithography Technique, *Nano Lett.*, 2, pp 739-745, 2002.

Burnside, S.D., Shklover V., Barbe C., Comte P., Arendse F., Brooks K., Gratzel M. , Self-Organization of TiO_2 Nanoparticles in Thin Films,. *Chem. Mater.,* 10, pp 2419-2425, 1998.

Burleson, D J., Lee, R. Penn., Two-Step Growth of Goethite from Ferrihydrite, *Langmuir,* 22, pp 402-409, 2006,

Byrappa, K., Yoshimura M., Handbook of Hydrothermal Technology: A Technology for Crystal Growth and Materials Processing. *New York: Noyes Publications,* pp 717-725, 2001.

Campbell, J. S., Graven, P., Young, P.W., Remvoal of carbon monoxide. In: Catalyst Handbook. *Wolfe Scientific Books ,* pp 97-126, 1970.

Campus, F., Bonhote, P., Gratzel, M., Heinen, S., Walder., L., Electrochromic Devices Based on Surface-Modified Nanocrystalline TiO_2 Thin film Electrodes, *Solar Energy and Solar Cells,* 56, pp 281-297. 1999.

Carpenter, E.E., Iron nanoparticles as potential magnetic carriers, *J. Magn. Magn. Mater.* 225, pp17-22, 2001

Chan. C.S., Stasio G. D., Welch, S. A., Girasole, M., Frazer, B. H., Nesterova, M.V., Fakra, S., Banfield., J.F., Microbial Polysaccharides Template Assembly of Nnaocrystal Fibers, *Science*, 303, pp 1656-1658, 2004.

Chang, Y., Teo, J. J., Zeng, H. C., Large-Scale Synthesis of High-Quality Ultralong Copper Nanowires, *Langmuir*, 21, pp 1074-1078, 2005.

Chemseddine, A., Moritz., T., Nanostructuring Titania: Control over Nanocrystal Structure, Size, Shape, and Organization, *Eur. J. Inorg. Chem.*, 1, pp 235-245, 1999.

Chen, Q., Qian Y., Chen Z., Zhou G., Zhang Y., Preparation of TiO_2 Powders with Different Morphologies by an Oxidation Hydrothermal Combination Method, *Mater. Letts.,* 22, pp 77-80, 1995.

Chen. C., Qi X., Zhou B., Photosensitization of Colloidal TiO_2 with a Cyanine Dye, *J. Photochem. Photobiol. A: Chem.*, 109, pp 155-158, 1997.

Chen, J.，Xu, L. N.， Li, W. Y.，Gou, X. α- Fe_2O_3 Nanotubes in Gas Sensor and Lithium-Ion Battery Applications, *Adv. Mater.* 17, pp 582-586, 2005.

Cheng, H., Ma J.， Zhao J， Qi, .L, Hydrothemal Preparation of Uniform Nanosize Rutile and Anatase Particles, *Chem. Mater.,* 7, pp 663-671, 1995.

Cheng, K.，He Y. P.，Miao Y. M.， Zou, B. S.， Wang Y. G.，Wang,T. H., Zhang, T.X., Du, L., Quantum Size Effect on Surface Photovoltage Spectra: Alpha- Fe_2O_3 Nanocrystals on the Surface of Monodispersed Silica Microsphere. *J. Phys. Chem.B*, 110, pp 7259-7264, 2006.

Choi, C.J., Dong, X.L., Kim, B. K., Microstructure and Magnetic Properties of Fe Nanoparticles Synthesized by Chemical Vapor Condensation, *Mater. Trans.* 42, pp 2046-2049, 2001.

Choi, S.H., Kim, E.-G., Hyeon, T. One-Pot Synthesis of Copper-Indium Sulfide Nanocrystal Heterostructures with Acorn, Bottle, and Larva Shapes, *J. Am. Chem. Soc.*, 128, pp 2520-2521, 2006.

Coakley, K. M., Liu, Y. X., Goh, C., Mc Gehee, M. D. Ordered organic-inorganic bulk heterojunction photovoltaic cells Source*, MRS Bulletin*., 30 (1), pp 37-40, 2005.

Collins, A., Cariazo, D., Davis, S. A., Mann, S. Spontaneous template-free assembly of ordered macroporous titania*, Chem Commun.* 5, pp 568-572, 2004.

Cornell, R.M., U. Schwertmann, << The Iron Oxides: Structure, Properties, Reactions, Occurrences and Uses >>, 2nd, *New York, Wiley-Vch GmbH & Co. KGaA.*, pp 11-30, 2002.

Cozzoli, P. D., Comparelli, R., Franizza, E., Curri, M. L., Agostiano, A., Laub, D., Photocatalytic Synthesis of Silver Nanoparticles Stabilized by TiO_2 Nanorods: A semiconductor/Metal Nanocomposite in Homogeneous Nonpolar Solution, *J. Am. Chem. Soc.,* 125, pp 3868-3879, 2003.

Dang, M.Z., Rancourt, D. G., Dutrizac, J. E., Lamarche, G., Provencher, R., Interplay of Surface Conditions, Particle Size, Stoichiometry, Cell Parameters, and Magnetism in Synthetic Hematite-like Materials, *Hyperfine Interactions*, 117, pp 271-319, 1998.

Dasilva SW, Pedroza, R.C. Sartoratto, PPC., Rezende, D.R., Raman spectroscopy of cobalt ferrite nanocomposite in silica matrix prepared by sol–gel method, *J. Non-crystal Alline Solid,* 352, pp1602-1606, 2006.

Deki, S., Y. Aoi, O. Hiroi, A. Kajinami. Titanium (IV) oxide Thin Films Prepared from Aqueous Solution, *Chem. Lett.*, pp433-434, 1996.

Diebold, U. The Surface Science of Titanium Dioxide*, Surface Science Report,* 48, pp53-229, 2003.

Domaradzki J, Kaczmarek D, Prociow E L, Borkowska A, Schmeisser D, Beuckert D, Microstructure and optical properties of TiO_2 thin films prepared by low pressure hot target reactive magnetron sputtering, *Thin Solid Film,* 513, pp 269-274, 2006

Dong, L.M., Han Z.D., Zhang, Y. M., Wu, Z., Zhang, X.Y. Synthesis of hexagonal barium ferrite nanoparticle by sol-gel method, *Rare Metals*, 25, pp605-608, 2006.

Eco Chemie B V, technical data sheet and manual of PGSTAT30, *Eco Chemie B V,* 2001.

Elsner, M., Haderlein, S.B.; Kelerhals, T., Luzi, S., Zwank, L., Angst, W. Schwarzenbach, R. P., Mechanisms and Products of Surface-Mediated Reductive Dehalogenation of Carbon Tetrachloride by Fe(II) on Goethite*Environ. Sci. Technol*. 38, pp2058-2066, 2004.

Fahmia, A., Minot, C., A Theoretical Investigation of Water-Adsorption on Titanium-dioxide surfaces, Surface Science, 304, pp 343-359, 1994.

Fanizza, E.; Cozzoli, P. D.; Curri, M. L.; Striccoli, M.; Sardella, E.; Agostiano, A., UV-Light-Driven Immobilization of Surface-Functionalized Oxide Nanocrystals onto Silicon *Adv. Func. Materials*., 17, pp201-211, 2007.

Forster, A. B., Fitremann, J. Renaud, P. Synthesis of (±)-Nephromopsinic, (-)-Phaseolinic, and (-)-Dihydropertusaric Acids*, Helvetica Chimica Acta*, 85, pp 3965-3974, 2002

Fu, S Y., Wei, C. C., Yang, J.M., and Chen T. H., Crystallite Size Variations of Nanosized Fe_2O_3 Powders during ç- to r-Phase Transformation, *Nano letters*, 2, No. 3, pp 245-252, 2002

Fu, Y. Y., Wang, R. M.; Xu, J., Chen, J., Yan, Y., Narlikar, A. V., Zhang, H. Synthesis of large arrays of aligned α-Fe_2O_3 nanowires, *Chem. Phys. Lett*., 379, Is 3-4, pp 373-379, 2003.

Fujishima, A., Honda, K., Electrochemical Photolysis of Water at a Semiconductor Electrode, *Nature*, 238, pp 37-38, 1972.

Gao, C., Li W., Hisao Morimoto, Yutaka Nagaoka, Toru Maekawa, Magnetic Carbon Nanotubes: Synthesis by Electrostatic Self-Assembly Approach and Application in Biomanipulations, *J, Phys. Chem. B* 110, pp7213-7220, 2006.

Gates, B.in, Y., Xia, Y. A Solution-Phase Approach to the Synthesis of Uniform Nanowires of Crystalline Selenium with Lateral Dimensions in the Range of 10-30 nm, *J. Am. Chem. Soc.,* 122, pp 12582-12583, 2000.

Georgakilas, Vasilios, Vasilios Tzitzios, Dimitrios Gournis and Dimitrios Petridis, Attachment of Magnetic Nanoparticles on Carbon Nanotubes and Their Soluble Derivatives, *Chem. Mater.,* 17, No. 7, pp 1613-1617, 2005.

Gerfin, T., Grätzel, M. Walder, L., Molecular and Supramolecular Surface Modification of Nanocrystalline TiO_2 films: Charge-Separating and Charge-Injecting Devices , *Progr. Inorg. Chem.,* 44, pp345-393, 1997.

Grätzel, M., Photoelectrochemical Cells, *Nature,* 414, pp 338-344, 2001.

Guirado, Francesc, Salvador Galí, Servando Chinchón, Jordi Rius, Crystal Structure Solution of Hydrated High-Alumina Cement from X-ray Powder Diffraction Data , *Angew. Chem. Int. Ed.,* 37(1-2), pp72-75, 1998.

Gupta, A. K., Gupta, M., Synthesis and surface engineering of iron oxide nanoparticles for biomedical applications, *Biomaterials*, 26, pp 3995- 4021, 2005.

Guo, C.W., Cao, Y., Xie, S. H., Dai W. L., and Fan K. N., Fabrication of Mesoporous Core-Shell Structured Titania Microspheres with Hollow Interior, *Chem. Commun.*, 6, pp700-701, 2003.

Hagfeldt, A., Grätzel, M.， Molecular Photovoltaics，Acc. *Chem. Res*. 33, pp269-277, 2000.

Holland, B. T., Blanford, C. F., Do, T., Stein, A., Synthesis of Macroporous Minerals with Highly Ordered Three-Dimensional Arrays of Spheroidal Voids, *Science*, 330, pp533-534, 1998.

Hou, K., Tian, B.,Li, F.; Bian, Z.,Zhao, D.,Huang, C. Highly Crystallized mesoporous TiO_2 films and their applications in dye sensitized solar cells, *J. Mater. Chem.,* 15, pp 2414-2416, 2005

Huang, Y., Duan X., Wei Q., and Lieber C. M., Directed Assembly of One-Dimensional Nanostructures into Functional Networks, *Science*, 291, pp 630-633, 2001.

Huffman, G.P., Ganguly, B., Zhao, J., Rao, K.R.P.M., Shah, N., Feng, Z., Huggins, F.E., Taghiei, M.M.,Lu, F., Wender, I., Pradhan, V.R., Tierney, J.W., Seehra, M.S., Ibrahim, M.M., Shabtai, J., Eyring, E. M., Structure and dispersion of iron-based catalysts for direct coal liquefaction, *Engergy & Fuels* 7, pp285-296, 1993.

Iidia, M., T. Sasaki, and M. Watanabe. Titanium Dioxide Hollow Microsphere with an Extremely Thin Shell, *Chem. Mater.,* 10, pp3780-3782, 1998.

Imai, H. Y. Takei, K. Shimizu, M. Mastsuda, and H. Hirashima.Direct Preparation of Anatase TiO_2 Nnaotubes in Porous Alumina Membranes, *J. Mater. Chem.,* 9, pp 2971-2972, 1999.

Imai, H., M. Matsuda, K. Shimizu, H. Hirashima, and N. Negishi. Preparation of TiO_2 Fibers with Well-Organized Structures, *J. Mater. Chem.*, 10, pp 2005-2006, 2000.

Imai, H., Terada, T., Yamabi S,. Self-Organized Formation of a Hierarchical Self-Similar Structure with Calcium Carbonate, *Chem. Comm.,* 2, pp 484-485, 2003.

Jana, N. R., Shape Effect in Nanoparticle Self-Assembly, *Angew. Chem. Int. Ed.*, 43, pp1536-1540, 2004.

Jiang, W.Q., Yang H.C., Yang S.Y., Hong, H.E., Hung, J.C., Chen, Y.C., and Hon, C.Y.. Preparation and properties of superparamegnetic nanoparticles with narrow size distribution and biocompatible, *J. Magn. Magn. Mater*. 283, pp 210-213, 2004.

Jung, J. H., H. Kobayashi, K. J. C. van Bommel, S. Shinkai, and T. Shimizu., Creation of Novel Helical Ribbon and Double-Layered Nanotube TiO_2 Structures Using an Organogel Template, *Chem. Mater.*, 14, pp 1445-1447, 2002.

Kavan, L., Rathousky, J., Grätzel, M., Shklover, V., Zukal, A, Mesoporous thin film TiO_2 electrodes, *Microporous /Mesoporous Mater*., 44-45, pp653-659, 2001.

Kim, C.K., Moon, B.K., Park, J.H., Choi, B.C., Seo. H. J, Solvethermal Synthesisi of Nanocrystalline TiO_2 in Toluene with Surfactant, *J. Crystal Growth*, 257, pp 309-315, 2003.

Kim, D.H.,A. Adnerson., Photoelectrocatalytic Degradation of Formic-Acid Using a Porous TiO_2 Thin-film electrode, Environ. *Sci. Technol.*, 28, pp 479-483. 1994.

Kim, D.K., Zhang, Y.,Voit, W., Kao, K.V., Kehr, J., Bjelke, B., Muhammed, M., Superparamagnetic iron oxide nanoparticles for bio-medical applications, *Scr. Mater.* 44, pp1713-1716, 2001.

Kim, Minsuk, Kwonnam Sohn, Hyon Bin Na, and Taeghwan Hyeon, Synthesis of Nanorattles Composed of Gold Nanoparticles Encapsulated in Mesoporous Carbon and Polymer Shells , *Nano Letters,* 2 (12), pp 1383-1387, 2002.

Kominami, H., M. Kohno, and Y. Kera., Synthesis of Brookite Type Titanium Oxide Nanocrystals in Organic Media, *J. Mater. Chem*., 10, pp 1151-1156, 2000.

Kong, X. Y., Ding Y., Yang R., and Wang Z L., Single-Crystal Nnaorings Formed by Epitaxial Self-Coiling of Polar Nanobelts, *Science*, 303, pp 1348-1351, 2004.

Konishi, Junko., Koji Fujita, Kazuka Nakanishi and Kazuyuki Hirao, Monolithic TiO_2 with Controlled Multiscale Porosity via a Template-Free Sol-Gel Process Accompanied by Phase Separation, *Chem. Mater.* 18, pp 6069-6074, 2006.

Korgel, B. A. Self-Assembled Nanocoils, *Science,* 303, pp 1308-1309, 2004.

Kormann, C., Bahnemann, D. W., Hoffmann, M. R. Preparation and characterization of quantum-size titanium dioxide, *J. Phys. Chem.* 92, pp 5196-5201, 1988.

Kowsowski, B.M., Paper presented at "iron oxides in colorant and chemical application "*Intertec. conferences. Wasahington, D.C.* 1993

Kwon, K-w., Bo H Domaradzki J, Lee and Moonsub Shim, Structural Evolution in Metal Oxide/Semiconductor Colloidal Nanocrystal Heterostructures, *Chem. Mater*., 18, pp 6357-6363, 2006

Lagemaat, V. J., frank, A.J., Effect of the Surface-State Distribution on Electron Transport in Dye-Sensitized TiO_2 Solar Cells: Nonlinear Electron-Transport Kinetics, *J. Phys. Chem. B*, 104, pp 4292-4297, 2000

Larsen, T.H., M. Sigman, A. Ghezelbash, R.C. Doty, and B. Korgel., Solventless Synthesis of Copper Sulfide Nanorods by Thermolysis of a Single Source Thiolate-Derived Precursor, *J. Am Chem. Soc.*, 125, pp 5638-5639, 2003.

Laudise, R. A. Hydrothermal Synthesis of Crystals, *C & EN* , Sept. 28, pp 30-43, 1987

Lazzeri, M., Vittadini, A., Selloni, A., Structure and Energetics of Stoichiometric TiO_2 Anatase Surfaces, *Phys. Rev. B,* 63, Art. No.155409, 2001.

Lazzeri, M., Vittadini,A., Selloni A., Structure and Energetics of Stoichiometric TiO_2 Anatase surfaces, *Phys. Rev. B*. 65, Art. No.119901,2002.

Lee, I., Han, S.W., Lee, S. J., Choi, H. J., Kim., K., Formation of Patterned Continuous Calcium Carbonate Films on Self-Assembled Monolayers via Nanopartile-Directed Crystallization, *Adv. Mater.*, 14, pp 1640-1643, 2002.

Lee, S. W.; Lee, S.K.; Belcher, A.M, Virus-Based Alignments of Inorganic Organic and Biological nanosized Materilas, *Adv. Mater.,* 15, pp 689-692, 2003.

Legrini, O., Oliveros E., Belcher A. M., Photochemical Processes for Water-Treatment., *Chem. Rev,* 93, pp 671-698, 1993.

Lehn, Jean- Marie, Towared Self-Organization and Complex Matter, *Science*, 295, pp 2400-2403, 2002.

Li, J, Zeng, H.C. Size-Tuning, Functionalization, and Reactivation of Au in TiO_2 Nanoreactors, *Angew. Chem., Int. Ed*. 44, pp 4342-4345, 2005.

Li, L., Ying C., Yang L., Dong L., Template-Free Synthesis and Photocatalytic Properties of Novel Fe_2O_3 Hollow Spheres*, J. Phys.Chem.C.*, 111, pp2123-2127, 2007.

Li, L., Fan, M., Brown, R.C.,Leeuwan, V.J.,Wang, J., Wang, W., Song, Y., Zhang, P. Critical reviews , *Environomental Science & Tech*., 36, pp 405-431, 2006.

Linsebigler A., Lu, G., Yates, T., Photocatalysis on TiO_2 Surfaces: Principles, Mechanisms, and Selected Results, *Chem. Rev*., 95, pp 735-758, 1995.

Lisiechi, I., Albouy, P. A., Pileni, P. M., Face-Centered Cubic supracrystals of cobalt nanocrystals, *Adv. Mater*., 15, pp 712-716, 2003.

Liu, B., Yu, H. S., Zhang, F., Li, L., Zhang, Q., Ren, L., Jiang, K., Ring-like Nanosheets Standing on Spindle-Like Rods: Unusual ZnO Superstructures Synthesized from a Flakelike Precursor Zn5(OH)8Cl2.H2O, *J. Phys, Chem. B,* 108, pp4338-4341, 2004.

Liu, Z.L., Wang, H.B., Lu, Q.H., Du, G.H., Peng, L., Du, Y.Q., Zhang, S.M. and Yao, K.L. Synthesis and characterization of ultrafine well-dispersed magnetic nanoparticles, *J. Magn. Magn. Mater.,* 283, pp 258-263, 2004.

Mahori, H., Hayashi, S., Umeyama, T., Eu, S., Oguro, A., Kang, S., Matano, Y., Shishido, T., Ngamsinlapasathian, S., Yoshikawa, S., Comparison of Electrode Structures and Photovoltaic Properties of Porphyrin-Sensitized Solar Cells with TiO_2 and Nb, Ge, Zr-Added TiO_2 Composite Electrodes , *Langmuir,* 22, pp11405-11411, 2006.

Marketa Zukalova, Arnost Zukal, Ladislav Kavan, Mohammad K. Nazeeruddin, Paul Liska and Michael Gratzel, Organized Mesoporous TiO_2 Films Exhibiting Greatly Enhanced Performance in Dye-Sensitized SolarCells Marke, *Nano Letters,* 5 (9), pp 1789-1792, 2005.

Masuda, Y., Jinbo, Y., Yonezawa, T., Koumoto, K., Templated Site-Selective Deposition of Titanium Dioxide on Self-Assembled Monolayers, *Chem. Mater*., 14, pp 1236-1241, 2002a.

Masuda, Y., Sugiyama, T., Koumoto, K., Micropatterning of Anatase TiO_2 Thin Films from an Aqueous Solution by a Site-Selective Immersion Method, *J. Mater. Chem.*, 12, pp 2643-2647, 2002b.

Mazeina, Lena, Navrotske, A., Enthalpy of Water Adsorption and Surface Enthalpy of Goethite (α-FeOOH) and Hematite (α-Fe_2O_3), *Chem. Mater*., 19, pp 825-833, 2007.

McCormick, M.L., Adriaens, P., Carbon Tetrachloride Transformation on the Surface of Nanoscale Biogenic Magnetite Particles*, Environ. Sci. Technol.* 38, pp 1045-1048, 2004.

Messer, B., Song, J. H., Huang, M., Wu, Y., Kim, F., Yang, P., Surfactant-Induced Mesoscopic Assemblies of Inorganic Molecular Chains, *Adv. Mater.,* 12, pp 1526-1528, 2000.

Microtrac Inc, MSDS and technical data sheet, *Micro Trac Inc,* 2007

Mohamed S. Hamdy, Otto Berg, Jacobus C. Jansen, Thomas Maschmeyer, Jacob A. Moulijn, Guido Mul, TiO_2 Nanoparticles in Mesoporous TUD-1: Synthesis, Characterization and Photocatalytic Performance in Propane Oxidation*, Chem. Eur. J*. 12, pp 620-628, 2006.

Morales, A.M., Lieber,C.M., A Laser Ablation Method for the Synthesis of Crystalline Semiconductor Nanowires, *Science,* 279, pp 208-211, 1998.

Moritz, T., Reiss, J., Diesner, K., Su, D., Chemseddine, A., Nanostructured Crystalline TiO2 through Growth Control and Stabilization of Intermediate Structural Building Units, *J. Phys, Chem. B,* 101, pp 8052-8053, 1997.

Motte, L., Billoudet, F., Lacaze, E., Pileni M. P., Self-Organization of Size-Selected Nanoparticles into Three-Dimensional Superlattices, *Adv. Mater.*, 8, pp 1018-1020. 1996.

Murray,C.B., Kagan,C. R., Bawendi M.G., Synthesis and Characterization of Monodisperse Nanocrystals and Close-Packed Nanocrystal Assemblies, *Annu. Rev. Mater. Sci.*, 30, pp545-610, 2000.

Naoi, K., Ohko, Y., Tatsuma, T., TiO_2 Films Loaded with Silver Nanoparticles: Control of Multicolor Photochromic Behavior, *J. Am. Chem. Soc.*, 126, pp 3664-3668, 2004.

Nazeeruddin, M.K., Kay, A., Rodicio, I., Humphry-Baker, R., Muller, E., Liska, P., Vlachopoulos, N., Grätzel, M., Conversion of Light to Electricity by Cis-X2bis (2,2'-Bipyridyl-4,4'-Dicarboxylate) Ruthenium (II) Charge-Transfer Sensitizers (X=Cl^-, Br^-, I^-, and SCN^-) on Nnaocrystalline TiO_2 electrodes, *J. Am. Chem. Soc.,* 115, pp 6382-6390, 1993.

Niederberger, M., Bartl, M. H.M.,Stucky, D., Benzyl Alcohol and Transition Metal Chlorides as a Versatile Reaction System for the Nonaqueous and Low-temperature Synthesis of Crystalline Nano-objects with Controlled Dimensionality, *J. Am. Chem. Soc.,* 124, pp13642-13643, 2002

Niu, H., Chen, Q., Ning, M., Jia, Y., Wang, X., Synthesis and One-Dimensional Self-Assembly of Acicular Nickel nanocrystallites under Magnetic Fields, *J. Phys, Chem. B,* 108, pp3996-3999, 2004.

Ohko, Y., Tatsuma, T., Fujii, T., Naoi, K., Niwa, C., Kubota, Y., Fujishima, A., Multicolour Photochromism of TiO_2 Films Loaded with Silver Nanoparticles, *Nat. Mater.*, 2, pp 29-31, 2003.

O'regan, M. Grätzel., A Low-Cost, High-Efficiency Solar-Cell Based on Dye-Sensitized Colloidal TiO_2 Films, *Nature*. 353, pp 727-740, 1991.

Ottermann, C R, Bange, K., Correlation beTween the density of TiO_2 films and their properties, *Thin solid films,* 286, pp 32-34, 1996.

Park, C. D., Magana, D., Stiegman, A. E., High-Quality Fe and γ-Fe_2O_3 Magnetic Thin Films from an Epoxide-Catalyzed Sol-Gel Process, *Chem Mater*, 19, pp 677-683, 2007.

Park, H., Choi, W., Effects of TiO_2 Surface Fluorination on Photocatalytic Reactions and Photoelectrochemical Behaviors, *J. Phys. Chem. B*, 108, pp 4086- 4093, 2004.

Park, S. J., Kim, S., Lee, S., Zheong, G., Khim, K. C., Hyeon,T., Synthesis and Magnetic Studies of Uniform Iron Nanorods and Nanospheres, *J. Am. Chem. Soc*.,122, pp 8581-8582, 2000.

Patzke, G.R., Krumeich, F., Nesper, R., Oxidic Nanotubes and Nanorods-Anisotropic Modules for a Future Nanotechnology, *Angew. Chem. Int. Ed.,* 41, pp 2446-2461, 2002.

Pėral, J., Ollis, D. F., Heterogeneous Photocatalic Oxidation of Gas-Phase Organics for Air Purification-Acetone, I-Butanol, Butyraldehyde, Formaldehyde, and Metal-Xylene Oxidation, *J. Catal.*, 136, pp 554-565, 1992.

Philip, E. M., Pemble, D., Sheel, W., Precursor-Directed Control of Crystalline Type in Atmospheric Pressure CVD Growth of TiO_2 on Stainless Steel, *Chem. Mater*, 18, pp 5750-5755, 2006.

Piotrowiak, P.,Galoppini, E.; Wei, Q., Meyer, G. J.,Wiewior, P. Subpicosecond Photoinduced Charge Injection from "Molecular Tripods" into Mesoporous TiO_2 Over the Distance of 24 Angstroms *J. Am. Chem. Soc*., 125, pp 5278-5279, 2003.

Polleux, J., Pinna, N., Antonietti, M., Niederberger, M., Ligand-Directed Assembly of Preformed Titania Nanocrystals into Highly Anisotropic Nanostructures, *Adv. Mater.,* 16, pp 436-439, 2004.

Puntes, V.F., Zanchet, D., Erdonmez, C. K., Alivisatos, A. P., Synthesis of hcp-Co Nanodiskes, *J. Am. Chem. Soc.,* 124, pp 12874-12880, 2002.

Qian, Y., Q. Chen, Z. Chen, C. Fan, G. Zhou, Preparation of Ultrafine Powders of TiO_2 by hydrothermal H_2O_2 Oxidation Starting from Metallic Ti, *J. Mater. Chem*., 3, pp 203-205, 1993.

Rabani, E., D.R. Reichman, P.L. Geissler, L.E. Brus., Drying-Mediated Self-Assembly of Nanoparticles, *Nature*, 426, pp 271-274, 2003.

Raghavender A.T., Pajic, Zadro, D., Milekovic, K., Rao, T., Jadhav, P.V., Ravinder, K. M., Synthesis and magnetic properties of $NiFe_{2-x}Al_xO_4$ nanoparticles, *J. Magnetism and Magnetic Materials,* 316, pp1-7, 2007.

Rao, C. N. R., Kulkarni G. U., Thomas P. J., Edwards, P.P., Size-Dependent Chemistry: Properties of Nanocrystals, *Chem-Eur. J.*, 8, pp29-35, 2002.

Reddy, K.M., Manorama, S.V., Reddy, A.R., Preparation, Characterization, and Spectral Studies on Nanocrystalline Anatase TiO_2, *J. Solid State Chem*, 158, pp180-186, 2001.

Salafsky, J. S,. A 'channel' design using single, semiconductor nanocrystals for efficient (opto)electronic devices, *Solid-State Electron.*, 45, pp 53-58, 2001.

Salgueiriño-Maceira, V., Correa-Duarte, M. A., Spasova, M., Liz-Marzán, L. M. Composite Silica Spheres with Magnetic and Luminescent Functionalities, *Adv. Funct. Mater*. 16, pp 509-514, 2006.

Samsonov, G.V., The Oxide Handbook. New York: *IFI/Plenum Press.* 9, pp463-464,1982.

Sartoratto, P.P.C., Calado, K.L., Pedroza, R.C., Da Silva, S.W., Morais, P.C., The thermal stability of maghemite-silica nanocomposites: An investigation using X-ray diffraction and Raman spectroscopy, *J. Alloys and compounds ,* 434, pp 650-654, 2007.

Sasaki, T., Watanabe, M., Hashizume, H., Yamada, H., Nakazawa., H., Macromolecule-Like Aspects for a colloidal Suspension of an Exfoliated Titanate. Pairwise Association of Nanosheets and Dynamic Reassembling Process Initiated from It, *J. Am. Chem. Soc.,* 118, pp 8329-8335, 1996.

Sasaki, T., Nakano, S., Yamauchi, S., Watanabe, M., Fabrication of Titanium Dioxide Thin Flakes and Their Porous Aggregate, *Chem. Mater.,* 9, pp 602-608, 1997.

Sasaki, T., Watanabe, M., Osmotic Swelling to Exfoliation. Exceptionally High Degree of Hydration of a Layered Titanate, *J. Am. Chem. Soc.,* 120, pp4682-4689, 1998.

Schnaitmann Dieter, Martin Bohmer, Manfred Urban, Process for the preparation of liquid pigment preparations, *US patent, No. 675448* ,1998.

Schűth, F., Non-siliceous Mesostructured and Mesoporous Materials, *Chem. Mater.*, 13, pp 3184-3195, 2001.

Seo, D.S., Lee, J. K., Kim, H., Preparation of nanotube-shaped TiO_2 powder *J. Cryst. Growth*, 229, pp 428-432, 2001.

Serpone, N., Lawless, D., Khairutdinow, R., Size Effects on the Photophysical Properties of Colloidal Anatase TiO_2 Particles: Size Quantization versus Direct Transitions in This Indirect Semiconductor, *J. Phys. Chem.*, 99, pp 16646-16654, 1995.

Sherman, D. M., Waite, T. D., Electronic spectra of Fe^{3+} oxides and oxide hydroxides in the near IR to near UV, *Am. Mineral*. 70, pp1262-1265, 1985,

Shimizu, K., Imai, H., Hirashima, H., Tsukuma, K., Low-Temperature Synthesisi of Anatase Thin films on Glass and Organic substrates by direct deposition from Aqueous Solutions, *Think Solid Films,* 351, pp 220-224, 1999.

Shull, C. G., Strauser, W. A., Wollan, E. O. Neutron Diffraction by Paramagnetic and Antiferromagnetic Substances , *Phys. Rev.*, 83, 2, pp 333-345,1951.

Song, G.P., Bo, J., Guo, R.,The characterization and property of polystyrene compounding of α-Fe_2O_3 in the nanoscale, *Colloid, Poly. Science,* 282, pp 656-658, 2004.

Smyth, J. R., Bish D. L., Crystal Structures and Cation Sites of the Rock-Forming Minerals, *Allen and Unwin, Boston,* pp 358-368, 1988.

Suber L., Fiorani D., Imperatori P., Foglia S., Montone A., Zysler R., Effects of thermal treatments on structural and magnetic properties of acicular α-Fe_2O_3 nanoparticles, *Nanostructured Materials,* 11, pp 797-803, 1999

Sugawara, A., T. Ishii, T. Kato., Self-Organized Calcium Carbonate with Regular Surface-Relief Structures, *Angew. Chem. Int. Ed.,* 42, pp 5229-5303, 2003.

Sugimoto, T., Zhou X., Muramatsu, A., Synthesis of Uniform Anatase TiO_2 Nanoparticles by Sol-Gel Method 3. Formation Process and Size Control, *J. Colloid Interface Sci.,* 259, pp 43-52, 2003.

Sun, S, Simone Anders, Hendrik F. Hamann, Thiele, J.U., Baglin, J.E.E., Thomason, T., Fullerton, C. Murray, B., Terris, B. D., Polymer Mediated Self-Assembly of Magnetic Nanoparticles, *J. Am. Chem.Soc.* 124 (12), pp 2884-2885, 2002.

Sun, X., Li Y., Synthesis and Characterization of Ion-exchangeable Titanate Nanotubes, *Chem. Eur. J.*, 9, pp 2229-2238, 2003.

Tachibana, Y., Hara, K., Sayama, K., Arakawa, H., Quantitative Analysis of Light-Haresting Efficiency and Electron-Transfer Yield in Ruthenium-Dye-Sensitized Nanocrystalline TiO_2 Solar Cells, *Chem. Mater.,* 14, pp 2527-2535, 2002.

Tang, B., Wang, G, Zhou L, Ge, J, Gui L, Facile Route to α-FeOOH and α-Fe_2O_3 Nanorods and Magnetic Property of α-Fe_2O_3 Nanorods *Inorg. Chem*., 45, 13, pp 5196-5200, 2006.

Tang, J , Redl F., Zhu Y, Theo Siegrist, Louis E. Brus, Michael L. S., An Organometallic Synthesis of TiO_2 Nanoparticles, *Nano Letters,* 5 , pp 543-548, 2005.

Tian, Z. R., Liu J., Xu H., Voigt, J. A., Mckenzie, B., Matzke, C.M., Shape-Selective Growth, Patterning, and Alignment of cubic Nanostructured Crystals via Self-Assembly, *Nano Lett.,*3, pp 179-182, 2003a.

Tian, Z.R., Liu J., J.A. Voigt, B. Mckenzie, Xu H., Hierarchical and Self-Similar Growth of Self-Assembled Crystals, *Angew.Chem. Int. Ed.*, 42, pp 413-417, 2003b.

Tian, Z. R. Voigt, J. A., Liu J, B. Mckenzie, Xu H., Large Oriented Arrays and Continuous Films of TiO_2 -Based Nanotubes, *J. Am. Chem. Soc.*, 125, pp 12384-12385, 2003c.

Trentler, T. J., Denler, T. E., Bertone, J. F., Agrawal, A.,Colvin, V. L. Synthesis of TiO_2 Nanocrystals by Nonhydrolytic Solution-Based Reactions, *J. Am. Chem. Soc*. 121, pp 1613-1614, 1999.

Topham, S., The history of the catalytic synthesis of ammonia., C*atalysis: Science and technology. Springer, Berlin,* 7, pp1-50, 1985.

Vittadini A., A. Selloni, F.P. Rotzinger, M. Gratzel., Structure and Energetics of Water Adsorbed at TiO_2 Anatase (101) and (001) Surfaces, *Phys. Rev. Lett.,* 81, pp 2954-2957, 1998.

Wang, C.C., Ying J. Y., Sol-Gel Synthesis and Hydrothermal Processing of Aanatase and Rutile Titania Nnaocrystals, *Chem. Mater.*, 11, pp 3113-3120, 1999.

Wang X., Chen X. Gao, L. Zheng, H, Ji M, Tang C., Shen Tao., Zhang Z., Synthesis of β-FeOOH and α-Fe_2O_3 nanorods and electrochemical properties of β-FeOOH, *J. Mater. Chem*. 14, pp 905-908, 2004.

Wang. Z.L., Structural Analysis of Self-Assembling Nanocrystal Superlattices, *Adv. Mater.,* 10, pp13-30, 1998.

Wang, Z. L., Liu Y., and Zhang Z., Handbook of Nanophase and Nanostructured Materials., New York: *Kluwer Academic/Plenum Publishers Press,* 1, pp1-2, 2003a.

WCASLAB, MSDS and Technical Data Sheet , *WcasLab, Inc*, 2007

Wei, Q. Kouske Hirota, Keisuke Tajima, K. Hasimoto, Design and Synthesis of TiO_2 Nanorod Assemblies and Their Application for Photovoltaic Devices , *Chem. Mater.* 18, pp 5080-5087, 2006.

Weng, C.C., Wei, K. H., Selective Distribution of Surface-Modified TiO_2 Nanoparticles in Polystyrene-b-poly (Methyl Methacrylate) Diblock Copolymer, *Chem. Mater*., 15, pp 2936-2941, 2003.

Whang, D., Jin, S., Wu, Y., Lieber, C.M., Large-Scale Hierarchical Organization of Nanowire Arrays for Integrated nanosystems, *Nano Lett.,* 3, 1255-1259, 2003.

Whitesides, G. M, Grzyboski, B. Self-assembly at all scales, *Science,* 295, pp 2418-2421, 2002.

Willis, Amanda L., Nicholas, J. Turro, Stephen O'Brien. Spectroscopic Characterization of the Surface of Iron Oxide Nanocrystals, *Chem. Mater*. 17, pp 5970-5975, 2005.

Wu, H., V. R. Thalladi, S. Whitesides, G. M. Whitesides., Using Hierarchical Self-Assembly To Form Three-Dimensional Lattices of Spheres, *J. Am. Chem. Soc.*, 124, pp14495-14502, 2002.

Xia, Y., Yang, P., Sun, Y., Wu, Y., Mayers, B., Gates, B., Yin, Y., Kim, F., Yan, H., One-Dimensional Nanostructures: Synthesis, Characterization, and Applications, *Adv. Mater.,* 15, pp 353-389, 2003a.

Xu, R, Zeng, H.C., Self-generation of tiered surfactant superstructures for one-pot synthesis of Co_3O_4 nanocubes and their close and non-close-packed organizations, *Langmuir,* 20, pp 9780-9790, 2004.

Yamabi, S., Imai, H., Crystal Phase Control for Titanium Dioxide Films by Direct Deposition in Aqueous Solutions, *Chem. Mater.,* 14, pp609-614, 2002a.

Yamabi, S., Imai, H., Growth Conditions for Wurtzite Zinc Oxide Films in Aqueous Solutions, *J. Mater. Chem.,* 12, pp 3773-3778, 2002b.

Yang, H.G., Zeng H C, Self-Aligned Growth of Hexagonal TiO_2 Nanosphere Arrays on α-MoO_3, (010) Surface, *Chem. Mater.*, 15, pp 3113-3120, 2003.

Yang, P., Zhao, D, Margolese, D.I, Chmelka, B.F., Stucky. G.D., Generalized Syntheses of Large-Pore Mesoporous Metal Oxides with Semicrystalline Frameworks, *Nature,* 396, pp152-155, 1998.

Yang, P.; Zhao, D.; Margolese, D. I.; Chmelka, B. F.; Stucky, G. D., Block Copolymer Templating Syntheses of Mesoporous Metal Oxides with Large Ordering Lengths and Semicrystalline Framework, *Chem Mater.*, 11, pp 2813-2826, 1999

Yang, P., Wire on Water, *Nature,* 425, pp. 243-244, 2003.

Yi, D. K., Su S. L., Georgia C. Papaefthymiou, Ying, Y., Nanoparticle Architectures Templated by SiO_2/Fe_2O_3 Nanocomposites*, Chem. Mater.*, 18, pp 614-619, 2006.

Yin, Y., Y. Lu, B. Gates, Xia,Y. S., Synthesis and Characterization of Mesoscopic Hollow Spheres of Ceramic Materials with Functionalized Interior Surfaces, *Chem. Mater.,* 13, pp 1146-1148, 2001.

Zeng H., J. Li, Liu, L. P., Wang, Z. L., Sun, S., Exchange-Coupled Nanocomposite Magnets by Nanoparticles Self-Assembly, *Nature,* 420, pp395-398, 2002.

Zhao, J., Huggins, F.E., Feng, Z., Lu, F., Shah, N. & Huffman, G. P., Structure of a Nanophase Iron Oxide Catalyst, *J. Catalysis*, 143, pp 499-509, 1993.

Zhao, J., Feng, Z., Huggins, F.E., Huffman, G.P. Binary iron oxide catalysts for direct coal liquefaction , *Engergy Fuels,* 8, pp 38-43, 1994a.

Zhao, J., Huggins, F.E.,Feng, Z. Lu, F., Shah, N. & Huffman, G. P., Role of Molybdenum at the Iron Oxide Surface, *J. Catalysis,* 148, pp194-197, 1994b.

Zhao, J., Huggins, F.E.,Feng, Z. Lu, F., Shah, N. & Huffman, G. P., Ferrihydrite: surface structure and its effects on phase transformation , *Clays and Clay Min.* 42, pp 737-746, 1994d.

Zhao, Y. Charles W. Dunnill, Zhu Y, Duncan H, Gregory, Walter Kockenberger, Li, Y, Hu W, Iftikhar Ahmad, and David G. McCartney, Low-Temperature Magnetic Properties of Hematite Nanorods, *Chem. Mater.*, 19, pp 916-921, 2007.

Zheng, T., Pang, J., Tan, G., He, J., McPherson, G. L., Lu, Y., Vijay. T. Zhan, J. Surfactant Templating Effects on the Encapsulation of Iron Oxide Nanoparticles within Silica Microspheres, *Langmuir,* 23, pp 5143-5147, 2007.

Zhong, W., Ding, W.P., Jiang, Y., Preparation and Magnetic Properties of Barium Hexaferrite Nanoparticles Produced by the Citrate Process, *J. Am Ceramic Soc.*, 80, pp3258-3262, 1997.

Zhong, Z., Yin, Y., Gates B., and Xia Y., Preparation of Mesoscale Hollow Spheres of TiO_2 and SnO_2 by Templating Against Crystalline Arrays of Polystyrene Beads, Adv. Mater., 12, 206-209, 2000.

Zhong, Z., Lin, M., Ng, V., Ng, G. X., Foo, Y., Gedanken, A., A Versatile Wet-Chemical Method for Synthesis of One-Dimensional Ferric and Other Transition Metal Oxides, *Chem. Mater*., 18, pp 6031-6036 , 2006

Zhong, Z., Ho, J., Teo, J., Shen, S., Gedanken, A., Synthesis of Porous α-Fe_2O_3 Nanorods and Deposition of Very Small Gold Particles in the Pores for Catalytic Oxidation of CO, *Chem. Mater*., 19, pp 4776-4782, 2007.

Zhu, K. Kopidakis, N., Neale, N. R., Lagemaat, J., Arthur, J. F., Influence of Surface Area on Charge Transport and Recombination in Dye-Sensitized TiO_2 Solar Cells, *J. Phys. Chem. B*, 110 (50), pp 25174-25180, 2006.

Zhu Y. C. and Ding, C. X. Oriented Growth of nano- TiO_2 Whiskers, *Nanostruct Mater*., 11, pp 427-431, 1999

PUBLICATIONS RELATED TO THE THESIS

1. Self-assembly of iron oxide nano-rods: experimental synthesis and instrumental characterization (prepared), Hong Yang, Qinmin Pan*

2. One step synthesis TiO_2 nanosphere within copolymer templating hollow ring (prepared), Hong Yang, Qinmin Pan*

3. Performance of Highly Porous TiO_2 Nanoparticles in Electron Transport (prepared). Hong Yang, Qinmin Pan*.